UNIVERSITÀ DEGLI STUDI DI MILANO

Department of Pharmaceutical Sciences

Doctorate School in Pharmaceutical Sciences (XXX Cycle)

Sector CHIM/08

NONCOVALENT FLUOROUS INTERACTIONS: NEW APPROACHES FOR DRUG DISCOVERY AND DRUG DELIVERY

Dr. Corinna GALLI

R10977

Faculty Advisor: Professor Sergio ROMEO

PhD Coordinator: Professor Giancarlo ALDINI

Academic year 2016-2017

Acknowledgements

Firstly, I would like to thank my advisor Professor Sergio Romeo for his mentorship, his continuous support over the years as well as for his patience and immense scientific knowledge.

The research presented here has also benefited from collaborations. I am grateful to Professor Giancarlo Aldini and his team for their helpful suggestions and for electrophoresis purification. I am grateful to Doctor Annapaola Andolfo from Protein Microsequencing Facility, San Raffaele Scientific Institute, for the helpful discussion and for all of her help with mass spectrometry studies.

I must also pay tribute to all the members of Professor Romeo laboratory, who have been a great intellectual resource and have made it fun to come to work, with a special thanks to Letizia Ceppi for helping me through the whole project.

My sincere thanks go to Professor Sandro Mecozzi, who provided me the opportunity to join his team at University of Wisconsin-Madison. Professor Mecozzi's creativity and scientific knowledge have been an inspiration that I will carry with me going forward.

Thank you to all his wonderful team, who made me feel at home, with a special thanks to Alexa Barres for her helpful advice.

Thanks to Dr. Tom Stringfellow for his NMR support and Doctor Martha Vestling for her mass spectrometry expertise.

Last but not the least, I would like to thank my family: my parents and my sister for their unwavering support, encouragement and love.

NONCOVALENT FLUOROUS INTERACTIONS:
NEW APPROACHES FOR DRUG DISCOVERY AND DRUG DELIVERY

By

Corinna Galli

Under the Supervision of

Professor Sergio Romeo

Abstract

The unique chemical properties of fluorine atom (high electronegativity, high ionization potential, low polarizability and low van der Waals interactions) modify the chemical properties of organic compounds as well as their reactivity when hydrogen atoms are replaced by fluorines. Actually, fluorocarbons show low polarity, which is responsible for the high hydrophobicity of these molecules. Additionally, the low polarizability of fluorines leads to weaker van der Waals interactions, which makes fluorocarbons lipophobic. Therefore, fluorinated compounds show an amphiphilic character that leads to the formation of the fluorous phase, which is separated to both aqueous and organic layers.

The aim of my project was applying the strong and noncovalent fluorous interactions to drug discovery and drug delivery.

The first part of my thesis is focused on the development of a new strategy for target identification able to overcome the several limitations associated to classic chemical proteomics techniques. Indeed, traditional chemical proteomics methodology uses agarose beads covalently bound to streptavidin as stationary phase for affinity purification. This resin is able to retain biotin-tagged proteins as well as sticky components abundant in the lysate. These contaminants might be aspecifically eluted with the biological targets, complicating the mass analysis and therefore the target identification. In order to increase the selectivity of the proteomics approach, we designed an innovative fluorous proteomics methodology using the strong fluorous-fluorous interactions as recognition system for affinity purification. Indeed, perfluorinated stationary phase can anchor only fluorinated species, avoiding aspecific binding. To test the fluorous proteomics approach, papain was considered as biological target. Fluorinated inhibitors of papain with different fluorinated-chain length were synthesized. The number of fluorine atom of the inhibitor is crucial for the interaction with the fluorinated stationary phase in the purification step. Actually, only papain inhibitors with a long fluorous alkyl chain are able to bind the fluorinated resin and therefore immobilize papain. In contrast, inhibitors with a short fluorous alkyl chain cannot bind the fluorinated stationary phase by means of fluorous-fluorous interactions. Consequently, papain cannot be anchored to the resin.

The second part of my thesis is focused on the application of fluorous interactions for drug delivery. This project was carried out in the School of Pharmacy, University of Wisconsin-Madison (Madison, WI, U.S.A.) under the supervision of Professor Sandro Mecozzi. The aim was designing and synthesizing semifluorinated dibranched polymers. The

synthesis of fluorinated molecules is a challenge, due to their poor reactivity and low solubility in commonly-used organic solvents. To increase the final yield, each step of the synthesis of the semifluorinated dibranched polymers was optimized. The dibranched fluorinated polymers will be used to prepare oil-in-water nanoemulsions for controlled drug release of paclitaxel. We reasoned that semifluorinated polymers with different chemical structures might lead to nanoemulsions with different stability and drug release profile. Small diameter of the nanoemulsion droplets and long half-lives are desired to maximize the tumoritropic accumulation of these nanosystems by EPR effect before drug release. This allows the release of the drug within the tumor instead of in the bloodstream, avoiding side effects due to the interaction of the drug with off targets and consequently reducing the systemic toxicity.

Table of Contents

List of Tables, Figures and Schemes

Chapter 1

Chapter 2

Chapter 3

Abbreviations

λ	wavelength
$[N_{1888}][NTf_2]$	methyltrioctylammonium bis(trifluoromethylsulfonyl)imide
1,2-DCE	1,2-dichloroethane
^{18}FDG	2-^{18}F-fluoro-2,2-deoxy-D-glucose
5-FU	5-fluorouracil
ABPP	activity-based probe profiling
ACT	artemisinin combination therapy
Aliquat® 336	tricaprylmethylammonium chloride
Arg	arginine
Asn	asparagine
BnBr	benzyl bromide
Boc	tert-butoxycarbonyl
bs	broad singlet
BTF	benzotrifluoride
CCCP	compound-centric chemical proteomics
CMC	critical micellar concentration
Cmp	compound
COX	cyclooxygenase
CQ	chloroquine
CV	column volume
Cys	cysteine

d	doublet
DCC	*N,N'*-dicyclohexylcarbodiimide
DCM	dichloromethane
dd	doublet of doublets
DHA	dihydroartemisinin
Diazald®	N-methyl-N-nitroso-p-toluenesulfonamide
DIC	N,N′-diisopropylcarbodiimide
DLS	dynamic light scattering
DMAP	4-dimethylaminopyridine
DMF	N,N-dimethylformamide
DMSO	dimethyl sulfoxide
DTT	dithiothreitol
ED_{50}	median effective dose
EDAC	N-(3-dimethylaminopropyl)-N′-ethylcarbodiimide hydrochloride
EDTA	ethylenediaminetetraacetic acid
EPR	enhanced permeability and retention effect
eq	molar equivalent
ESI	electrospray ionization
Et_2O	diethyl ether
EtOAc	ethyl acetate
FC-12	fluorohexanes
FDA	food and drug administration
F_nH_m	(fluorinated alkyl) alkyl diblocks

F-SPE	fluorous solid phase extraction
Gly	glycine
HATU	*N*-[(Dimethylamino)-1*H*-1,2,3-triazolo-[4,5-*b*]pyridin-1-ylmethylene]-*N*-methylmethanaminium hexafluorophosphate *N*-oxide
HBTU	2-(1H-benzotriazol-1-yl)-1,1,3,3-tetramethyluronium hexafluorophosphate
HCTU	2-(6-Chloro-1-H-benzotriazole-1-yl)-1,1,3,3-tetramethylaminium hexafluorophosphate
HFE-7100	perfluorbutyl methyl ether
His	histidine
HMEC	human mammary epithelial cells
HMGCoA	3-hydroxy-3-methylglutaryl-coenzyme A
HOBt	1-hydroxybenzotriazole
HPLC	high-performance liquid chromatography
iBuOCOCl	isobutyl chloroformate
IC_{50}	half maximal inhibitory concentration
ID	injected dose
IL	ionic liquids
LC-MS/MS	liquid chromatography tandem-mass spectrometry
Leu	leucine
logD	logarithmic coefficient of distribution
m	multiplet
MALDI	matrix-assisted laser desorption/ionization
MCT	medium chain triglycerides

mPEG	methoxy poly(ethylene glycol)
MRI	magnetic resonance imaging
Ms	methanesulfonyl
N/P ratio	nitrogen to phosphorous ratio
NMM	4-methylmorpholine
NMR	nuclear magnetic resonance
o.n.	overnight
PEG	poly(ethylene glycol)
PET	positron emission tomography
PFCE	perfluoro-15-crown-5-ether
PFCs	perfluorocarbons
PFOA	perfluorooctanoic acid
PFOB	perfluorooctyl bromide
PFOS	perfluorooctane sulfonate
Phe	phenylalanine
PTX	paclitaxel
RES	reticuloendothelial system
R_f	retention factor
rt	room temperature
s	singlet
SAR	structure activity relationship
SDS	sodium dodecyl sulfate
SDS-PAGE	sodium dodecyl sulfate polyacrylamide gel electrophoresis

t	triplet
$t_{1/2}$	half-life
TBABr	tetrabutylammonium bromide
TBAI	tetrabutylammonium iodide
TBTU	O-(benzotriazol-1-yl)-N,N,N′,N′-tetramethyluronium tetrafluoroborate
TCTU	(O-(6-Chloro-1-hydrocibenzotriazol-1-yl)-1,1,3,3-tetramethyluronium tetrafluoroborate)
TEA	trimethylamine
TFA	trifluoroacetic acid
THF	tetrahydrofuran
TLC	thin layer chromatography
TMS	tetramethylsilane
U	enzyme unit
UV	ultraviolet light
Z	carbobenzyloxy

Chapter 1

Introduction

1.1 Historical Development

Elemental fluorine was isolated by Henry Moissan in 1886. However, the industrial production of fluorine began during World War II, when isotopic enrichment of natural uranium into its radioactive isotope was required in order to build nuclear weapons. For this purpose, high-temperature electrolysis was applied to prepare large quantities of elemental fluorine and fluorhydric acid needed to get uranium hexafluoride (UF_6), which is used for uranium enrichment. This led to the birth of fluorine industry.[1]

Industrial application of fluorinated organic molecules started with the market of Freon-12 (CCl_2F_2) by General Motors to replace more toxic compounds used in kitchen refrigerators. Polytetrafluoroethylene (Teflon™) was serendipitously discovered by Dr. Roy Plunkett in 1938 while working on refrigerants. An accidental polymerization afforded a waxy substance showing unique chemical and physical properties.[2] In fact, Teflon™ is characterized by high thermal stability, exceptional mechanical properties at extreme temperatures, excellent chemical resistance and dielectric properties, oil and water repellence and low flammability.[3] Thanks to these properties, Teflon™ has found several applications, such as electrical cable insulation, stain repellant, non-stick coating for cookware and lubrificant.[4] It is also applied in the medical field as graft material in surgery, heart patches and coating on catheters, since it prevents the adhesion of bacteria on the catheter surface avoiding hospital-acquired infections.[5]

For many years, fluorine chemistry remained confined to the field of polymers and materials rather than medicinal chemistry. Organic fluorinated compounds are not common in nature. It is remarkable that

fluorine is present in less than 15 natural products and the only one known at that time was fluoroacetic acid, a potent poison.[1,6] For these reasons, the investigation of fluorinated-drug field started later, in the early 1950s. It is noteworthy that the introduction of a single fluorine atom in a drug can modify deeply its biological properties. In fact, in 1957 Dr. Charles Heidelberger demonstrated that 5-fluorouracil (5-FU) – synthesized by introducing a fluorine atom in the 5 position of uracil – was able to inhibit the thymidylate synthase. This blocked the synthesis of thymidine and, consequently, the synthesis of DNA.[7,8]

Nowadays, 20% of pharmaceuticals on the market contains fluorine. Atorvastatin – HMGCoA reductase inhibitor used to treat hypercholesterolaemia – was the most sold drug worldwide in 2012. It went on market in 1997 and over 15 years, atorvastatin has been made over $125 billion in sales.[9] Many selective serotonin reuptake inhibitors contain fluorine atoms. In fact, it was demonstrated that the presence of a trifluoromethyl group in *para* position in the aromatic ring of fluoxetine gives selectivity toward the serotonin transport.[10] Other examples of best-seller fluorinated drugs are ciprofloxacin (a broad-spectrum antibiotic belonging to the quinolone class), lansoprazole (a proton-pump inhibitor) and fluticasone propionate (a glucocorticoid used to treat asthma and allergic rhinitis).[8] The interest for fluorine in medicinal chemistry has been increased in the recent years. Actually, new fluorinated drugs have been approved by FDA or are under clinical study. Among them, afatinib (approved in 2015) and dacomitinib (phase III study) are active against non-small-cell lung carcinoma while evacetrapib and darapladib (both in phase III study) are under development as drugs for treatment of atherosclerosis.[11,12,13,14]

1.2 Properties of Fluorine

The structure and the atomic properties of fluorine atom affect deeply both chemical and physical characteristics of fluorinated molecules. Fluorine is the most electronegative element in the periodic table and shows very high ionization potential and very low polarizability.[1] When bound to carbon, it forms the strongest bond in organic chemistry.[15] The extreme stability of C-F bond is increased when the number of fluorine atoms bound to the same carbon atom increases. This improved stabilization is found also in the length of C-F bonds in the series CH_3F (140 pm) > CH_2F_2 (137 pm) > CHF_3 (135 pm) > CF_4 (133 pm). The main reason for this stabilization is the excellent overlap between the fluorine 2s and 2p orbitals with the corresponding carbon orbitals; this allows the occurrence of dipolar resonance structures for multiply fluorine-substituted carbon, as shown in **Figure 1.1**.[2]

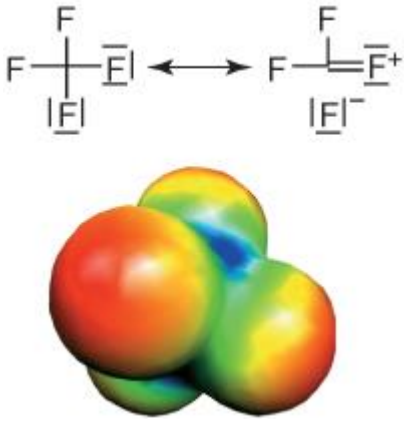

Figure 1.1 Resonance stabilization of C-F bond in CF_4. The electrostatic potentials are mapped on the electron isodensity surface (calculation at the MP2/6-31+G* level of theory; red denotes negative and blue positive partial charges).[2]

Because of the high electronegativity of fluorine, C-F bond is polarized from the sp^3 carbon (δ^+) to the fluorine (δ^-) that is in the opposite

direction of C-H bond. The high electronegativity and the low polarizability of the fluorine atom are responsible for the ionic character of C-F bond as well as the stronger energy of this bond if compared with the bond between carbon and the other halogens. Moreover, the low polarizability implies lower van der Waals interactions, often increasing local lipophilicity of a molecule despite the higher electronegativity.[15]

Fluorine shows a greater van der Waals radius (1.47 Å) than hydrogen (1.20 Å), being actually closer to that of oxygen (1.52 Å).[16] The larger volume of fluorine than hydrogen volume is responsible for the molecular steric congestion observed when hydrogens are replaced with fluorines. In particular, replacing a single hydrogen with fluorine has limited steric effect and this does not affect the conformation of the whole molecule. However, the substitution of a methylene (CH_2) with a difluoromethylene group (CF_2) can lead to a dramatic modification in conformation.[17]

Table 1.1 summarizes some properties of hydrogen, fluorine and oxygen.

Atom	Pauling's Electronegativity	Bond Length (CH_2-X, Å)	Van der Waals Radius (Å)	Bond Energy (CH_2-X, kcal/mol)	Ionization Potential (kcal/mol)	Atom Polarizability (Å^3)
H	2.20	1.09	1.20	99	313.6	0.667
F	3.98	1.39	1.47	116	401.8	0.557
O	3.44	1.43	1.52	85	314.0	0.82

Table 1.1 Properties of hydrogen, fluorine and oxygen.

1.3 Physical Properties of Fluorinated Molecules

The physical properties of fluorinated molecules depends mainly on the high electronegativity of fluorine, its small size and its very low polarizability. As mentioned before, C-F bond is strongly polarized. However, perfluorocarbons (PFCs) are nonpolar. In fact, local dipole moments within the same molecule cancel out, leading to a nonpolar molecule.[2]

Due to the low polarizability, fluorinated molecules – even the lightly fluorinated compounds – show weak intra- and intermolecular interactions. Consequently, they are characterized by very high vapor pressure if compared to that of their hydrogenated analogues. This means that fluorinated molecules are volatile.[1] Perfluorinated compounds have lower boiling points than hydrocarbons with similar molecular weights. If perfluorinated compounds and homologous hydrocarbons are compared, they show similar boiling points. However, the molecular masses of PFCs are about four times higher than hydrocarbons ones, as shown in **Figure 1.2**.[2]

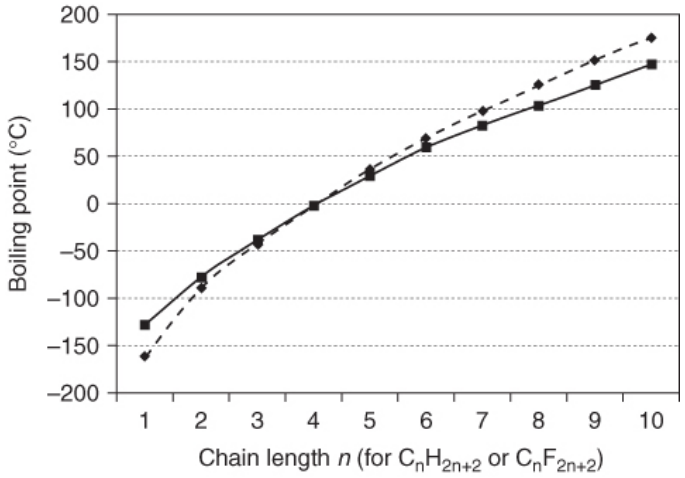

Figure 1.2 The boiling points of homologous alkanes (♦) compared with those of the corresponding perfluoroalkanes (■).[2]

It is noteworthy that branching does not affect the boiling point strongly. The boiling point of PFCs is only 25-30 °C higher than that of noble gases with similar molecular weights. This is due to the low polarization that affords a "perfect" fluid behavior to these molecules. The boiling points of fluoromethanes do not increase according to the number of fluorines present in the molecule, conversely to the boiling points of chloro- and bromomethanes. As shown in **Table 1.2**, the boiling point increases from CH_4 to CH_2F_2 and then decreases until CF_4.[1]

Compound	Boiling point (°C)	Compound	Boiling point (°C)	Compound	Boiling point (°C)
CH_4	-161	CH_4	-161	CH_4	-161
CH_3F	-78.6	CH_3Cl	-24.2	CH_3Br	3.6
CH_2F_2	-51.6	CH_2Cl_2	40.1	CH_2Br_2	98.2
CHF_3	-82.2	$CHCl_3$	61.3	$CHBr_3$	149.5
CF_4	-128	CCl_4	98.2	CBr_4	189.5

Table 1.2 Boiling points of halomethanes.[1]

Hemifluorinated molecules have local carbon-fluorine dipole moments that generate strong electrostatic interactions. Moreover, a correlation is observed between boiling points and dipolar moments. Actually, comparing the boiling point of methane and fluoromethanes, it results that nonpolar CH_4 and CF_4 show the lowest boiling points while CH_2F_2 – which has the strongest molecular dipole moments – has the highest boiling point. **Figure 1.3** illustrates the relationship between dipole moment and boiling point for methane and fluoromethane series.[1,2]

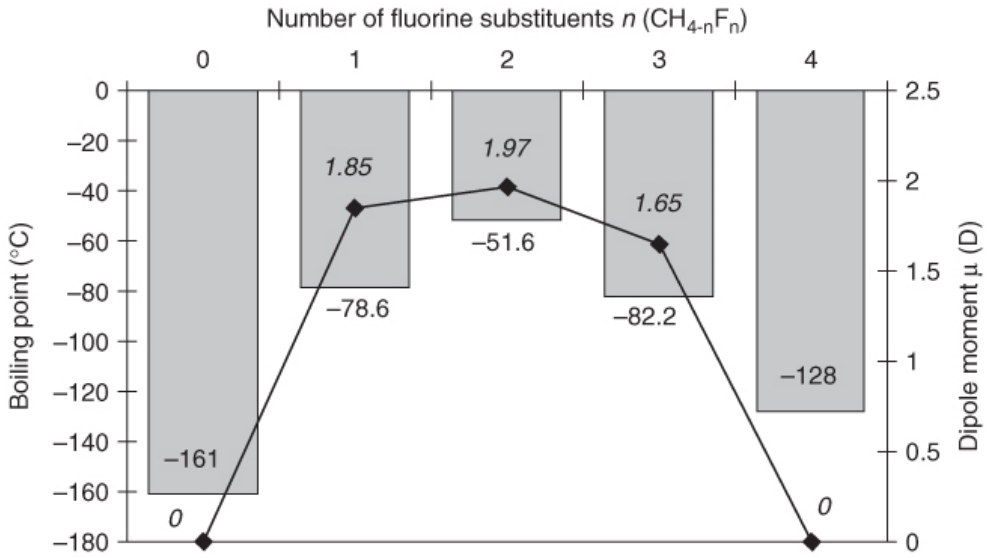

Figure 1.3 Boiling points (gray bars) and dipole moments (◆, values in italics) of methane and the different fluoromethanes $CH_{4-n}F_n$.[2]

Weak intermolecular interactions are also responsible for the very low surface tension (γ) of perfluorinated compounds. In fact, they always show a lower surface tension than the one of the corresponding hydrocarbons. Consequently, PFCs can wet any surface. Moreover, the introduction of a polar hydrophilic group in a perfluorinated alkyl chain affords a very active fluorosurfactant that can reduce the surface tension of water from 72 dyn/cm to 15-20 dyn/cm compared with 25-35 dyn/cm for the corresponding hydrocarbon surfactant.[2] Similarly, the critical micelle concentration (CMC) of fluorinated surfactants is lower than their hydrogenated counterparts CMC.[18] It has been estimated that the contribution of a CF_2 in a linear fluorocarbon chain towards the energy of micellization is equivalent to 1.5 CH_2 in a linear hydrocarbon chain. Fluorinated amphiphiles can self-assemble into Langmuir monolayers, spherical or cylindrical micelles, and bilayer pyramidal columns in organic, aqueous, or fluorous solvents.[15,19,20] However, these systems show different properties if compared with the

ones obtained from hydrogenated analogues. Because of the greater van der Waals radius of fluorine than hydrogen radius, perfluoroalkyl chains are bulkier than the hydrocarbon counterpart. Consequently, disk-like and rod-like cylindrical micelles are preferred than spherical micelles.[21]

1.4 Reactivity and Chemical Properties of Fluorinated Molecules

C-F bond is thermodynamically stabilized by the optimum overlap between the 2s and 2p orbitals of fluorine and the corresponding orbitals of carbon. In PFCs, there is also a kinetic stability coming from the steric shielding of the central carbon atom by the fluorine substituents.[2,15] Actually, the three electron lone pairs of fluorine atom and the negative partial charge represent a steric and electrostatic shield against nucleophilic attack of the central carbon atom. Moreover, CF_3 group is much more sterically demanding than CH_3 substituent and is bulkier than isopropyl group. This is more easily understandable comparing the van der Waals volumes of CH_3 (16.8 $Å^3$) and CF_3 (42.6 $Å^3$), as shown in **Figure 1.4**. The steric hindrance and the electrostatic shield arising from the presence of many adjacent fluorines bound to a carbon backbone is the major responsible factor for the relative inertness of PFCs.[2,22]

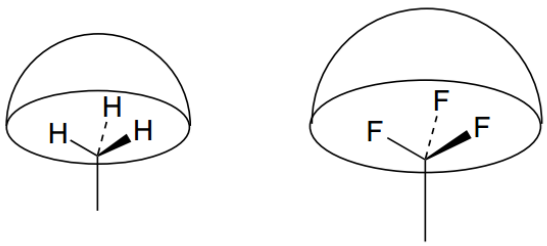

16.8 $Å^3$ 42.6 $Å^3$

Figure 1.4 Van der Waals volumes of CH_3 and CF_3 groups.[22]

Fluoroalkyl substituents have always a strong electron-withdrawing effect. Consequently, they increase the acidity of neighboring hydrogen atoms (**Table 1.3**). As expected, the inductive effect falls off with distance, while the presence of a double bond relays the effect. The strong inductive effect of fluoroalkyl substituents increases the acidity of alcohols (**Table 1.3**). It is noteworthy that perfluoro-*t*-butanol has a pK_a value close to acetic acid pK_a. Fluorine atoms bound to a phenyl ring are not only inductively electron-withdrawing since their electron lone pairs can be donated to the aromatic ring through resonance.

Carboxylic acid	pK_a	Alcohol	pK_a
CH_3COOH	4.76	CH_3CH_2OH	15.9
CH_2FCOOH	2.59	CF_3CH_2OH	12.4
CHF_2COOH	1.34	CCl_3CH_2OH	12.2
CF_3COOH	0.52	$(CF_3)_2CHOH$	9.3
$CF_3CH_2CH_2COOH$	4.15	$(CH_3)_3COH$	19.2
$CF_3CH=CHCOOH$	3.48	$(CF_3)_3COH$	5.1
C_6H_5COOH	4.21	C_6H_5OH	10.0
C_6F_5COOH	1.75	C_6F_5OH	5.5

Table 1.3 pK_a values of some carboxylic acids and alcohols.[2,22]

The inductive effect of fluorination lowers the strength of organic bases (**Table 1.4**). Tertiary perfluoroalkylamines do not show basic properties. Actually, perfluoroethylamine can be used as solvent in reaction involving Lewis acid like $TiCl_4$ or BF_3, without observing a reaction between the fluorinated base and the Lewis acid.[22]

Amine	pK_b
$CH_3CH_3NH_2$	3.3
$CF_3CH_2NH_2$	8.1
$C_6H_5NH_2$	9.4
$C_6F_5NH_2$	14.36

Table 1.4 pK_b values of some amines.[2,22]

Despite the electron lone pairs and the high electronegativity, fluorine is a poor acceptor of hydrogen bond because of the low polarization of its s and p electrons.[2]

The introduction of fluorines in aromatic systems changes the electrostatic distribution of the molecular surface deeply. Noteworthy, the fluorination of aromatic rings in molecules of pharmaceutical interest may create new binding sites localized in proximity of the fluorine atoms.[23] For that reason, mono- or difluorination of phenyl groups in drugs can improve the protein binding. For example, it was demonstrated that fluorinated inhibitors and HMGCoA reductase form complexes involving an ion-dipole interaction between an aromatic fluorine and the guanidinium side chain of Arg590 (**Figure 1.5**). The distance F···N was found to be 2.9 Å.[23,24]

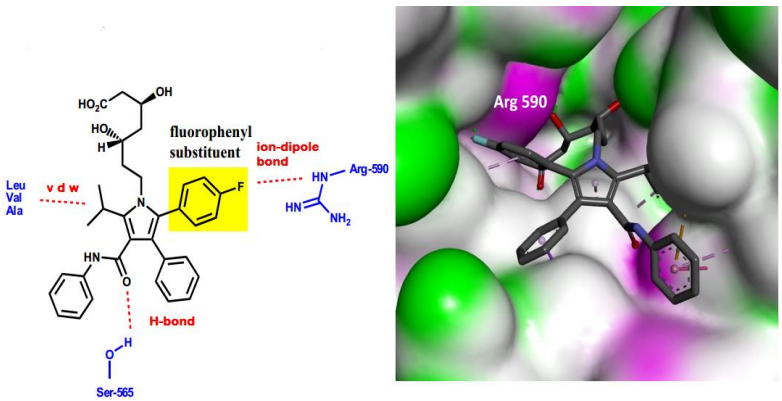

Figure 1.5 Ion-dipole bond between atorvastatin and Arg590 in the binding pocket of HMGCoA reductase.

Moreover, a systematic scan of substituents belonging to the series of 7-(substituted aryl)-3,5-dihydroxy-6-heptenoic (and heptanoic) acids and their lactones demonstrated that the inhibitors showing the highest activity borne a 4-fluorophenyl moiety.[23] This suggests that aromatic fluorine can play an important role in the activity of molecules with medicinal interest.

1.5 Perfluorocarbons

Horváth and Rábai introduced the term "fluorous" in 1994 in analogy to "aqueous".[25] Fluorous was defined as "of, relating to, or having the characteristics of highly fluorinated saturated organic materials, molecules, or molecular fragments";[26] that means PFCs are fluorous molecules. PFCs are more chemically and thermally stable than hydrocarbons since the strong C-F bond gets stronger because of the high degree of fluorination, rising from 116 kcal/mol up to 127 kcal/mol in PFCs.[27] An additional element of stability is represented by the steric hindrance arising from the coating of fluorine substituents, since it protects the carbon backbone against nucleophilic attack.[28] The low polarization and the larger size of fluorine compared to hydrogen (1.47 Å vs 1.20 Å) affect the molecular conformation of PFCs.[2] Actually, mean volumes of CF_2 and CF_3 groups are estimated to be 38 $Å^3$ and 92 $Å^3$, while mean volumes of CH_2 and CH_3 groups are 27 $Å^3$ and 54 $Å^3$ respectively.[29] Moreover, the CF_3 group is larger than an isopropyl substituent.[29] For these reasons, fluorinated chains are bulkier than alkyl chains, with cross sections around 27-30 $Å^2$ and 18-21 $Å^2$ respectively.[29] The steric repulsion between fluorine atoms bound to the carbon backbone in the relative 1,3-positions as well as the larger van der Waals radius of fluorine cause a stretching and a twisting of the

carbon backbone by 12° on average.[29,30] This results in a 15/7 helix, with left and right helices being in equal proportions.[29] This is the reason why perfluoroalkyl chains adopt an all-trans helical structure rather than the planar "zig-zag" conformation of linear hydrocarbons (**Figure 1.6**).[2] The repulsive stretching of 1,3-difluoromethylene groups is also responsible for the rigidity of perfluoroalkyl chains. In fact, PFCs are rigid, rod-like molecules since they lack the conformational flexibility of hydrocarbons. It has been demonstrated that trans/gauche interchange enthalpies are at least 25% higher for linear PFCs than for the non-fluorinated analogue, and this reduces the conformational freedom of perfluoroalkyl chains.[29] Consequently, PFCs show higher level of packing if compared to hydrocarbons, which is responsible for the assembly properties of PFCs.

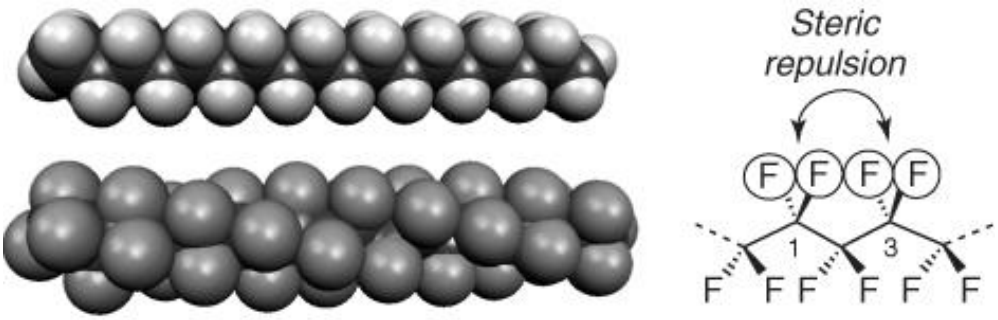

Figure 1.6 The linear "zig-zag" conformation of octadecane compared with the helical perfluorooctadecane.[2]

Due to the very low polarizability of fluorine, van der Waals interactions between perfluoroalkyl chains are very weak.[15] As a result, the cohesive energy in liquid PFCs are low. Weak van der Waals interactions are responsible for many properties of PFCs, such as very low surface tension, high fluidity, low dielectric constant, high vapor pressure, high compressibility, and high gas solubilities.[31,32]

Intermolecular interactions can be quantified by the Hildebrand parameter (δ), calculated as the root square of the cohesive energy density of a liquid. The cohesive energy density is correlated to the polarity of the molecules. For low molecular weight compounds, the cohesive energy density is the energy of vaporization in calories per cubic centimeter and is an evaluation of the degree of van der Waals forces between molecules in the liquid. The lower the Hildebrand parameter is, the weaker the intermolecular interactions are.[33] It is remarkable that molecules with similar δ are miscible with or soluble in one another. **Table 1.5** lists δ for some perfluorinated and non-fluorinated solvents.

Solvent	**δ ($MPa^{1/2}$)**
O_2	11.4
Perfluorohexane	12.1
Perfluoroheptane	12.3
Perfluoro(methylcyclohexane)	12.5
Hexane	14.9
α,α,α-Trifluorotoluene	16.8
Toluene	18.2
Cyclohexane	18.8
Benzene	18.8
Acetonitrile	24.3
Methanol	29.7
Water	48.0

Table 1.5 Hildebrand parameters (δ) for perfluorinated and non-fluorinated solvents.[33,29, 34]

Because of the disparity in cohesive energy densities between liquid PFCs and liquid non-fluorinated hydrocarbons, these entities are not miscible.[29] It is remarkable that PFCs show amphiphilic properties. The local dipole moments of each C-F bond within the same molecule cancel out, leading to a hydrophobic character. Additionally, low van der Waals interactions give a lipophobic behavior. This amphiphilic character provides the driving force to PFCs to segregate away from both polar and non-polar solvents.[35] Consequently, when PFCs are mixed with water and organic solvents, they usually form a unique phase called the fluorous phase, which is separated to both the aqueous and the organic layers (**Figure 1.7**). This allows PFCs to make stronger intermolecular interactions with each other. Molecules showing this kind of behavior are called fluorophilic, in analogy to hydrophilic and lipophilic.

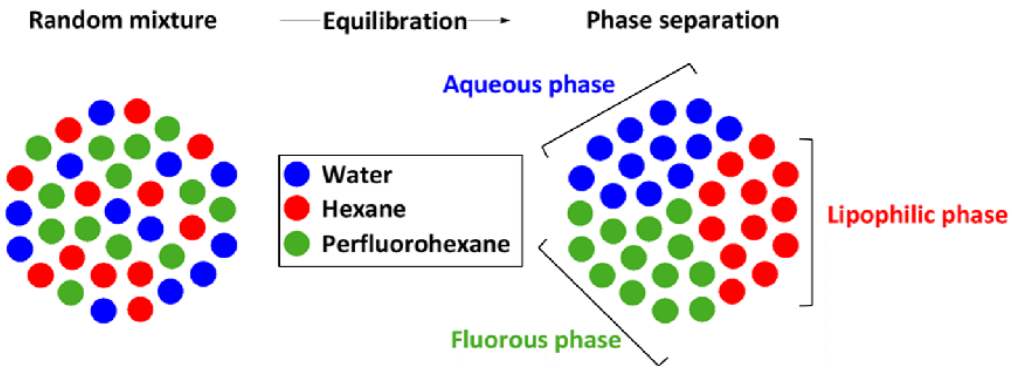

Figure 1.7 Schematic representation of the fluorous phase formation.

The term "fluorophilicity" is referred to the affinity of a given compound for the fluorous phase. It was demonstrated that there is not a simple relationship between the total number of fluorine atoms and the phase preference of molecules bearing perfluoroalkyl chains (also

called "fluorous ponytails", $R_{fn}=F(CF_2)_n$).[33] Some factors must be taken into account when an increased in the fluorophilicity is desired:[33]

- The fluorine content.

  At least 60 wt.% fluorine is needed. It is remarkable that the maximum fluorine weight percentage is not 100%. For example, perfluorohexane has 78 wt.% fluorine. An organic molecule can be converted into a fluorous compound by adding fluorous ponytails. Moreover, a molecule is more fluorous when the fluorine atoms are distributed throughout the whole molecule rather than in one moiety.[36]
- The lengths and the number of the fluorous ponytails.

  Longer fluorous chains as well as increasing the number of the same ponytail lead to a higher partition coefficient.
- The molecular structure. The number of functional groups that may be involved in intermolecular interactions, such as hydrogen bonds, should be limited. However, trifluoromethyl substituents, either introduced as such or part of OCF_3 and SCF_3 groups, are highly effective in increasing fluorophilicity. Thus, the trifluoromethyl group might be considered as a strong fluorophilic group because of its fluorine content and low formula weight.
- The structure of the fluorous ponytail. Several factors, such as branching, hetero atoms as part of $-CF_2OCF_2-$, $-CF_2SCF_2-$, or $–CF_2N(R_f)_2-$ segments or conformational flexibility *versus* rigidity are expected to affect the fluorophilicity of a given compound.

It is important to note that perfluoroarenes cannot be considered as fluorous molecules. Actually, they are more polar than perfluoroalkanes and tend to partition into the organic phase rather than the fluorous layer.

1.6 (Fluorinated Alkyl) Alkyl Diblocks

(Fluorinated alkyl) alkyl (F_nH_m) diblocks are composed by a fluorinated moiety bound to an alkyl chain by a covalent bond. This leads to both steric and energetic frustrations and therefore properties of this new entity are different from those of the parent moieties. F_nH_m are amphiphilic (fluorinated and alkyl chains display different affinities), amphisteric (the two chains show different conformations, cross sections, and steric hindrance), and amphidynamic (they have different dynamic features since the fluorinated moiety is stiff, rod-like, and prone to aggregation while the other one is more flexible and prone to bend).[29] **Figure 1.8** illustrates the properties of linear F_nH_m.

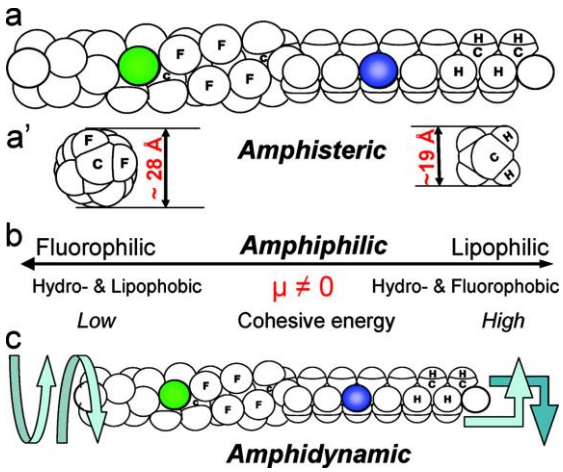

Figure 1.8 Linear F_nH_m diblocks are (a) amphisteric (a': cross sections of the fluorinated and non-fluorinated blocks), (b) amphiphilic, and (c) amphidynamic.[29]

The amphisteric, amphiphilic, and amphidynamic character of F_nH_m diblocks affects their properties. Indeed, they possess a dipole moment and surface activity that are essentially not observed in perfluorinated chains as well as in alkyl chains. In contrast to PFCs, the C-F bond dipoles in F_nH_m diblocks do not all cancel out and they are oriented

opposite to those of C-H bond dipoles, leading to a significant dipolar character.[29] Due to the strongly electron-withdrawing effect of fluorinated chains, shift of electronic charges leading to the creation of an electric dipole is observed at their junction with the alkyl chains. The terminal CH_3 and CF_3 groups of the F_nH_m diblocks also take part to dipoles. The total moment dipole of the molecule is not aligned with the axis of the molecule since the axes of CH_3 and CF_3 groups form an angle with the axis of the F_nH_m diblocks, as illustrated in **Figure 1.9**.

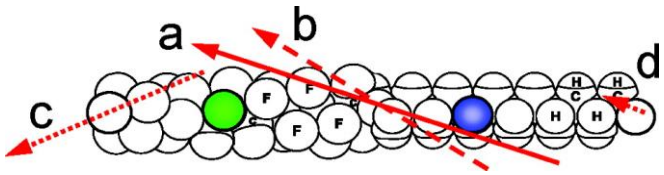

Figure 1.9 F_nH_m diblocks host a strong dipole (a), with components arising from (b) the F_n-H_m junction, (c) the terminal CF_3, and (d), to a much lesser extent, the terminal CH_3.[29]

Since F_nH_m diblocks are fluorophilic (and lipophobic) at one end and lipophilic (and fluorophobic) at the other one, they show an amphiphilic character. It is remarkable the absence of a hydrophilic moiety in contrast to conventional surfactants. Because of their combined amphisteric, amphiphilic, and amphidynamic character, F_nH_m diblock molecules are used to prepare self-assembled colloids such as Langmuir monolayer, bilayer membranes, vesicles as well as micelles when the surfactant concentration exceeds the critical micelle concentration (CMC).

1.7 Fluorine in Medicinal Chemistry

The introduction of fluorine substituents into a molecule affects its physical and chemical properties deeply and, thus, its biological

activities. Actually, absorption, distribution, interaction with biological targets as well as metabolism and elimination of a drug are modified by the introduction of fluorine atoms.

Fluorine atoms are introduced in pharmaceuticals mainly for three topics:

1. Increase the metabolic stability.

   Hepatic enzymes, especially P450 cytochromes, oxidize lipophilic drugs limiting their bioavailability. In order to increase the bioavailability of pharmaceuticals, metabolic sites can be blocked by introducing fluorine substituents. It is important to verify that the introduction of a new group does not affect the binding with the molecular target and thus the biological activity of the molecule. For example, the cholesterol-absorption inhibitor ezetimibe was obtained starting from the lead SCH 48461 by introducing two fluorine atoms on aromatic rings (**Figure 1.10**).[37,38] These modifications block the oxidation of the phenyl ring to phenol as well as the dealkylation of the methoxy group.

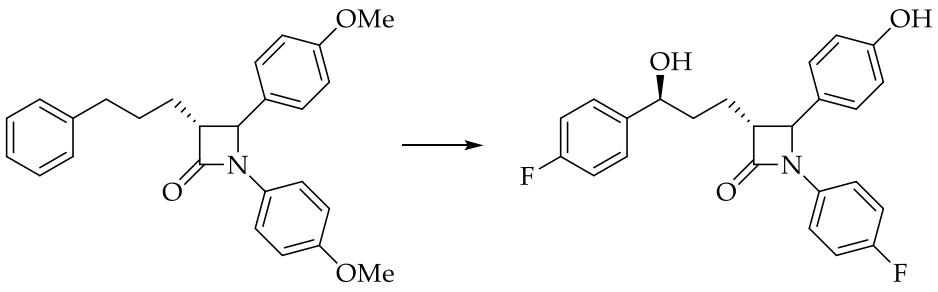

SCH 48461
ED50 (hamster) = 2.2 mg/kg

Ezetimibe
ED50 (hamster) = 0.04 mg/kg

Figure 1.10 Development of ezetimibe by lead optimization of SCH 48461.

Another example supporting the strong impact of fluorine atoms on metabolic stability of drugs is represented by the selective cyclooxygenase II (COX-II) inhibitor celecoxib.[39,40] It was discovered replacing a fluorine atom of the lead compound by a methyl group. This reduced the very high half-life to a more acceptable value (**Figure 1.11**).

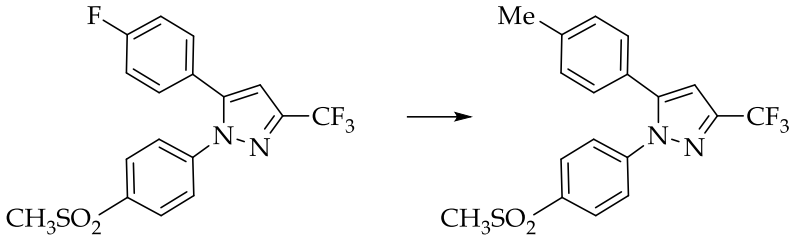

Early COX II inhibitor
$t_{1/2}$ (rat) up to 220 h

Celecoxib analogue
$t_{1/2}$ (rat) = 3.5 h

Figure 1.11 Development of celecoxib.[40]

It is noteworthy that in some cases the introduction of fluorine atoms does not prevent the oxidative metabolism.[41] This is observed in phenyl rings bearing a nitrogen substituent in the para position to the fluorine substituent. In fact, a rearrangement takes place during metabolic oxidation and fluorine moves to an adjacent carbon atom. The corresponding phenol metabolite in para position to the nitrogen substituent is observed.

2. Modify physicochemical properties (acidity/basicity and molecular lipophilicity) that affect the membrane permeability and therefore the drug bioavailability.

   The introduction of fluorine atoms changes the acidity or the basicity of neighboring ionizable functional groups and therefore the absorption properties of the drug are affected. For example, a

basic group can be required for interacting with a biological target, but at the same time, this basic function can also be responsible for the limited ability of the drug to pass throughout the cell membranes, leading to a low bioavailability. Van Niel *et al.* demonstrated that the introduction of fluorines in the serotonin 5-HT_{1D} agonist indole-derivatives reduces the pK_a of these compounds significantly.[42] The reduction of basicity was found to facilitate absorption, especially for oral drug administration. However, the decreased basicity lowered the affinity of these compounds for the receptor (**Table 1.6**).

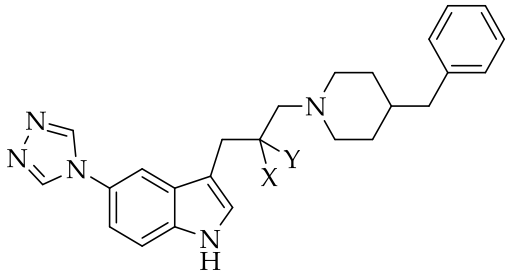

X	Y	log P	log D (pH=7.4)	pK_a	IC_{50}	EC_{50}
H	H	4.97	2.34	9.7	0.3 nM	0.6 nM *very low bioavailability*
F	H	4.63	3.25	8.7	0.9 nM	0.9 nM *moderate bioavailability*
F	F	4.89	4.80	6.7	78 nM	*Affinity decreased due to lowering of pKa*

Table 1.6 Influence of fluorine atoms on the pK_a, on the bioavailability and on the receptor binding for a set of 5-HT_{1D} agonists.[42] The nonfluorinated molecule is a very potent receptor ligand with a very low bioavailability. The

monofluorinated derivative has a lower pK_a and is able to bind the target, resulting in a compound of increased bioavailability. The difluorinated derivative, however, is no longer basic enough to achieve high binding affinity for the 5-HT_{1D} receptor.

Absorption and distribution are also controlled by the balance of lipophilicity and hydrophilicity in a drug. Lipophilicity is often required to reach a good binding affinity with the target.[43] However, a high lipophilicity results in a reduced solubility in polar, aqueous medium. A measure for the lipophilicity of a molecule is the logarithmic coefficient (logD) for distribution (D) of a compound between octanol and water at pH 7.4. Replacement of hydrogen by fluorine leads to a more lipophilic compound. The logD of 293 compounds has been evaluated in order to investigate the effect of the replacement of hydrogens by fluorines on the lipophobicity.[44] The histogram of changes in logD upon one H/F exchange is represented in **Figure 1.12**.

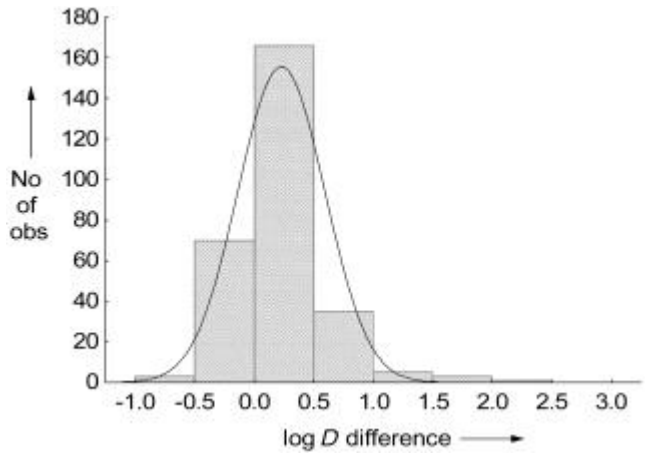

Figure 1.12 Histogram of changes in logD observed upon substitution of a hydrogen by a fluorine.[44]

The plot shows a Gaussian distribution in which the substitution of just one hydrogen by fluorine increases the lipophilicity of

about 0.25 log units. It is noteworthy that the tail of the Gaussian curve extends below zero. This means that there are few cases in which the replacement of a hydrogen with a fluorine decreases the lipophilicity. This was observed in molecules bearing an oxygen close to the fluorine atom. It was found that the lipophilicity decrease occurs when the O⋯F distance of at least one low-energy conformer in a molecule is smaller than 3.1 Å, and this might be explained by solvation effects.

3. Increase the binding affinity of a drug.

   Due to the difference in size and electronegativity between hydrogen and fluorine atoms, the replacement of hydrogens by fluorines may modify the molecular conformation and therefore the affinity for the biological target. For example, methoxy groups bound to a phenyl ring without orto substituents favor a planar conformation and lie on the plane of the ring.[45] In contrast, trifluoromethoxy groups bound to a phenyl ring without orto substituents tend to turn out of plane because of their larger size. For that reason, trifluoromethoxy substituent is not an isosteric replacement of methoxy group since it adopts a different conformation. Because of the polarized nature of C-F bond, C-F can interact with a biological target mainly through electrostatic interactions, such as dipole-dipole and charge-dipole interactions. However, these intermolecular electrostatic interactions are weak,[46] in contrast to intramolecular electrostatic interactions which are stronger. Electrostatic interactions are pronounced when substituents close to the C-F bond bear a formal charge. For example, the gauche conformers of the 2-fluoroethylammonium ion and the protonated 2-fluoroethanol are preferred because these keep the partially-negative fluorine

atoms close to the formally positively-charged nitrogen or oxygen (**Figure 1.13**).

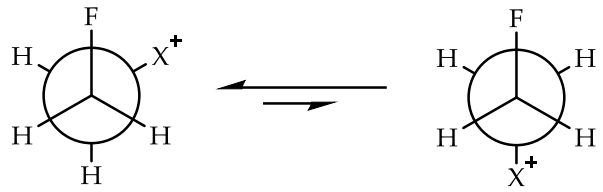

1 (X^+= -NH_3^+): -5.8 kcal/mol
2 (X^+= -OH_2^+): -7.2 kcal/mol

0.0 kcal/mol

Figure 1.13 Conformations of 2-fluoroethylammonium ion and protonated 2-fluoroethanol.[46]

It is more interesting to note how hyperconjugation can affect the preferred conformation of a fluorinated molecule. For example, there are two possible conformers for 1,2-difluoroethane, where the fluorine atoms are either gauche or anti. It was demonstrated by NMR and molecular modelling studies that the gauche conformer is more stable, showing a reduction in energy than the anti conformer. This result may be unexpected because of the steric repulsion of fluorine atoms in the gauche conformer (**Figure 1.14**).

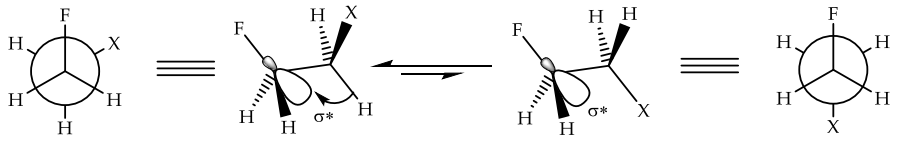

1 (X=F): -0.8 kcal/mol
2 (X=OH): -0.3 kcal/mol
3 (X=OAc): -0.95 kcal/mol
4 (X=NH_2): -1.0 kcal/mol
5 (X=NHAc): -1.8 kcal/mol

0.0 kcal/mol

Figure 1.14 Hyperconjugation effect.[46]

In the gauche conformer of compound **1** (**Figure 1.14**), both σ*CF orbitals are aligned with adjacent C-H bonds. Consequently, C-H

bonds can donate electron density into the σ*CF orbitals. This process is called hyperconjugation. The electron density donation into an antibonding orbital is equivalent to a partial break of the bond and for that reason the C-F bonds of compound **1** becomes longer and partially lose their covalent character. Nevertheless, the bonds are still strong because the fluorine atoms are now more negative and consequently are more strongly attracted to the partially-positive carbon atoms. As a result, hyperconjugation is a stabilizing effect that lowers the energy of the gauche conformer of compound **1**. In the anti conformer of compound **1**, each σ*CF orbital is aligned with an adjacent C-F bond, which is polarized and less electron donor than a C-H bond and then hyperconjugation is not observed. The gauche effect is also found in molecules containing F-C-C-O and F-C-C-N (compounds **2-5, Figure 1.14**). Typically, the more electronegative substituents are, the stronger the gauche effect is. Hyperconjugation can also be observed with lone pairs or π-systems as electron donors. In each case, the favored conformation shows the electron-donating group aligns with the σ*CF orbital (**Figure 1.15**).

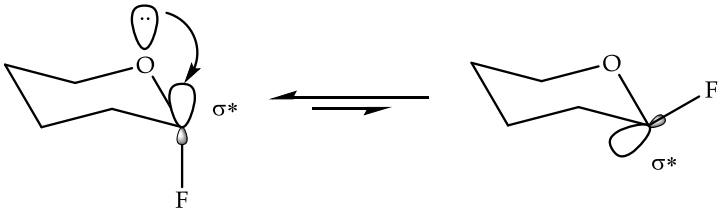

Figure 1.15 Conformations of 2-fluorotetrahydro-2H-pyran.[46]

An example of the F-C-C-O gauche effect and its influence on the biological active conformation is provided by fluorinated analogues of indinavir, an HIV protease inhibitor. X-ray crystallography showed that indinavir binds to HIV protease with the central carbon chain. Structure-activity relationship (SAR) study led to the synthesis of fluorinated analogues **1** and **2**, as shown in **Figure 1.16**. Compound **1** was found to be equipotent with indinavir, while compound **2** was 14-fold less potent. This different potency might be explained with the F-C-C-O gauche effect, which reinforces (compound **1**) or destabilizes (compound **2**) the bioactive conformation of the carbon chain.

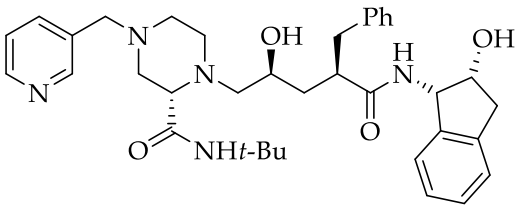

Indinavir

K_i=1.9 nM

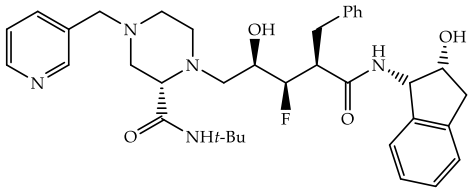

1

K_i=2.0 nM

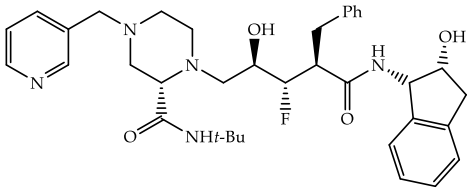

2

K_i=27 nM

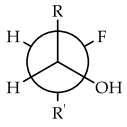

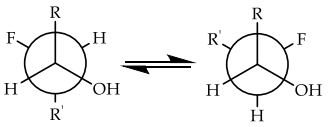

Figure 1.16 HIV protease inhibitor indinavir and its fluorinated analogues **1** and **2**.[46]

1.7.1 Bioisosterism

Bioisosterism is defined as the ability of atoms or functional groups with similar sizes or shapes to be interchanged without substantially altering biological behavior such as binding affinity.[45] Fluorine can sterically mimic a hydrogen and stereoelectronically mimic a hydroxyl group.[1] Fluorovinyl group (C=CHF) represents a nonhydrolyzable isostere of the peptidic bond, which can be used as peptidomimetic moiety for the design of protease inhibitors. The fluorine atom of fluorovinyl group takes the position of the oxygen of the carbonyl group of the peptide bond while the planarity of the vinyl group ensures a good match in size and geometry. Indeed, the double bond provides a good mimic of bond length and bond angles of the peptidic unit while its rigidity permits the control of the cis/trans conformation of the peptidic bond. Trifluoroethylamines are metabolically stable isosteres of amides. In fact, the trifluoromethyl group can mimic the carbonyl function of the amide, leading to a stable, nonbasic amine. Fluoro-C-glycosides, difluorodisaccharides, and fluorophosphonates can be applied as stable, nonhydrolyzable replacements for disaccharides, phosphates, sulfates. **Figure 1.17** resumes the fluorinated mimics of some functional groups.

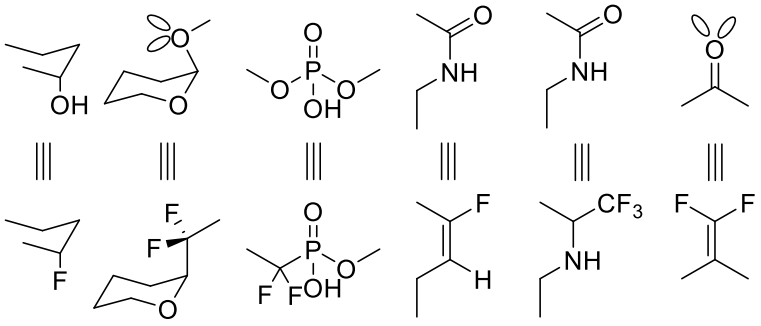

Figure 1.17 Fluorinated mimics of some functional groups.[1]

1.8 Biomedical Applications of Perfluorocarbons

The unique properties of PFCs allow the application of these molecules to biological and medical fields. In the following section the biocompatibility of perfluorocarbons as well as their biomedical applications will be discussed.

1.8.1 Biocompatibility of Perfluorocarbons

The biocompatibility of fluorocarbons is well-known. Perfluorinated saturated hydrocarbons with little amphiphilic character for *in vivo* applications seem to be harmless and physiologically inactive, although macrophage activation and flu-like symptoms might be observed.[47] Fluorocarbons injected intravenously are opsonized and phagocytosed by monocytes and macrophages of the reticuloendothelial system and stored temporarily in the liver, spleen and bone marrow.[48,49] They diffuse throughout the cell membrane to reach the bloodstream, are taken up by lipid carriers, brought to the lungs and eventually excreted unmodified with expired air.[47] It is remarkable that the strong C-F bonds are resistant to enzymatic metabolism. Typically, half-lives of PFCs range from days to week.[47] The introduction of a fluorinated chain to a molecule usually reduces both hemolytic activity and toxicity.[29,50] However, compounds in which short alkyl chains are bound to a branched fluorinated moiety show high inhalation toxicity due to their increased susceptibility to nucleophilic attack.[29] Some fluorous surfactants such as perfluorooctane sulfonate (PFOS) and perfluorooctanoic acid (PFOA) are resistant to degradation and toxic. Actually, they can lead to hepatotoxicity, immunotoxicity,

developmental toxicity, and can also have effects on thyroid hormones.[51] PFCs tend to bioaccumulate because of their lipophobic nature that makes biological recognition and elimination difficult. Bioaccumulation is an important issue since toxicological tissue and organ residual concentrations might be reached in animals as well as in humans.[52] Unlike organochlorines, PFCs accumulate mainly in blood, liver, kidney, and gallbladder and show high affinity for blood proteins, especially albumin.[53,54] In particular, perfluorinated surfactants are expected to bind blood and liver proteins due to their ionic character and enter the enterohepatic circulation.[55]

1.8.2 Fluorous Molecules as Artificial Blood Substitutes

The first biomedical application has been as artificial blood substitutes. Liquid fluorocarbons show low cohesive energy density and are able to dissolve gases with similar cohesive energy density such as O_2 and CO_2, as demonstrated by their Hildebrand parameters. As a result, PFCs can act as liquid carriers of oxygen with several applications, for example temporary blood substitutes as well as oxygenation liquids for tissues during organ transplantations or in ocular surgery.[1] Perfluorooctyl bromide (PFOB) has been studied to treat respiratory distress syndrome.[56,57] PFOB can be instilled neat into the patient's lungs in order to reduce the gas-liquid interface as well as the alveolar surface tension. PFOB can also improve lung oxygenation in patients with severe respiratory failure because of its ability to dissolve O_2.[58] PFOB has been investigated as a blood substitute used as fluorocarbon-in-water emulsion.[57,59] For example, Oxygent is a lecithin-stabilized emulsion of PFOB able to deliver O_2 to tissues. However, FDA did not approved Oxygent for human use since it showed an increase in

incidence of stroke among Oxygent-treated patients and for that reason phase 3 trials have been halted.[47]

1.8.3 Fluorous Molecules in Imaging

Ultrasound imaging technique is easier than other ones such as MRI and PET. However, it requires efficient contrast agents to highlight the difference between tissues.[1] The contrast agents used in ultrasound imaging are micron-size gas bubble products that are injected into the bloodstream. Gas bubbles can reflect sound waves more effectively than red blood cells, providing a bright contrast. The unique properties of PFCs (very low water solubility, high vapor pressure relative to molecular weight, and biological inertness) allow the application of these compounds as contrast agents. In fact, PFC vapor counterbalances the surface tension and blood pressure forces that push the gases inside the bubbles toward dissolution. Typically, the bubble wall is made up of phospholipids, proteins or biodegradable synthetic polymers. PFCs used as contrast agents are formulated as emulsions.

PFCs are also being investigated for magnetic resonance imaging (MRI) applications. ^{19}F atom has a nuclear spin of ½ and a high gyromagnetic ratio, which means that this isotope is very responsive to MRI measurements. Furthermore, it has a 100% natural abundance. Since there is no fluorine naturally occurring in biological tissue, any exogenous fluorine can be detected.[60] In combination with gadolinium contrast agent, fluorocarbons have been applied in cardiovascular MRI to detect angiogenesis in sclerotic aortic valves or quantify atherosclerotic lesions.[61,62]

Another non-invasive technique is represented by positron emission tomography (PET).[63] The isotope fluorine-18 has a half-life of 109 minutes and decays by positron emission. Therefore, molecules containing this isotope can be taken into account for PET. This technique provides functional or metabolic evaluation of normal tissue or disease conditions and its role in cancer radiotherapy planning is relevant. There are several fluorinated radiotracer, for example 2-^{18}F-fluoro-2,2-deoxy-D-glucose (^{18}FDG), fluorinated nucleosides, fluorinated aminoacids (^{18}F-fluoroethyl-L-tyrosine (FET), ^{18}F-fluorothymidine (FLT), ^{18}F-fluoro-α-methyltyrosine (FMT)), as well as fluorinated peptides. In particular, ^{18}FDG is largely used in oncology.[63] ^{18}FDG is a fluorinated analog of glucose which can be taken by cell in a similar way than glucose, phosphorylated by hexokinase to give ^{18}FDG-6-phosphate but cannot undergo glycolysis. Uptake of fluorine-18 provides a direct measure of the rate of glucose metabolism in the part of the body under study. ^{18}FDG is the most applied radiolabel in PET because of:

- increased glucose metabolism in tumors;
- low positron energy with high abundance (96%) and a path length in tissue of approximately 0.1-0.2 cm;
- long half-time of the isotope (109 minutes), allowing complex imaging studies such as dynamic studies and investigations of slow metabolic processes;
- good efficacy;
- safety, due to the low emitting energy that represents a minimal risk for the patient.

1.8.4 Fluorocarbons in Drug and Gene Delivery

Due to their physicochemical properties, PFCs have been investigated for pulmonary drug delivery.[64] In fact, they can distribute homogeneously throughout the lungs because of their low viscosity and low surface tension. However, drugs are poor-soluble in PFCs. In order to overcome this issue, different approaches have been investigated. Among them, fluorocarbon-based nanoemulsions have been prepared.[15] In this system, the hydrophobic drug is dissolved in the lipid surfactants and the colloid is stabilized by the fluorocarbon.

Fluorocarbon-based emulsions were studied to inject volatile anesthetics into the bloodstream. The advantage is that the onset of the anesthesia is more rapid because the intravenous delivery of volatile anesthetics eliminates the time the volatile anesthetic needs to equilibrate with the lungs.[65]

A new class of hemifluorinated dibranched amphiphiles characterized by a fluorophilic (fluorous chain), lipophilic (alkyl chain), and hydrophilic (polar head) moieties has been synthetized.[66] The fluorinated surfactants were able to stabilize nanoemulsions containing 20% of the volatile anesthetic sevofluorane and 10% of the FDA-approved PFOB to slow ripening. In one case, the surfactant was able to dramatically slow the ripening and stabilize the nanoemulsion for over 1 year. This suggests their potential for clinical use.

Due to the ability of amphiphilic fluorinated polymers to self-assemble into stable micelles, these molecules have been taken into account to encapsulate and deliver hydrophobic anticancer agents. For example, fluorinated amphiphilic copolymers bearing a hydrophilic block, represented by a PEG-polyaspartamide unit, and a fluorocarbon-containing side-chain were synthesized and used to prepare flutamide-

loaded micelles.[67] It was demonstrated that micelles were able to successfully deliver the anticancer agent flutamide to cells *in vitro*. In this colloidal system, the fluorocarbon moiety is not involved in the encapsulation of the hydrophobic drug but rather stabilizes the aggregate by the fluorophobic effect.

Hyperthermia has been recently investigated as an adjuvant treatment to traditional therapies with anticancer drugs based on thermoresponsive molecules.[68] It has been demonstrated that the local application of heat can sensitize tumors to chemotherapy, radiotherapy and immunotherapy. Several mechanisms of antitumor activity are induced by local hyperthermia, such as loss of membrane integrity, upregulation of heat shock proteins, activation of immune cells and necrotic cell death. Since highly-fluorinated compounds show excellent thermomorphic properties, undergo temperature-dependent miscibility with aqueous environments and are biocompatible, they have been taken into account to combine conventional chemotherapy with local hyperthermia.[68] For example, the alkylating agent chlorambucil was bound to perfluoroalkyl chains using an ester linkage as a cleavable site. These compounds were tested in various cancer cell lines both under normal conditions (37 °C) and under mild hyperthermia (42 °C). It was demonstrated that these molecules were more cytotoxic when local hyperthermia was applied. Moreover, these results were also confirmed in mice. Analogues bearing the hydrocarbon chain instead of the fluorous chain did not show thermoresponsive behavior. The mechanism of cell death induced by these molecules was the same as chlorambucil since it involved DNA damage. The mechanism of thermal activation might involve both the increased solubility at the tumor site under hyperthermia and the hydrolysis of the ester linker, leading to the release of the fluorinated chain. Anticancer agents in

which the fluorous chain was covalently linked to the drug by non-cleavable moieties did not exhibit such extensive thermoresponsive activity.

Perfluorinated molecules have also been investigated for gene delivery.[69,70] Due to their hydrophobic and lipophobic character, perfluorinated compounds are able to improve the affinity of cationic polymers to cell membrane and across its lipidic bilayer. Moreover, the low surface energy allows perfluorocarbon molecules to strongly interact each other at low concentrations. This permits the formation of polyplexes with nucleic acid at low nitrogen to phosphorous ratio (N/P ratio), needed to minimize the toxicity on the transfected cells.[71] Fluorinated dendrimers characterized by excellent transfection efficacy and low cytotoxicity were synthetized. It was demonstrated that the fluorinated moiety plays a relevant role since fluorination on dendrimers enhances cellular uptake, endosomal escape, serum resistance of dendrimer/DNA polyplexes as well as modulates the DNA packing/unpacking ability of dendrimers.[71]

1.9 References

1. Bégué, J. P. & Bonnet-Delpon, D. *Bioorganic and Medicinal Chemistry of Fluorine*. (Wiley, 2008).
2. Kirsch, P. *Modern Fluoroorganic Chemistry. Synthesis, Reactivity, Applications.* (Wiley-VCH, 2004).
3. Hansen, N. M. L., Jankova, K. & Hvilsted, S. Fluoropolymer Materials and Architectures Prepared by Controlled Radical Polymerizations. *Eur. Polym. J.* **43,** 255–293 (2007).
4. Plunkett, R. http://www.2.dupont.com/Phoenix Heritage/en US/1938 detail.html.
5. Ebnesajjad, S. *Introduction to Fluoropolymers. Materials, Technology, and Applications.* (In William Andrews: Kidlington, Oxford; Waltham, Mass., 2013).
6. Chan, K. K. . & O'Hagan, D. *The Rare Fluorinated Natural Products and Biotechnological Prospects for Fluorine Enzymology*. (Natural Product Biosynthesis by Microorganisms and Plants, 2012).
7. Heidelberger, C., Chaudhuri, N. K., Danneberg, P., Mooren, D. & Griesbach, L. Fluorinated Pyrimidines, a New Class of Tumor-Inhibitory Compounds. *Nature* **179,** 663–666 (1957).
8. Wang, J. *et al.* Fluorine in Pharmaceutical Industry: Fluorine-Containing Drugs Introduced to the Market in the Last Decade (2001−2011). *Chem. Rev.* **114,** 2432–2506 (2014).
9. *Lipitor Becomes World's Top-Selling Drug*. (Grain's New York Business via Associated Press, 2011).
10. Louis Goodman and Alfred Gilman. *The Pharmacological Basis of Therapeutics*. (McGraw-Hill, 2011).
11. Minkovsky, N. & Berezov, A. BIBW-2992, a Dual Receptor Tyrosine Kinase Inhibitor for the Treatment of Solid Tumors.

Curr. Opin. Investig. Drugs **9,** 1336–46 (2008).

12. Cao, G. *et al.* Evacetrapib Is a Novel, Potent, and Selective Inhibitor of Cholesteryl Ester Transfer Protein that Elevates HDL Cholesterol without Inducing Aldosterone or Increasing Blood Pressure. *J. Lipid Res.* **52,** 2169–2176 (2011).
13. Nicholls, S. J. *et al.* Effects of the CETP Inhibitor Evacetrapib Administered as Monotherapy or in Combination with Statins on HDL and LDL Cholesterol. A Randomized Controlled Trial. *JAMA* **306,** 2099–2109 (2011).
14. Thompson, P. L., Nidorf, S. M. & Eikelboom, J. Targeting the Unstable Plaque in Acute Coronary Syndromes. *Clin. Ther.* **35,** 1099–1107 (2013).
15. Krafft, M. P. Fluorocarbons and Fluorinated Amphiphiles in Drug Delivery and Biomedical Research. *Adv. Drug Deliv. Rev.* **47,** 209–228 (2001).
16. Smart, B. E. Fluorine Substituent Effects (on Bioactivity). *J. Fluor. Chem.* **109,** 3–11 (2001).
17. O'Hagan, D. & Rzepa, H. S. Some Influences of Fluorine in Bioorganic Chemistry. *Chem. Commun.* 645–652 (1997).
18. Krafft, M. P. & Riess, J. G. Perfluorocarbons: Life Sciences and Biomedical Uses-Dedicated to the Memory of Professor Guy Ourisson, a True RENAISSANCE Man. *J. Polym. Sci. Part A Polym. Chem.* **45,** 1185–1198 (2007).
19. Sadtler, V. M., Giulieri, F., Krafft, M. P. & Riess, J. G. Micellization and Adsorption of Fluorinated Amphiphiles: Questioning the 1CF2≈1.5 CH2 Rule. *Chem. Eur. J.* **4,** 1952–1956 (1998).
20. Percec, V. *et al.* Self-Assembly of Semifluorinated Janus-Dendritic Benzamides into Bilayered Pyramidal Columns. *Angew. Chem. Int. Ed.* **44,** 4739–4745 (2005).

21. Stahler, K., Selb, J. & Candau, F. Multicompartment Polymeric Micelles Based on Hydrocarbon and Fluorocarbon Polymerizable Surfactants. *Langmuir* **15,** 7565–7576 (1999).
22. Chambers, R. *Fluorine in Organic Chemistry*. (Blackwell Publishing Ltd., 2004).
23. Razgulin, A. V & Mecozzi, S. Binding Properties of Aromatic Carbon-Bound Fluorine. *J. Med. Chem.* **49,** 7902–7906 (2006).
24. da Costa, R. F., Freire, V. N., Bezerra, E. M. & Cavada, B. S. Explaining Statin Inhibition Effectiveness of HMG-CoA Reductase by Quantum Biochemistry Computations. *Phys. Chem. Chem. Phys.* **14,** 1389–1398 (2012).
25. Horvath, I. T. & Rabai, J. Facile Catalyst Separation without Water-Fluorous Biphase Hydroformylation of Olefins. *Science (80-.).* **266,** 72–75 (1994).
26. Gladysz, J. A., Curran, D. P. & Horvath, I. T. in *Handbook of Fluorous Chemistry* 1–4 (Wiley-VCH: Weinheim, 2004).
27. Patai, S. & Rappoport, Z. *The Chemistry of Halides, Pseudo-Halides, and Azides*. (Rev.ed; Wiley: Chichester, Eng.; New York, 1995).
28. Krafft, M. P. in *Handbook of Fluorous Chemistry* 478–490 (Wiley-VCH: Weinheim, 2004).
29. Krafft, M. P. & Riess, J. G. Chemistry, Physical Chemistry, and Uses of Molecular Fluorocarbon-Hydrocarbon Diblocks, Triblocks, and Related Compounds-Unique 'Apolar' Components for Self-Assembled Colloid and Interface Engineering. *Chem. Rev.* **109,** 1714–1792 (2009).
30. Monde, K., Miura, N., Hashimoto, M., Taniguchi, T. & Inabe, T. Conformational Analysis of Chiral Helical Perfluoroalkyl Chains by VCD. *J. Am. Chem. Soc.* **128,** 6000–6001 (2006).
31. Riess, J. G. Oxygen Carriers (' Blood Substitutes ') - Raison d'Etre,

Chemistry, and Some Physiology. *Chem. Rev.* **101,** 2797–2919 (2001).

32. Krafft, M. P. & Riess, J. G. Highly Fluorinated Amphiphiles and Colloidal Systems, and Their Applications in the Biomedical Field. A Contribution. *Biochimie* **80,** 489–514 (1998).
33. Kiss, L. E., Kovesdi, I. & Rabai, J. An Improved Design of Fuorophilic Molecules: Prediction of the ln P Fluorous Partition Coefficient, Fluorophilicity, Using 3D QSAR Descriptors and Neural Networks. *J. Fluor. Chem.* **108,** 95–109 (2001).
34. Barton, A. F. M. *Handbook of Solubility Parameters and Other Cohesion Parameters*. (CRC Press, 1983).
35. Gladysz, J. A. & Emnet, C. in *Handbook of Fluorous Chemistry* 11–23 (Eds. Wiley-VCH: Weinheim, 2004).
36. de Wolf, E., Ruelle, P., Deelman, B. & Koten, G. Van. Prediction of Partition Coefficients of Fluorous and Nonfluorous Solutes in Fluorous Biphasic Solvent Systems by Mobile Order and Disorder Theory. *J. Phys. Chem. B* **108,** 1458–1466 (2004).
37. van Heek, M. *et al.* In Vivo Metabolism-Based Discovery of a Potent Cholesterol Absorption Inhibitor, SCH58235, in the Rat and Rhesus Monkey through the Identification of the Active Metabolites of SCH48461. *J. Pharmacol. Exp. Ther.* **283,** 157–163 (1997).
38. Clader, J. W. The Discovery of Ezetimibe: A View from Outside the Receptor. *J. Med. Chem.* **47,** 1–9 (2004).
39. Smith, D. H., van de Waterbeemd, H. & Walker, D. K. in Vol. 13 (Wiley-VCH: Weinheim, 2001).
40. Penning, T.D., et al. Synthesis and Biological Evaluation of the 1,5-Diarylpyrazole Class of Cyclooxygenase-2 Inhibitors: Identification of 4-[5-(4-methylphenyl)-3-(trifluoromethyl)-1H-

pyrazol-1-yl]benzenesulfonamide (SC-58635, Celecoxib). *J. Med. Chem.* **40,** 1347–1365 (1997).

41. Park, B. K., Kitteringham, N. R. & O'Neill, P. M. Metabolism of Fluorine-Containing Drugs. *Annu. Rev. Pharmacol. Toxicol.* **41,** 443–470 (2001).
42. van Niel, M. B. & et al. Fluorination of 3-(3-(piperidin-1-yl)propyl)indoles and 3-(3-(piperazin-1-yl)propyl)indoles Gives Selective Human 5-HT1D Receptor Ligands with Improved Pharmacokinetic Profiles. *J. Med. Chem.* **42,** 2087–2104 (1999).
43. *Protein-Ligand Interactions*. (Wiley-VCH: Weinheim, 2003).
44. Bohm, H. *et al.* Fluorine in Medicinal Chemistry. *ChemBioChem* **5,** 637–643 (2004).
45. Muller, K., Faeh, C. & Diederich, F. Fluorine in Pharmaceuticals: Looking Beyond Intuition. *Science (80-.).* **317,** 1881–1886 (2007).
46. Hunter, L. The C–F Bond as a Conformational Tool in Organic and Biological Chemistry. *Beilstein J. Org. Chem.* **14,** 6, No. 38 (2010).
47. Riess, J. G. Perfluorocarbon-Based Oxygen Delivery. *Artif. Cells Blood Substitutes Biotechnol.* **34,** 567–580 (2006).
48. Miller, M. L., Wesseler, E. P., Jones, S. C. & Clark, L. C. J. Some Morphologic Effects of Inert Particulate Loading on Hemopoietic Elements in Mice. *RES J. Reticuloendothel. Soc.* **20,** 385–398 (1976).
49. Ni, Y., Klein, D. H. & Song, D. Recent Developments in Pharmacokinetic Modeling of Perfluorocarbon Emulsions. *Artif. Cells Blood Substitutes Immobil. Biotechnol.* **24,** 81–90 (1996).
50. Filler, R., Kobayashi, Y. & Yagupolskii, L. M. *Organofluorine Compounds in Medicinal Chemistry and Biomedical Applications*. (Elsevier: Amsterdam, 1993).
51. Olsen, G. W. *et al.* Half-Life of Serum Elimination of

Perfluorooctanesulfonate, Perfluorohexanesulfonate, and Perfluorooctanoate in Retired Flurochemical Production Workers. *Environ. Health Perspect.* **115,** 1298–1305 (2007).

52. Kelly, B. C., Gobas, F. A. C. & McLachlan, M. S. Intestinal Absorption and Biomagnification of Organic Contaminants in Fish, Wildlife and Humans. *Environ. Toxicol. Chem.* **23,** 2324–2336 (2004).
53. Renner, R. Growing Concern over Perfluorinated Chemicals. *Environ. Sci. Technol.* **35,** 154A–160A (2001).
54. Jones, P. D., Hu, W., De Coen, W. M., Newsted, J. L. & Giesy, J. P. Binding of Perfluorinated Fatty Acids to Serum Proteins. *Environ. Toxicol. Chem.* **22,** 2639–2649 (2003).
55. Giesy, J. P. & Kannan, K. Perfluorochemical Surfactants in the Environment. *Environ. Sci. Technol.* **36,** 147A–152A (2002).
56. Riess, J. G. in *Handbook of Fluorous Chemistry* 521–573 (Wiley-VCH: Weinheim, 2004).
57. Riess, J. G. Highly Fluorinated Systems for Oxygen-Transport, Diagnosis and Drug-Delivery. *Colloids Surfaces-Physicochemical Engeenering Asp.* **84,** 33–48 (1994).
58. Wolfson, M. R., Greenspan, J. S. & Shaffer, T. H. Pulmonary Administration of Vasoactive Substances by Perfluorochemical Ventilation. *Pediatrics* **97,** 449–455 (1996).
59. Riess, J. G. Highly Fluorinated Amphiphilic Molecules and Self-Assemblies with Biomedical Potential. *Curr. Opin. Colloid Interface Sci.* **14,** 294–304 (2009).
60. Tirotta, I. *et al.* 19F Magnetic Resonance Imaging (MRI): from Design of Materials to Clinical Applications. *Chem. Rev.* **115,** 1106–1129 (2015).
61. Caruthers, S. D. *et al.* In Vitro Demonstration Using 19F Magnetic

Resonance to Augment Molecular Imaging with Paramagnetic Perfluorocarbon Nanoparticles at 1.5 Tesla. *Invest. Radiol.* **41,** 305–312 (2006).

62. Waters, E. A. *et al.* Detection and Quantification of Angiogenesis in Experimental Valve Disease with Integrin-Targeted Nanoparticles and 19-Fluorine MRI/MRS. *J. Cardiovasc. Magn. Reson.* **10,** (2008).
63. Menaa, F., Menaa, B. & Sharts, O. N. Importance of Fluorine and Fluorocarbons in Medicinal Chemistry and Oncology. *J. Mol. Pharm. Org. Process Res.* **1,** 1–6 (2013).
64. Lehmler, H. *Perfluorocarbon Compounds as Vehicles for Pulmonary Drug Delivery*. *Expert Opinion on Drug Delivery* **4:3,** (2007).
65. Fast, J. P., Perkins, M. G., Pearce, R. A. & Mecozzi, S. Fluoropolymer-Based Emulsions for the Intravenous Delivery of Sevoflurane. *Anesthesiology* **109,** 651–656 (2008).
66. Parlato, M. C., Jee, J. P., Teshite, M. & Mecozzi, S. Synthesis, Characterization, and Applications of Hemifluorinated Dibranched Amphiphiles. *J. Org. Chem.* **76,** 6584–6591 (2011).
67. Piccionello, A. P. *et al.* Fluorinated and Pegylated Polyaspartamide Derivatives to Increase Solubility and Efficacy of Flutamide. *J. Drug Target* **20,** 433–44 (2012).
68. Clavel, C. M., Nowak-Sliwinska, P., Paunescu, E. & Dyson, P. J. Thermoresponsive Fluorinated Small-Molecule Drugs: a New Concept for Efficient Localized Chemotherapy. *Med. Chem. Commun.* **6,** 2054–2062 (2015).
69. Zhou, Q. *et al.* Ultrasound-Mediated Local Drug and Gene Delivery Using Nanocarriers. *Biomed Res. Int.* **2014,** (2014).
70. Yan, G. *et al.* Tunable Dynamic Fluorinated Poly(orthoester)-Based Drug Carriers for Greatly Enhanced Chemotherapeutic

Efficacy. *Polym. Chem.* **8,** 2063–2073 (2017).

71. Wang, M., Liu, H., Li, L. & Cheng, Y. A Fluorinated Dendrimer Achieves Excellent Gene Transfection Efficacy at Extremely Low Nitrogen to Phosphorus Ratios. *Nat. Commun.* **5,** 1–8 (2014).

Chapter 2

Noncovalent Fluorous Interactions: New Approaches for Drug Discovery

2.1 Proteomics Approaches in Drug Discovery

Chemical proteomics is an emerging research field that integrates biochemistry, cell biology, organic synthesis, mass spectrometry and bioinformatics analysis.[1,2] It is involved in both investigation and characterization of drug-target interactions in samples from cell lines or tissues.[1] Despite several experimental procedures are employed by chemical proteomics, two techniques are more common:[3]

- activity-based probe profiling (ABPP), which focuses on the enzymatic activity of specific classes of proteins
- compound-centric chemical proteomics (CCCP), which investigates drug-target interactions and therefore the molecular mechanism of action of bioactive small molecules.

Figure 2.1 compares these two approaches.

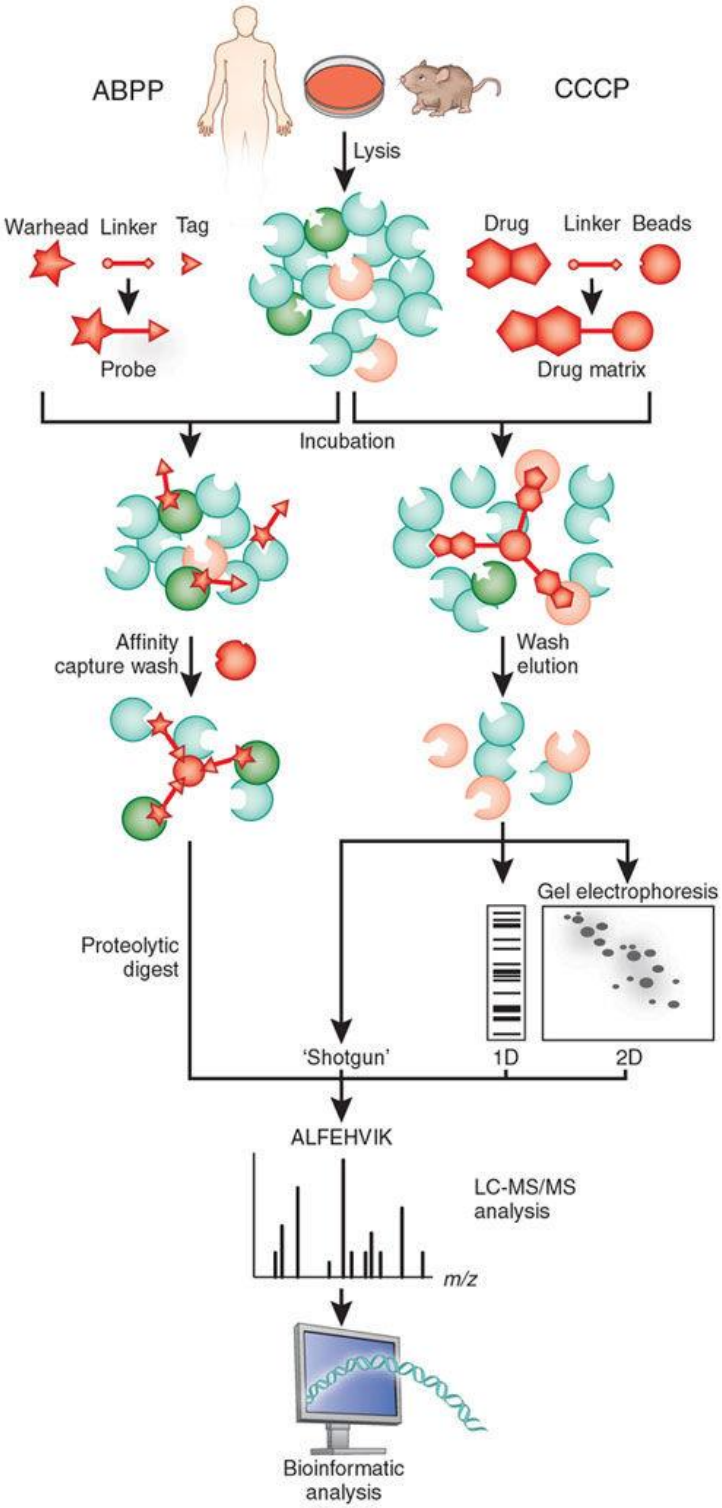

Figure 2.1 Comparison of activity-based probe profiling (ABPP) and compound-centric chemical proteomics (CCCP).[2]

ABPP approach involves small-molecular probes composed by three different moieties:

- a reactive group
- a tag
- a linker

The reactive group should be able to covalently bind the active catalytic site of the target protein as well as be inert towards other species present in the biological sample. Two general classes of reactive groups can be distinguished:

- electrophilic groups that bind nucleophilic active site of the target protein
- photoreactive groups that label residue of the target protein following UV irradiation.

ABPP probes also show a tag involved in target characterization. Indeed, the tag must strongly bind the resin during affinity purification step, allowing a quick isolation of the target protein. Biotin is widely used as tag, since it can strongly interact with immobilized streptavidin. Noteworthy, if the active probe must be modified to allow the immobilization on the stationary phase, the modified compound should be tested with an appropriate biological assay to demonstrate the activity is retained.

The reactive group and the tag are connected by a linker which acts as a spacer. This avoids steric hindrance that would prevent the interaction between the reactive group and the target protein as well as the bound of the tag to the resin. Hydrophilic spacers – such as diethylene glycol – are widely used as linker, while hydrophobic alkyl chains might promote non-specific binding of proteins and therefore increase the complexity of the collected sample. Actually, the elution of proteins that unspecifically interact with the stationary phase during affinity purification complicates the sample analysis.

Therefore, cleavable linkers were designed, allowing the release of only proteins bound to the probe, while proteins that non-specifically bound to the resin remain anchored to the stationary phase. Cleavable linkers commonly used for drug discovery show acylhydrazone unit (that can be cleaved by hydrazides),[4] peptide spacer (cleavable by proteolysis approach),[5] acid-labile groups,[6] and the photolabile 1-(2-nitrophenyl)ethyl moiety.[7,8] In ABPP technique, the cell lysate is incubated with the probe and the captured proteins are purified by affinity chromatography and then digested with trypsin. The peptides are identified by LC-MS/MS and bioinformatics analysis.[1,3]

In contrast to ABPP, CCCP approach is more focused on target discovery. In this technique, a bioactive compound is immobilized on an inert and biocompatible matrix without loss of biological activity. The cell lysate is incubated with the affinity matrix and the proteins of interest are selectively eluted. These proteins can be either purified by SDS-PAGE before digestion or processed in a gel-free method (shotgun proteomics). After proteins digestion with trypsin, peptides are analyzed by LC-MS/MS and bioinformatics analysis.[2,3]

Chemical proteomics approaches have several advantages.[2,3] First, chemical proteomics is useful to study previously uncharacterized proteins by means of drug-target interactions. Moreover, this approach can be applied to the whole proteome or sub-proteomes as well as to recombinant proteins. This permits the investigation of proteins in their natural state and environment, including endogenous abundance levels, post-translational modifications, point or deletion mutants, presence of natural binding molecules such as proteins and nucleic acids. Furthermore, chemical proteomics can be performed in any cell type, tissue or species (humans, animals, plants and microorganisms), allowing the exploration of drug mechanisms in physiological and clinical samples (such as tumor tissue) or toxicity profiles

in healthy samples.[2] Despite these advantages, chemical proteomics also suffers from several disadvantages. First, in order to link bioactive molecules on the stationary phase, a functional group (usually amines, carboxyl acids or hydroxyls) is required. If the active small molecule does not show the tag, it must be introduced without losing the bioactivity. Moreover, this technique should be performed under non-denaturing conditions to avoid proteins unfolding. This could be an issue for membrane proteins – especially those with several transmembrane domains – which require more drastic conditions in order to be extracted from intact biological membranes. Furthermore, proteins which are naturally abundant in the lysate, such as hemoglobin and albumin, show affinity for small molecules. Consequently, these proteins are anchored to the resin and eluted even if they are not the biological target. Moreover, abundant proteins are "sticky" and tend to unspecifically interact with the stationary phase. To identify the so-called background binding, a negative control is required. Controls are usually represented by inactive analogs of the active small molecules. Target proteins can be identified by comparing the proteins captured with the active molecule with those isolated by the negative control. Besides, the most common biochemical affinity-pair biotin-streptavidin is expensive and it is difficult to fully recover the bound target protein by elution.[9] Finally, the biotinylated tag undergoes fragmentation during MS/MS analysis, complicating the tandem mass spectrometry spectral interpretation.[10]

2.2 Fluorous Interactions as New Tag for Chemical Proteomics

In order to overcome the issues related to traditional chemical proteomics techniques, fluorous interactions were investigated as tool for proteomics approaches.[11] It has been demonstrated that organic compounds bearing a perfluoroalkyl chain can be easily separated from a non-fluorinated mixture by solid-phase extraction (F-SPE).[12] The purification of fluorinated organic compounds by means of F-SPE is more similar to a filtration rather than a chromatography and the separation is based on the presence/absence of the fluorinated tag instead of polarity or other molecular characteristics involved in traditional chromatography.

F-SPE can be standard or reverse.[13] Standard F-SPE is the most common and involves a fluorous solid phase – typically silica gel functionalized with fluorocarbon chains – and a fluorophilic, non-fluorous solvent as eluent. **Figure 2.2** illustrates the purification of fluorinated-tagged molecules by standard F-SPE.

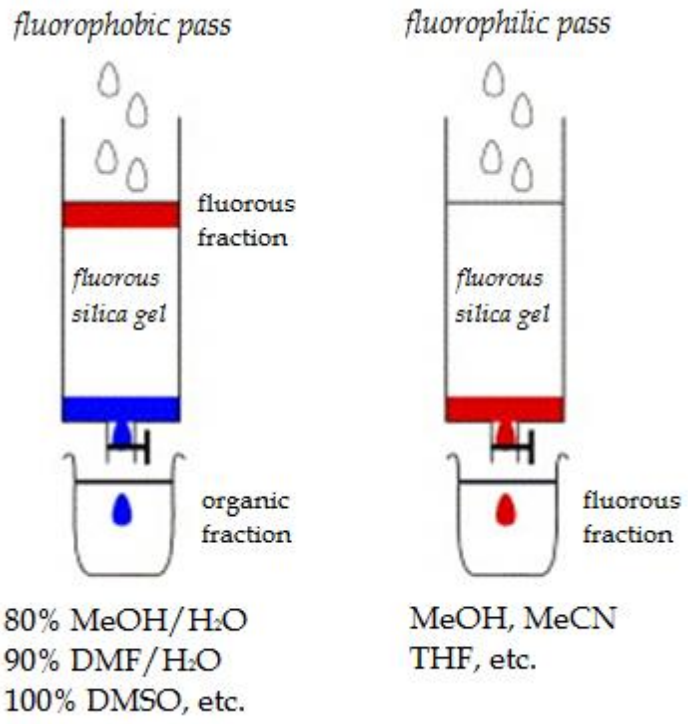

Figure 2.2 Purification of fluorinated molecules by standard F-SPE. The organic fraction is blue and the fluorous fraction is red.[13]

The crude mixture is loaded into the fluorous silica gel and then non-fluorinated components are eluted with a fluorophobic solvent such as 70-80% MeOH-H_2O or 80-90% DMF-H_2O. 100% DMSO might be used if a component of the crude product is water-sensitive. During this step, fluorinated molecules remain anchored to the resin because of the strong, non-covalent fluorine-fluorine interactions between the fluorinated organic compounds and the fluorous stationary phase. Then, a fluorophilic solvent like water-free MeOH, CH_3CN, THF is used to elute the fluorinated organic molecules. It is noteworthy that the fluorous silica gel can be washed with fluorophilic solvents (MeOH, THF or acetone) and reused, reducing both waste disposal and cost.

Reverse F-SPE is a more recent technique in which the philicities of solid phase and eluent are reversed.[13] **Figure 2.3** illustrates the purification of fluorinated-tagged molecules by reverse F-SPE.

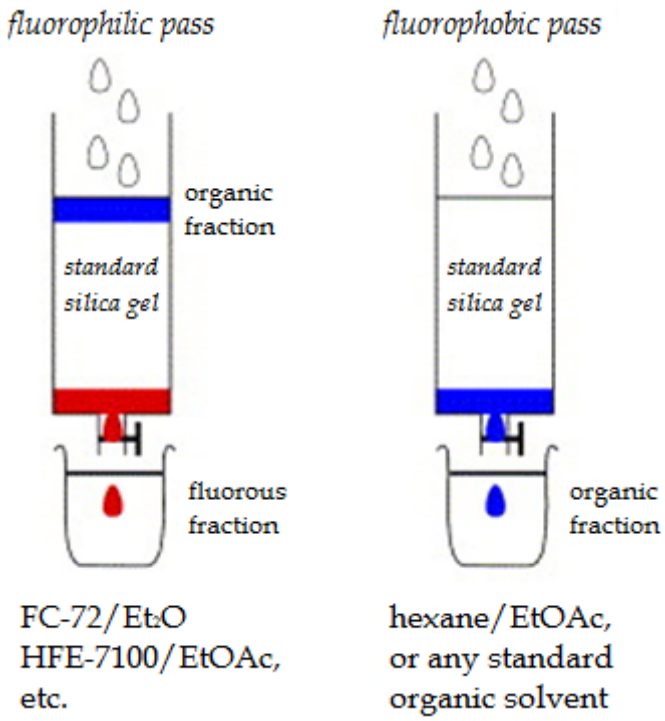

Figure 2.3 Purification of fluorinated molecules by reverse F-SPE. The organic fraction is blue and the fluorous fraction is red.[13]

A mixture containing non-fluorous and fluorous organic compounds is charged onto regular silica gel. A fluorophilic solvent is used to elute the fluorinated component. Common fluorophilic solvents applied in this step are mixtures of FC-12 (perfluorohexanes) and diethyl ether as well as HFE-7100 (perfluorobutyl methyl ether) blended with ethyl acetate, ether or another organic cosolvent. Then, a fluorophobic elution is achieved with regular solvents in order to recover the non-fluorinated fractions.

Brittain *et al.* combined standard F-SPE with proteomics introducing the concept of "fluorous proteomics".[11] They selectively labeled a specific peptide class with a perfluorinated alkyl chain. The tagged peptides were isolated by F-SPE and analyzed by MALDI-MS or ESI-MS, as shown in **Figure 2.4**.

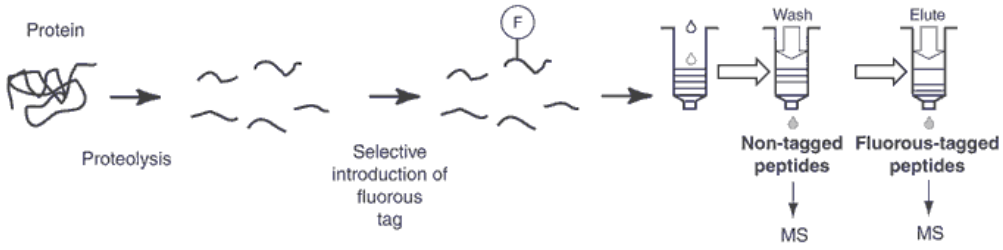

Figure 2.4 Fluorous proteomics approach used to isolate specific classes of peptides.[11]

This methodology overcomes many of the limitations of classic bioaffinity-based enrichment techniques. Indeed, fluorous proteomics allows separation strategies that cannot be accomplished with traditional bioaffinity pairs. Brittain *et al.* demonstrated that doubly-tagged (branched) peptides can be separated from singly-tagged (linear) peptides by using a fluorous proteomics approach while this separation cannot be achieved varying the number of biotin unit used as a tag. Therefore, this methodology allows not only the isolation of fluorinated-tagged entities from non-fluorinated molecules, but also the separation of fluorinated species based on the features of the fluorinated tag. Furthermore, fluorous proteomics avoids inefficient recovery of tagged peptides and tag fragmentation during MS/MS analysis that occur in conventional chemical proteomics. It was demonstrated that fluorinated affinity labels are completely compatible with commercially-available software for protein identification such as MASCOT, providing an unequivocally identification of tagged proteins. Moreover, the fluorous proteomics approach is easier than the classic proteomics technique and is less expensive since the fluorous stationary phase can be recycled. It is noteworthy that solvents involved in the elution steps (water and methanol) do not interfere with MS/MS allowing the direct MS analysis of isolated peptides. Finally, unlike traditional bioaffinity reagents, fluorous proteomics might be directly applied to the isolation of different functional classes of small molecules in metabolomics studies.

2.3 Background and Project Aim

Professor Romeo group synthesized molecules with antimalarial activity by applying the so-called "double drug" approach.[14] It is based on the design of molecules showing two moieties that are able to interact with different targets. The synthesized compounds were characterized by primaquine, atovaquone, 4-aminoquinolinic core as well as statin group (β-hydroxyl-γ-aminoacid) as potent and non-selective plasmepsin inhibitor (**Figure 2.5**). Actually, the statin would mimic the tetrahedral intermediate observed during the hydrolysis of the peptide bond by plasmepsin.

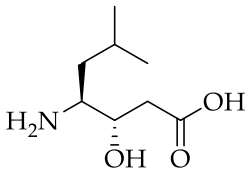

Figure 2.5 Chemical structure of statin (β-hydroxyl-γ-aminoacid; IUPAC nomenclature: (3S,4S)-4-amino-3-hydroxy-6-methylheptanoic acid).

RV97 is characterized by the primaquine core bound to a dipeptidyl unit. This moiety is linked to the statin – represented by Ile-Leu dipeptide functionalized with butyl amide – by 4,4'-oxybisbenzoic acid, an aromatic linker optimized previously,[15] as shown in **Figure 2.6**.

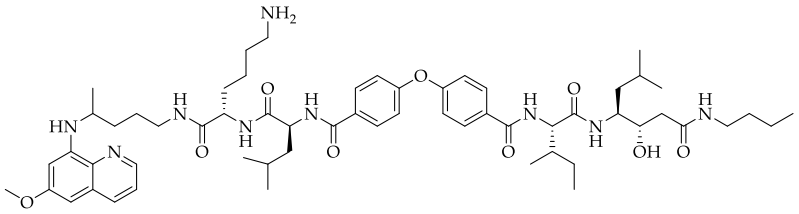

Figure 2.6 Chemical structure of **RV97** (D10: IC_{50} = 400 nM; W2: IC_{50} = 700 nM).

Primaquine shows a different mechanism of action if compared to statin, since it is a liver schizonticide. Therefore, primaquine and statin recognize their different targets. It has recently been demonstrated that primaquine side effects might be reduced by binding the drug to a peptidyl unit.[16] The quinolinic core promotes the membrane crossing, acting as a double-drug carrier. It has been demonstrated that **RV97** blocks *P. falciparum* growth during the intraherythrocytic stage on both chloroquine-sensitive (D10) and chloroquine-resistant (W2) strains. **RV97** showed an *in vivo* antiplasmodial activity comparable to that of chloroquine (ED_{50} = 6.11 mg/Kg) as well as a good inhibition of plasmepsin I, II, IV (Plm I: 110 nM; Plm II: 0.4 nM; Plm IV: 0.5 nM). In order to reduce the molecular weight as well as the peptidic character of **RV97**, the number of aminoacids present in the molecule was reduced. Therefore, antimalarial agents with a simpler structure characterized by 4,4'-oxybisbenzoic acid core were synthesized. **Table 1.2** lists some synthesized antimalarial molecules with a simplified chemical structure.

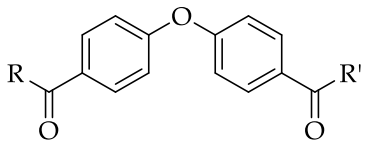

Entry	R	R′	D10 IC_{50} (nM)[a]	W2 IC_{50} (nM)[a]
AN12	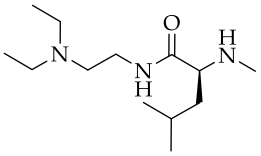	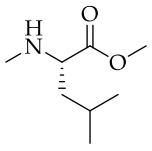	12.97	8.46
AN15	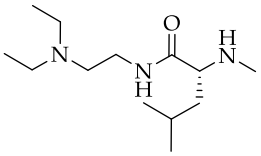	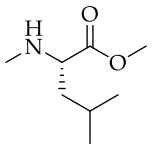	3000	1100
AO07	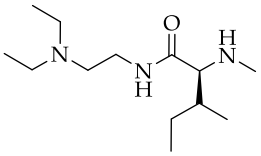	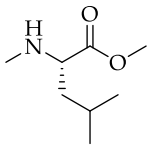	5.83	2.76
AO26	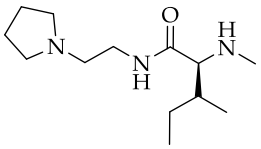	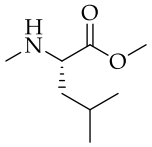	0.49	0.34
DC18	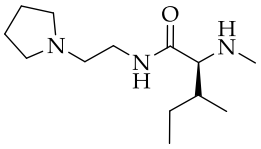	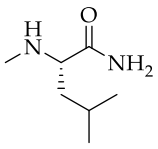	2.45	3.13
DHA			5.63	2.29
CQ			23	410

Table 2.1 Chemical structures of 4,4′-oxybisbenzoic acid derivatives and their antimalarial activities against D10 and W2 *P. falciparum* strains.
[a]Results are the mean of two experiments performed in duplicate.

The antimalarial activity of **AN12** (**Table 2.1**) was thirty-fold higher on D10 and eighty-fold higher on W2 strains if compared to **RV97**. To investigate the influence of the stereochemistry on the biological activity, the diastereoisomer of **AN12** was synthesized (**AN15**). **AN15** showed loss of antiplasmodial activity against both D10 and W2 *P. falciparum* strains. This suggested that the interaction with the biological target is highly specific and

the spatial orientation of the left-handed moiety of these antimalarial compounds inside the binding pocket is crucial for the antiplasmodial activity. Due to the promising results achieved for **AN12**, SAR study was focused on the R substituent modification, keeping the R' function constant. In particular, it was observed that the replacement of leucine with isoleucine increased the activity on both D10 and W2 strains (**AO07**). The substitution of the linear, tertiary amine of **AN12** with the cyclopentylamine group (**AO26**) further improved the biological activity. However, **AO26** might be metabolized easily. In order to improve the metabolic stability of **AO26**, the methyl ester was replaced by a primary amide, leading to **DC18**. This molecule showed an antimalarial activity against W2 strains comparable to dihydroartemisinin one. Furthermore, **DC18** showed a toxicity on human mammary epithelial cells (HMEC) in the micromolar range (IC_{50} > 30 µM). The parasitemia was decreased of 70% after 4-day intraperitoneal injection of **DC18** to mice infected with *P. vinkei*. However, the parasitemia rose again from the fifth day of treatment. This might be explained by the metabolism of **DC18** (microsomial clearance: 85.50 µl/min/mg).

The above-mentioned results suggested that this new class of antiplasmodial compounds is effective against both D10 and W2 *P. falciparum* strains. Nevertheless, the biological target(s) of these molecules is (are) still unknown. The identification of the target protein(s) of these antimalarial agents would permit rational SAR study as well as facilitate the drug discovery. Moreover, the target of these compounds might be innovative, allowing the exploration of new strategies for malaria therapy. The identification of new target proteins involved in this pathology would be very useful to overcome the imminent problem related to the development of resistance to currently-used antimalarial drugs. In fact, the mortality due to malaria has significantly increased at the end of the last century.[17] This trend has been associated to the development of resistance by *P. falciparum* against

quinolines, especially chloroquine.[18] In order to face this problem, combination therapy involving artemisinin derivatives (ACT, artemisinin combination therapy) was tested. However, in 2006 a case of resistance to artemisinin has been reported in Ta Sanhal, a village near the border between Cambodia and Thailand. The development of resistance to artemisinin observed in southeast Asia is due to the massive use of ACT.[19] Noteworthy, artemisinin and its derivatives are the most effective drugs for malaria and nowadays cannot be replaced by other commercially-available molecules. For this reason, the possibility that malarial parasites develop resistance to artemisinin is a problem of global health. To overcome the resistance issue, molecules with innovative mechanisms of action as well as active on new targets are strongly needed.

To identify the biological target of the 4,4'-oxybisbenzoic acid class of antimalarial agents, the chemical proteomics approach described by Ki Duk Park has been applied (**Figure 2.7**).[4]

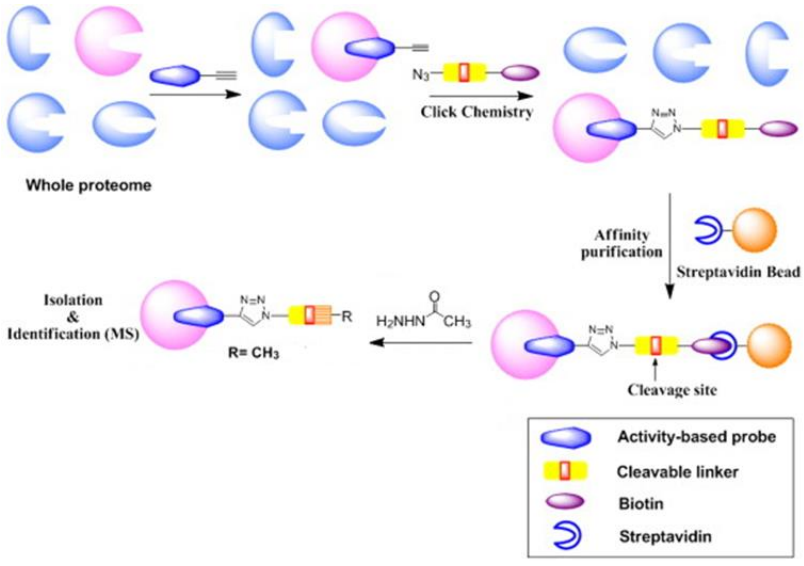

Figure 2.7 Chemical proteomics approach for target identification.[4]

According to this approach, **DC18** was used as active compound and it was modified by introducing a terminal alkyne group. The retention of the antimalarial activity was tested (**Figure 2.8**).

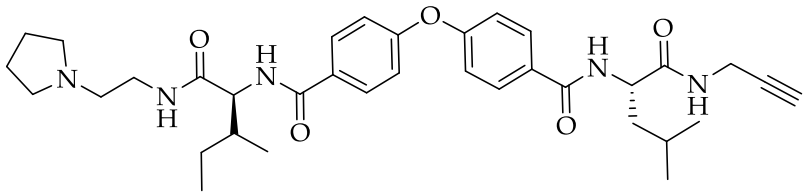

Figure 2.8 Derivatized **DC18** used as tag compound for target identification (D10: IC_{50} = 8 nM; W2: IC_{50} = 12 nM).

The modified tag compound was then incubated in *P. falciparum* lysate to permit the interaction with the biological targets. By means of click chemistry reaction, the tag compound bound to the target proteins was captured taking advantage of a suitable cleavable linker. This linker was composed by a terminal azide, an acylhydrazone linker and a terminal biotin unit. Indeed, the azide was required to react with the alkyne by the click chemistry reaction while the biotin was involved in the affinity purification. The high selectivity of this approach arose from the presence of the cleavable acylhydrazone. In fact, an exchange acylhydrazone/acetyl hydrazide allowed the selective elution of the target due to the presence of the acylhydrazone unit only in the incubated compound while the naturally biotinylated proteins remained anchored to the streptavidin beads. Then, the eluted proteins were purified by SDS-PAGE, digested and the peptides analyzed by LC-MS/MS. Bioinformatics analysis afforded the primary structure of the isolated proteins. This approach allowed the identification of 11 *Plasmodium* proteins as potential targets of **DC18**. The isolation of a small number of potential biological targets starting from a complex lysate underlines the effectiveness of this method. However, this traditional proteomics approach shows several limitations. In particular, the click

chemistry reaction between the tag compound – bearing the target proteins – and the cleavable linker would lead to the formation of a large entity. This might complicate the click chemistry reaction, limiting the entire chemical proteomics approach. Indeed, only tagged-protein captured by the cleavable linker can be anchored to the resin. Moreover, several steps are needed, making the methodology lengthy and therefore not applicable to high-throughput screening. Furthermore, the stationary phase used to purify the lysate is agarose beads covalently bound to streptavidin. This resin is able to retain biotin-tagged proteins as well as "sticky" components, which are abundant in the lysate, albumin and hemoglobin among them. These contaminants are called background proteins and are often aspecifically eluted with the biological targets. This complicates the mass analysis and consequently the target identification.

Therefore, a new recognition system lacking of the limitations displayed by biotin-streptavidin pair must be investigated. In particular, the new recognition system should be involved in interactions strong enough to apply the affinity purification. However, it must be more selective to avoid the aspecific binding issue and therefore facilitate the target identification. Moreover, the whole proteomics approach should be improved to reduce the number of steps involved in the methodology as well as minimize the sample handling that might cause loss of proteins or contaminations.

Therefore, the project aim was designing and validating an innovative proteomics technique for target identification based on the strong and non covalent fluorous interactions. Indeed, fluorine atoms can strongly interact each other and therefore fluorous interactions might be considered as a new recognition system for chemical proteomics. This would simplify the proteomics approach since the click chemistry would not be required. Indeed, the tag compound bound to the protein might be directly anchored to the fluorinated stationary phase, avoiding the capture by the cleavable

linker. The selectivity would be ensured by the fluorous interactions between the resin and the tagged protein. Therefore, this new recognition system should be able to simplify both the synthesis and the affinity chromatography.

Figure 2.9 illustrates the designed fluorous proteomics technique.

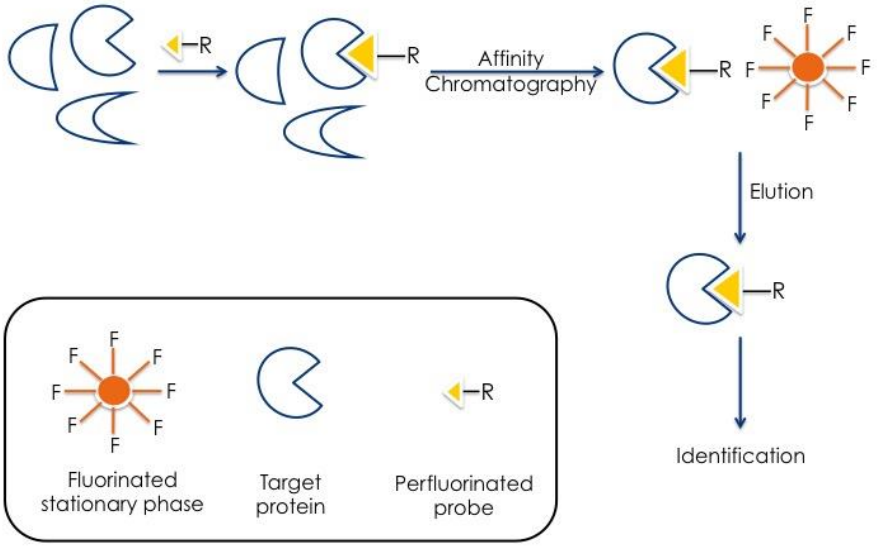

Figure 2.9 Innovative fluorous proteomics approach.

The fluorous proteomics approach requires the introduction of a perfluoroalkyl chain in a bioactive compound. Then, the fluorinated derivative is incubated with the lysate to permit the interaction with the target. The fished protein is isolated by affinity chromatography using a perfluorinated stationary phase and taking advantage of the strong and non-covalent fluorous interactions. Then, the target is purified by SDS-PAGE and identified by LC-MS/MS. This approach overcomes some limitations of the traditional chemical proteomics approach:

- The click-chemistry reaction is avoided since the fluorinated tag is already present in the active compound

- There is no need to synthesize a cleavable linker. Indeed, the selective elution arises from the strong fluorous interactions that can be overcome by a fluorophilic solvent such as methanol.
- Only fluorinated molecules can interact with the fluorinated stationary phase, avoiding aspecific binding.[20] This strongly reduces the amount of contaminants and background proteins present in the eluted sample that would complicate the target identification.

To validate the described fluorous proteomics approach, papain was selected as target protein. Papain is a cysteine endopeptidase extracted from *Carica papaya* with a molecular weight of about 23,800 Dalton. It is characterized by a single peptide chain of 211 residues folded into two parts forming a cleft.[21] The structure is stabilized by three disulfide bonds and shows seven subsites able to accommodate a single amino acid residue of a peptide substrate.[22] The catalytic site is formed by the triad Cys25-His159-Asn175.[23] Since papain is commercialized in its inactive form, it must be activated before use by reducing the disulfide bonds. It is irreversibly inhibited by diazomethyl ketones, which form a covalent bond with Cys25.[23] **Figure 2.10** shows the chemical structure of one of the diazomethyl ketone papain inhibitors described in the literature.[23]

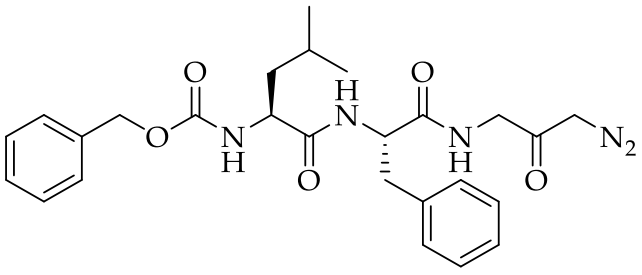

Figure 2.10 Chemical structure of a diazomethyl ketone inhibitor.[23]

Papain was chosen to validate the fluorous proteomics technique for several reasons:

- it is a small protein with a simple structure
- it is commercially available
- it is not expensive
- it shows homology with mammalian cysteine proteases involved in several diseases related to tissue degeneration and therefore is well studied[24]
- its activation is completed in 45 minutes
- diazomethyl ketones are selective papain inhibitors easy to synthesize
- diazomethyl ketones covalently bind papain
- its complete inhibition by diazomethyl ketones is achieved rapidly (15 minutes)

With the aim of validating the fluorous proteomics approach, the papain substrate 4-nitrophenyl((benzyloxy)carbonyl)glycinate and fluorinated diazomethyl ketone inhibitors were synthesized. Both the activation of papain and its inhibition were tested by UV assay. Then, the inhibited papain was isolated by fluorous proteomics following the procedure described previously (**Figure 2.9**). The eluted sample was analyzed by SDS-PAGE and mass spectrometry.

2.4 Synthetic Schemes

2.4.1 Synthesis of Compound 2-1

Scheme 2.1 shows the synthesis of compound **2-1**, which acts as substrate for papain.

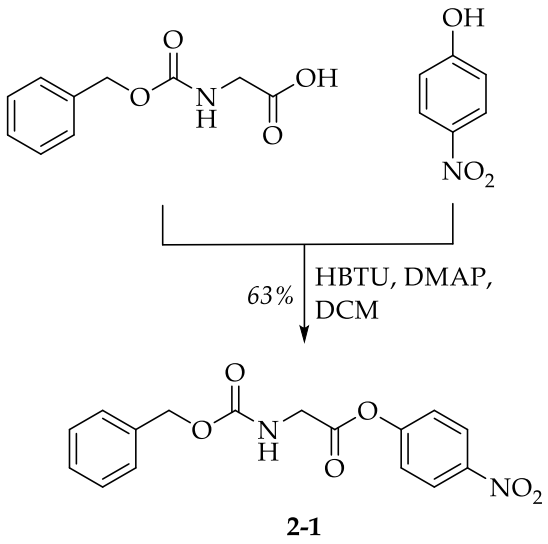

2-1

Scheme 2.1 Synthesis of papain substrate.

Compound **2-1** is achieved by esterifying Z-Gly-OH with p-nitrophenol, using HBTU and DMAP as coupling reagents.

2.4.2 Synthesis of Compound 2-2 and Compound 2-3

Scheme 2.2 shows the synthesis of compounds **2-2** and **2-3**. These molecules are fluorinated inhibitors of papain.

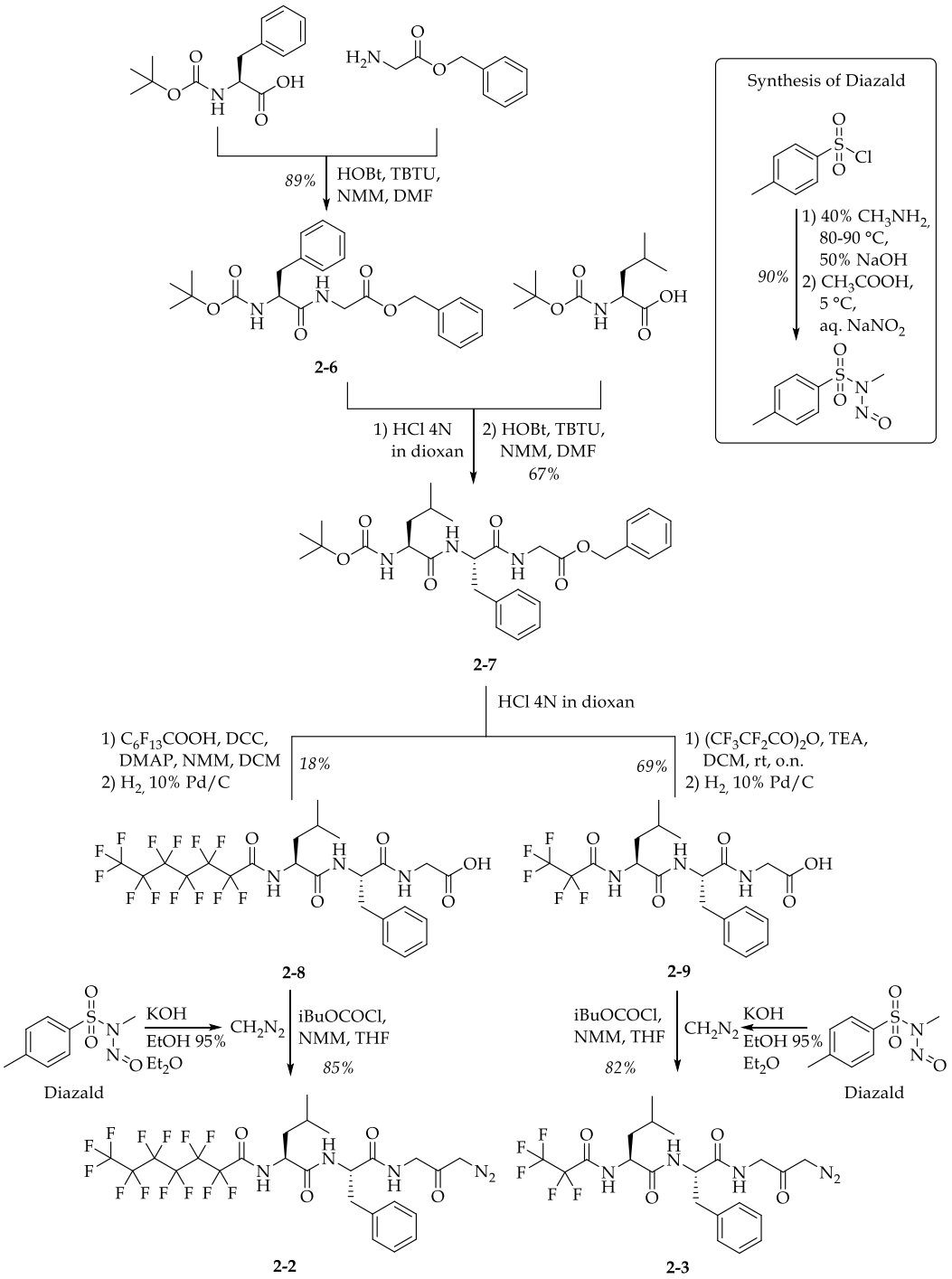

Scheme 2.2 Synthetic scheme of compounds **2-2** and **2-3**.

The synthesis of compounds **2-2** and **2-3** starts with a coupling reaction between Boc-L-Phe-OH and Gly benzyl ester using TBTU and HOBt as coupling reagents to give intermediate **2-6**. Then, intermediate **2-6** is Boc-deprotected before coupling with Boc-L-Leu-OH to afford intermediate **2-7**, which is in common for the syntheses of compounds **2-2** and **2-3**. Indeed, intermediate **2-7** is Boc-deprotected, reacted with perfluoroheptanoic acid or pentafluoropropionic anhydride and then deprotected by hydrogenolysis to give intermediate **2-8** and **2-9** respectively. Both intermediate **2-8** and **2-9** are reacted with diazomethane prepared previously from Diazald®, to afford compounds **2-2** and **2-3** respectively. The box at the top right-handed side of **Scheme 2.2** shows the synthesis of Diazald® starting from p-toluensulfonyl chloride, methylamine and sodium nitrite.

2.4.3 Synthesis of Compound 2-4

Scheme 2.3 shows the synthesis of compound **2-4**, which acts as fluorinated inhibitor of papain with a different chemical structure if compared to compounds **2-2** and **2-3**.

Intermediate **2-10** is prepared according to the general method described by Elshani *et al*, starting from 2-bromoacetic acid and 1H,1H-pentadecafluoroheptanol.[25] Intermediate **2-10** is coupled with Boc-deprotected intermediate **2-7** to afford intermediate **2-11** with a good yield. For this reaction, DIC is chosen as coupling reagent. Intermediate **2-11** is then deprotected by hydrogenolysis and reacted with diazomethane, prepared previously from Diazald®, to give compound **2-4**.

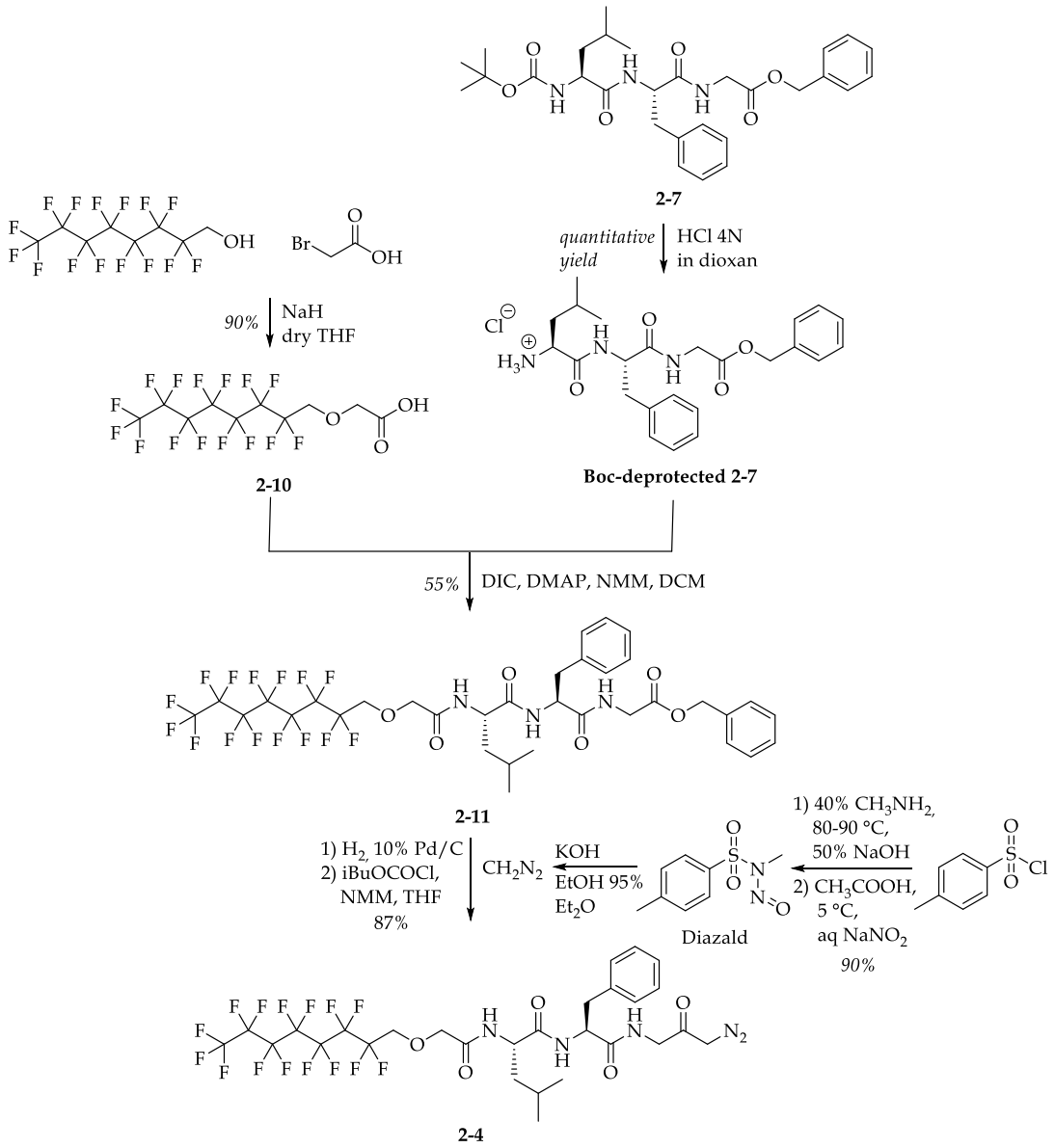

Scheme 2.3 Synthesis of compound **2-4**.

2.4.4 Synthesis of Compound 2-5

The synthesis of the compound **2-5** is shown in **Scheme 2.4**.

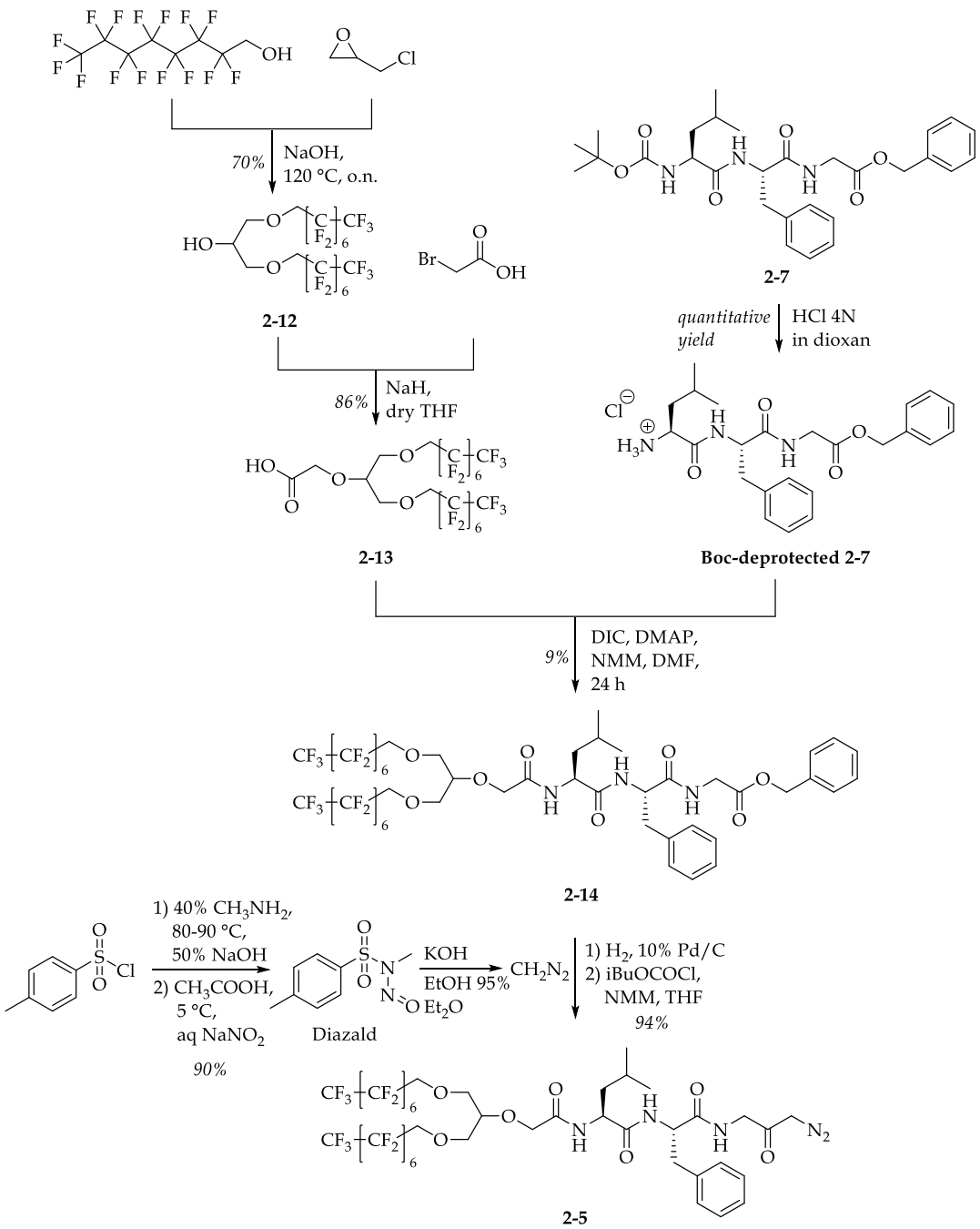

Scheme 2.4 Synthetic scheme of compound **2-5.**

The synthesis of compound **2-5** starts with the nucleophilic reaction between 1H,1H-pentadecafluoroheptanol and epichlorohydrin to afford dibranched intermediate **2-12**, which is then reacted with bromoacetic acid to give intermediate **2-13**. Then, intermediate **2-13** is coupled with Boc-deprotected intermediate **2-7** to afford intermediate **2-14** using DIC as coupling reagent. Intermediate **2-14** is then deprotected by hydrogenolysis and reacted with diazomethane, prepared previously from Diazald®, to give compound **2-5**.

2.5 Reactions and Mechanisms

2.5.1 Coupling Reaction

The generation of amide bonds is an important step for the synthesis of molecules of biological interest. The first step for the formation of a peptide bond is the activation of the carboxylic group, then the nucleophilic attack of the amine on an activated carboxylic acid is required. The carboxylic acid activation can be achieved by using the so-called coupling reagents. Notably, the configuration of the involved amino acids – especially when the chiral center is in the α-position – must be retained during the peptide synthesis, regardless the coupling technique used (in solution or solid-phase approaches). Thus, the main challenge in the peptide synthesis is the choice of suitable coupling reagents that must ensure the accomplishment of high yield as well as no racemization observed.

The main mechanisms responsible for the racemization of α-amino acids are enolization and, when possible, formation and enolization of an 5(4H)-oxazolone (oxazolonium ion for N-alkyl amino acids), as shown in **Figure 2.11**.[26]

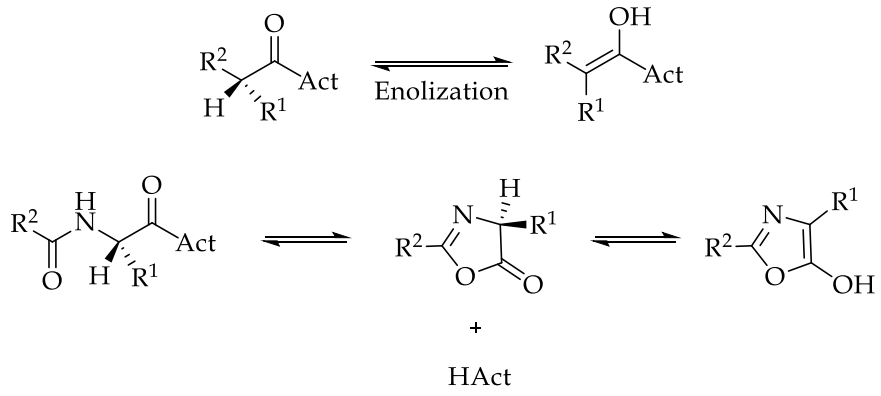

Figure 2.11 Mechanisms responsible for the racemization during peptide synthesis.[26] (Act: Activating group).

The method of activation of the carboxylic group deeply affects the degree of racemization. The presence of a base promotes the racemization since the proton in the α-position can be easily removed. Moreover, if the activating group (Act-) is a good leaving group promoting the formation of the 5(4H)-oxazolone, the proton in the α-position will be more acidic and therefore more easily removed by the base. However, the presence of a base and a good leaving group are often required since they lead to a better coupling yield.

Despite several classes of coupling reagents might be distinguished, the main groups are represented by carbodiimides and benzotriazoles. **Figure 2.12** shows some components of each class.

CARBODIIMIDES

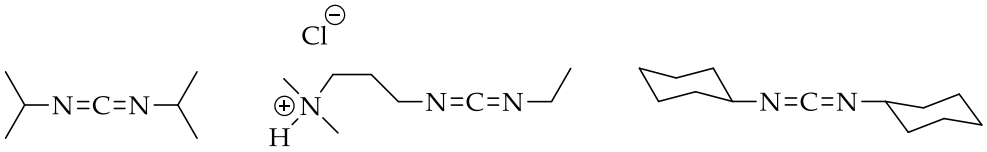

DIP EDC (EDAC, WSC) DCC

BENZOTRIAZOLES

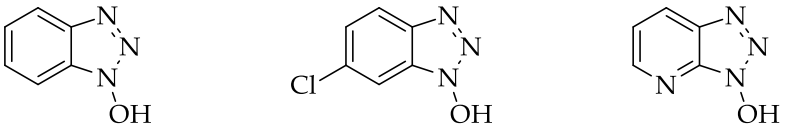

HOBt Cl-HOBt HOAt

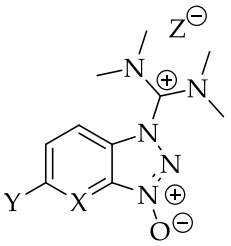

Z = PF_6, BF_4
X = CH, N
Y = H, Cl

HBTU X = CH, Y = H, Z = PF_6
TBTU X = CH, Y = H, Z = BF_4
HCTU X = CH, Y = Cl, Z = PF_6
TCTU X = CH, Y = Cl, Z = BF_4
HATU X = N, Y= H, Z = PF_6

Figure 2.12 Carbodiimides and benzotriazoles coupling reagents.

Carbodiimides have been used as coupling reagents since 1955, DCC being the most widely employed. The mechanism of activation performed by carbodiimides is represented in **Figure 2.13**.

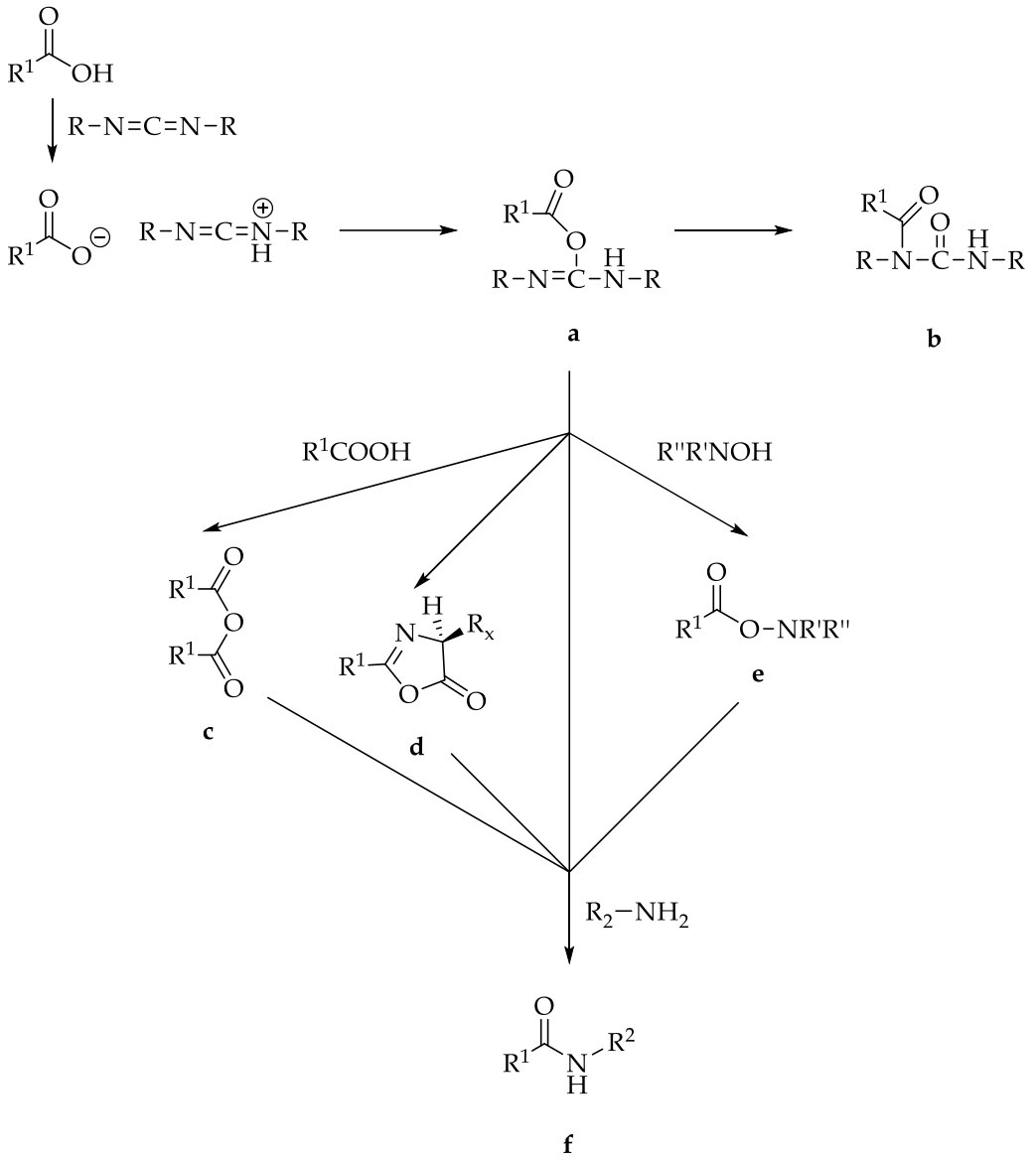

Figure 2.13 Mechanism of carboxylic acid activation observed with carbodiimides.

First, a proton is transferred to the carbodiimide followed by addition of the carboxylic acid to give the O-acylisourea (**Figure 2.13**, **a**). This intermediate is highly reactive and therefore can attack the amino acid providing the corresponding amide (**Figure 2.13**, **f**). However, the O-acylisourea might rearrange to afford the corresponding N-acylurea (**Figure 2.13 b**), which is not reactive. The O-acylisourea might also react with another carboxylic acid group leading to the corresponding symmetric anhydride (**Figure 2.13**, **c**)

which is an excellent acylating agent. O-acylisourea can undergo intramolecular cyclization to give a 5(4H)-oxazolone if the carboxylic acid is a N-carboxamide or a carbamate α-amino acid (Boc, Fmoc) (**Figure 2.13**, **d**). The 5(4H)-oxazolone can act as acylating agent. However, it is less powerful than O-acylisourea or the symmetric anhydride. Moreover, tautomerization of O-acylisourea to give the enol form might lead to racemization. A nucleophilic agent, such as hydroxylamine derivative (R'R''NOH) can react with the O-acylisourea, affording the corresponding active ester (**Figure 2.13**, **e**) which is less reactive but more stable. Notably, the solvent used for the coupling reaction affects the rate at which the O-acylisourea forms. When the activation is accomplished in a solvent with low dielectric constant (such as DCM), the O-acylisourea is obtained instantaneously. However, when a more polar solvent (such as DMF) is used, a mixture of starting amino acid, symmetric anhydride, N- acylurea and urea is formed. In order to reduce the epimerization as well as increase the yield while using carbodiimides as coupling reagents, the addition of HOBt as an additive may be taken into account.[27] HOBt acts as a nucleophilic agent by reacting with the O-acylisourea to give the corresponding active ester (**Figure 2.14**).

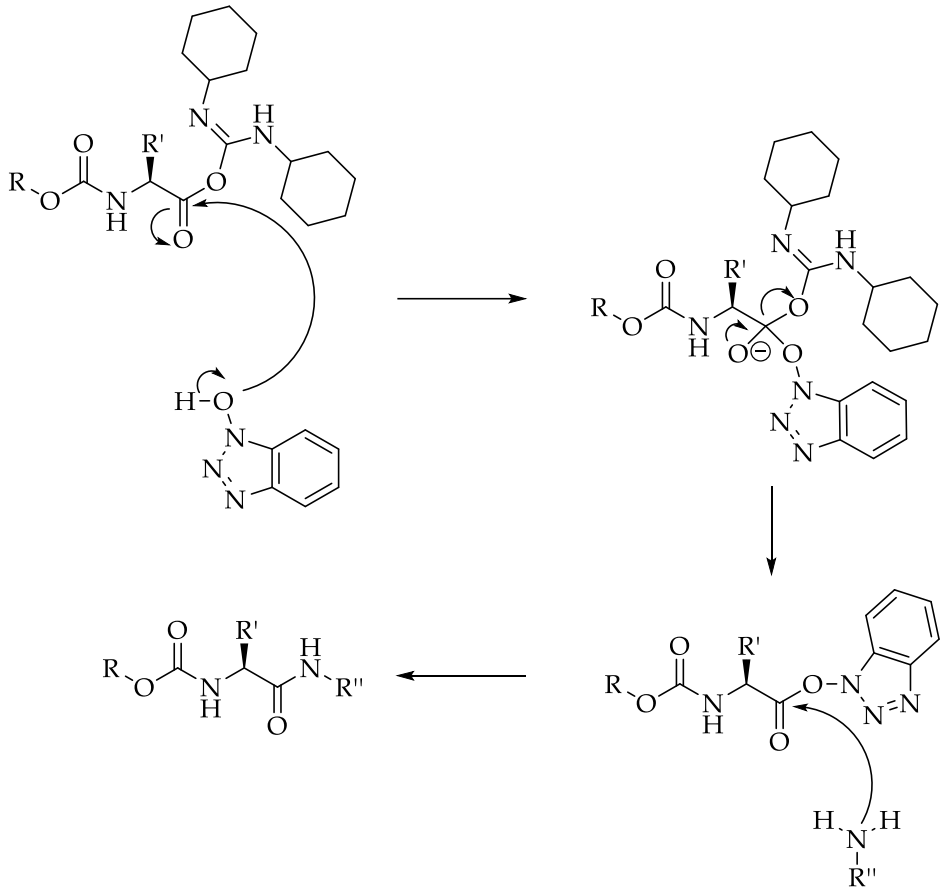

Figure 2.14 Mechanism of activation by HOBt when used as an additive with carbodiimides.[27]

The main advantage in using this additive as trapping agents of the O-acylisourea is its ability to increase the concentration of the active species when DMF is used as a solvent as well as reduce racemization of the carboxylic function.

Another important class of coupling reagents is represented by 1-H-benzotriazoles. Several salts are associated to this class, including uronium, aminium, phosphonium, immonium, and carbonium salts.[27] HATU (**Figure 2.12**) is the most reactive among all as well as the most expensive. The presence of chlorine is responsible for the greater reactivity of HCTU and TCTU compared to HBTU and TBTU (**Figure 2.12**). The chemical species that

react with the salt is the deprotonated carboxylic function, thus a small amount of a base is needed. **Figure 2.15** shows the mechanism of activation observed with 1-H-benzotriazole-based coupling reagents.

The acyloxy-phosphonium species cannot be isolated and therefore they react instantaneously with the benzotriazole derivative to afford an intermediate which reacts with the ilino-ammonium component leading to the corresponding amide.

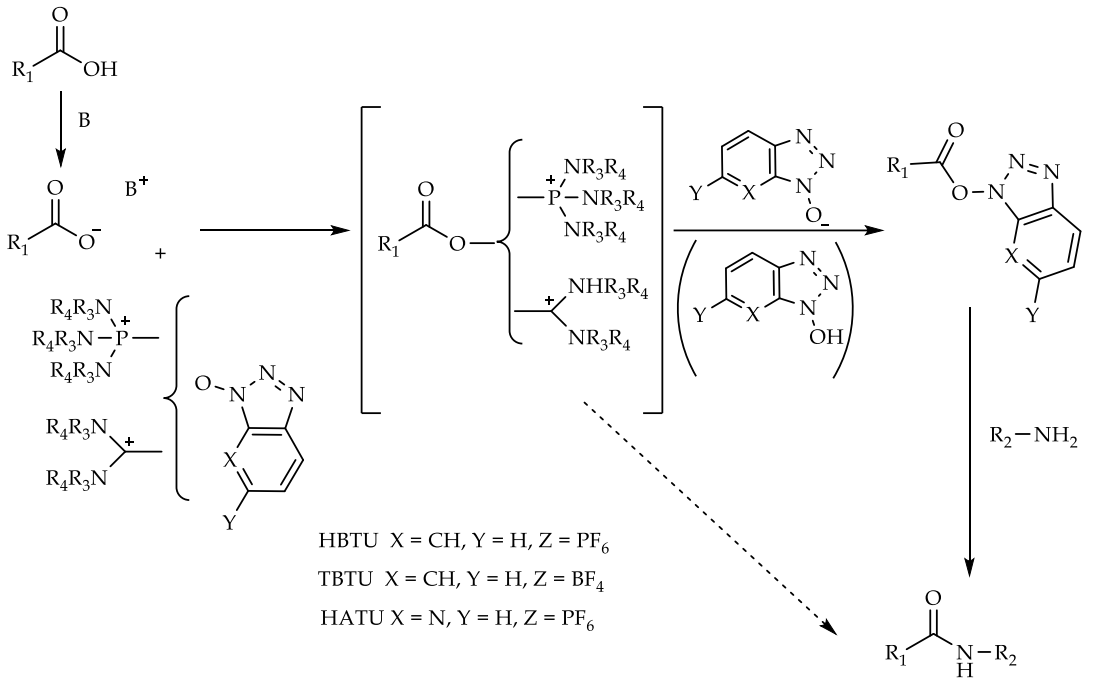

Figure 2.15 Mechanism of activation observed with 1-H-benzotriazole-based coupling reagents.

2.5.2 Diazomethane and Diazomethyl Ketone Syntheses

The formation of diazomethyl ketone derivatives requires the preparation of diazomethane first, which is immediately reacted with a carboxylic acid to give the corresponding diazomethyl ketone, as shown in **Figure 2.16**.

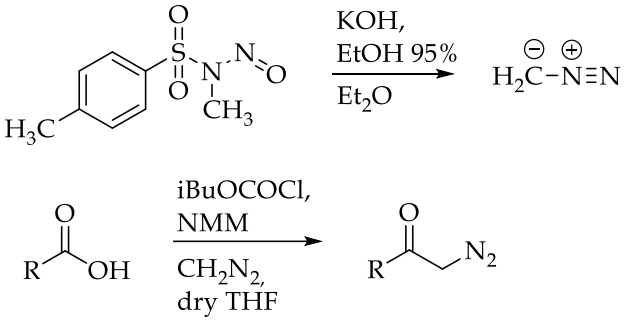

Figure 2.16 Synthesis of diazomethyl ketone derivative.

Diazomethane (CH_2N_2) is a yellow gas at rt. It is extremely poisonous and is a potent carcinogen. Diazomethane is also a sensitizer and long-term, low-level exposures can lead to asthma-like symptoms. Moreover, diazomethane is highly instable since it can explode if exposed to sharp surfaces or certain chemicals such as drying agents. Therefore, it is conserved and handled as diethyl ether solution to prevent accidents. Diazomethane is usually prepared in the exact amount needed for the synthesis of diazomethyl ketones, in order to avoid the storage of the remaining solution of diazomethane. Diazald® (N-methyl-N-nitroso-paratoluenesulfonamide) is usually used as precursor. Diazald® undergoes an internal rearrangement, then it is deprotonated by a base (such as KOH) and a dissociation leads to the diazomethane gas. **Figure 2.17** illustrates the above-described mechanism.

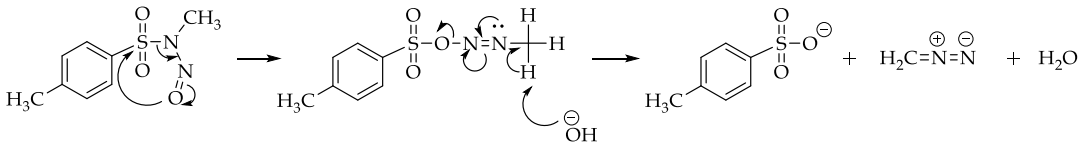

Figure 2.17 Mechanism of formation of diazomethane starting from Diazald®.

Diazomethane bears a negative charge on the carbon, as demonstrated by its resonance structures (**Figure 2.18**).

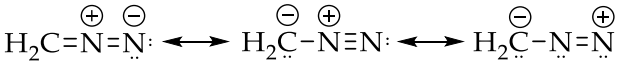

Figure 2.18 Resonance structures of diazomethane.

Diazomethane is largely used in organic chemistry because of its ability to act as methylating agent for carboxylic acids. This can be also used as effective way to destroy the unreacted gas. Indeed, diazomethane is destroyed by adding acetic acid, which acts as a scavenger leading to the formation of harmless methyl acetate and nitrogen gas (**Figure 2.19**).

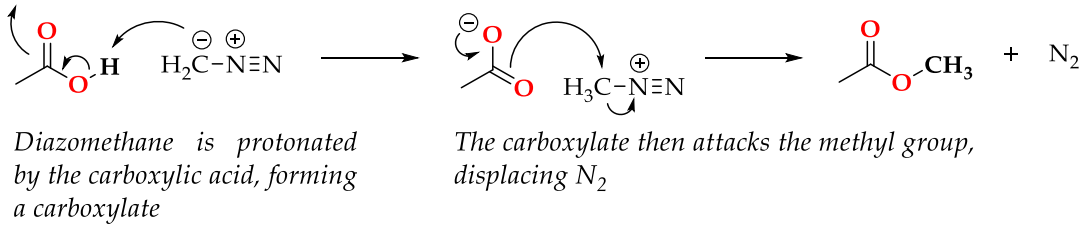

Figure 2.19 Inactivation of diazomethane by acetic acid.

As mentioned before, diazomethane is the starting material to prepare diazomethyl ketone derivatives. The procedure involves the reaction between a carboxylic acid and isobutyl chloroformate, leading to an unstable anhydride, which cannot be isolated. This intermediate then reacted with the diazomethane to afford the desired diazomethyl ketones, as shown in **Figure 2.20**.

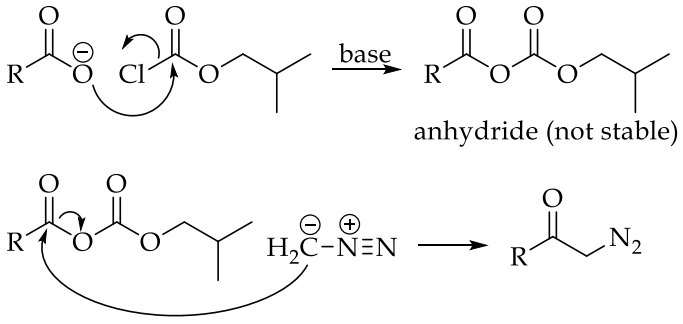

Figure 2.20 Mechanism of diazomethyl ketone synthesis.

2.5.3 Papain Inactivation by Diazomethyl Ketone Inhibitors

The proposed mechanism for the inactivation of papain by diazomethyl ketones is shown in **Figure 2.21**.[28]

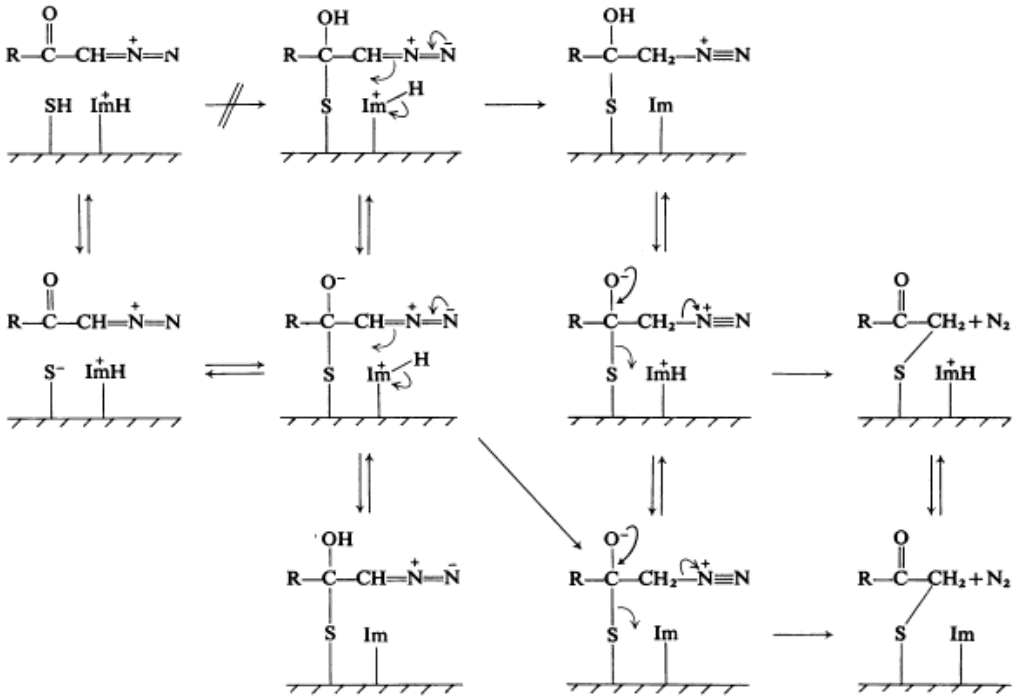

Figure 2.21 Mechanism of papain inactivation.[28]

The thiol group of Cys25 is part of the catalytic triad as it is transiently acylated during catalysis. The observation that diazomethyl ketones do not react with low-molecular-weight thiols, such as β-mercaptoethanol and cysteine, suggests that the mechanism of papain inhibition involves neighboring groups in the catalytic pocket, as well as the formation of a transient thiohemiketal, the protonation by the imidazolium ion of His159 and the alkylation on sulphur. Notably, the atom that is protonated by the imidazolium ion of papain is the same as the atom that is finally bonded to the sulphur atom of papain. It is supposed that S-C bond formation occurs by

the setting-up of a three-membered cyclic transient state. Therefore, the side chain of His159 must be rotated to reduce the steric hindrance and therefore permits the catalysis.

2.6 Fluorinated Papain Inhibitors

In the following paragraphs, the structure of diazomethyl ketone papain inhibitors, the optimization of their synthesis as well as the stability of the obtained fluorinated molecules are discussed.

2.6.1 Chemical Structure of Fluorinated Papain Inhibitors

Fluorinated papain inhibitors we designed for the application of the fluorous proteomics approach are low-molecular-mass molecules that consist of three parts. One moiety is represented by a peptidyl fragment with a suitable sequence for the interaction with papain binding pocket. The second part is represented by the reactive diazomethyl ketone group, which can covalently bind Cys25 in the catalytic site and thus inhibit papain. The third moiety is a fluorinated chain responsible for the interaction with the fluorinated stationary phase during affinity purification. The length of the fluorous chain is crucial, since it is involved in the formation of the fluorous phase during purification. Indeed, a long fluorinated chain (C_6F_{13}) is required to allow the interaction with the stationary phase during affinity purification. Interestingly, if the fluorous alkyl chain is very long (> C_8F_{17}), the synthesis of these compounds becomes a challenge. This is due to the poor reactivity of molecules showing a high degree of fluorination and to problems concerning the solubility of the starting materials in the common organic solvents which might arise. Indeed, highly fluorinated compounds tend to segregate

forming the fluorous phase, making the interaction with other reactants difficult. However, a short chain cannot interact with the fluorinated stationary phase and therefore the fluorinated molecule would not be retained in the column during affinity chromatography. The fluorinated inhibitors synthesized for the fluorous proteomics approach have different chain length, as **Figure 2.22** shows.

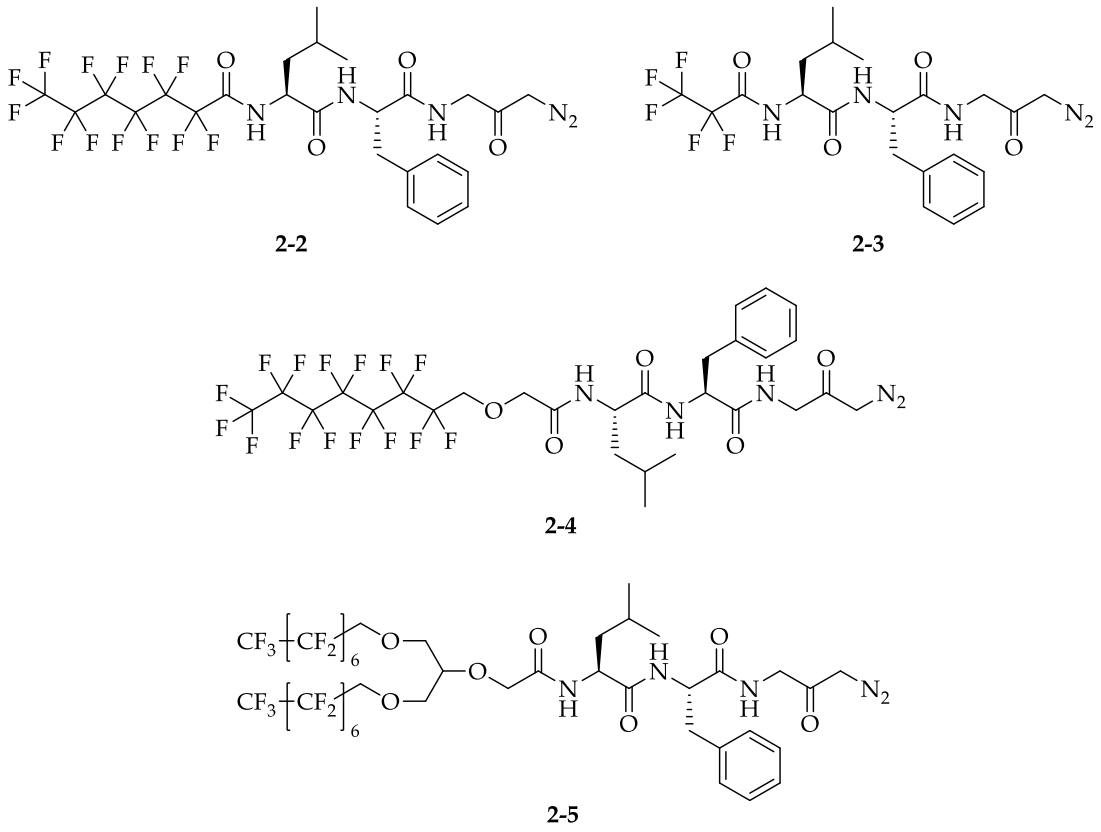

Figure 2.22 Synthesized fluorinated diazomethyl ketone inhibitors.

The fluorinated alkyl chain is directly bound to the peptidyl fragment in compounds **2-2** and **2-3** while compounds **2-4** and **2-5** show an ether bridge linking the two moieties. The short spacer introduced in compounds **2-4** and **2-5** distances the fluorinated alkyl chain from the peptidyl unit, minimizing steric hindrance during affinity purification. Moreover, compounds **2-2**, **2-3**

and **2-4** are linear semifluorinated molecules while compound **2-5** is dibranched. Consequently, compound **2-5** is a doubly-tagged molecule and therefore can be taken into account to design innovative separation schemes. Actually, a mixture of linear and branched fluorinated species might be separated by fluorous proteomics approach because of their different chemical structures.

2.6.2 Synthesis Optimization of Fluorination Reaction

As mentioned before, compound **2-2** bears the long fluorinated alkyl chain directly bound to the peptidyl fragment while compound **2-4** has an ether spacer placed between the fluorous chain and the peptidyl unit. The absence of a spacer in compound **2-2** complicates the synthesis of this molecule. Indeed, the reactivity of fluorocarbons is greatly reduced when the fluorous moiety is directly bound to the reactive functional group.[29] This can be explained taking into account the strong electron-withdrawing effect of the fluorous chain. Therefore, the fluorination of intermediate **2-7** was difficult and different reaction conditions were investigated.

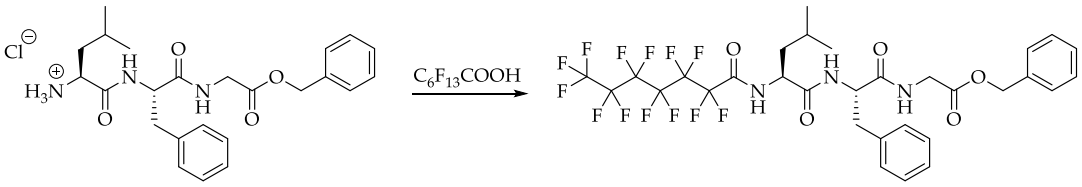

Deprotected 2-7

Entry	Reagents	Reaction Conditions	Yield (%)
1	EDAC DMAP	o.n., rt	0
2	TBTU	o.n., rt	0
3	$SOCl_2$ pyridine	1) 3 h, reflux 2) o.n., rt	0
4	DCC DMAP	o.n., rt	18

Table 2.2 Optimization of fluorination reaction of intermediate **2-7**.

The reaction was firstly carried out using common coupling reagents (**Table 2.2**, entries 1 and 2). Since the desired product was not achieved, the activation of perfluoroheptanoic acid to perfluoroheptanoil chloride was performed (**Table 2.2**, entry 3) without good results. Fluorination reaction was successful only using DCC as coupling reagent (**Table 2.2**, entry 4).

In contrast, intermediate **2-11** was achieved with a good yield (55%) and therefore the optimization of the reaction conditions was not required. In fact, the presence of the ether linker separates the fluorinated alkyl chain from the reactive carboxylic group in intermediate **2-10**, shielding the electron withdrawing effect of fluorine atoms and therefore promoting the coupling with the peptidyl fragment (Boc-deprotected intermediate **2-7**) to afford intermediate **2-11**.

2.6.3 Stability of Highly Fluorinated Intermediate 2-8

Since the introduction of a perfluorinated alkyl chain deeply modifies the chemical properties of the whole molecule, we wondered if fluorinated inhibitors were stable in the aqueous buffer used to perform the fluorous proteomics approach. We reasoned that the perfluorinated alkyl chain directly bound to the peptidyl fragment by amide bond – as in compound **2-2** – might show a strong electron-withdrawing effect, making the amide bond labile and therefore easy to hydrolyze. Consequently, the fluorinated chain might be lost, compromising the fluorous proteomics study. In contrast, the presence of a perfluorinated alkyl chain might protect the amide bond from the hydrolysis because of steric hindrance arising from fluorine atoms that might mask the amide bond. These hypotheses led us to test the stability of highly fluorinated molecules in the aqueous buffer. The medium chosen for this test is the same used to activate papain before performing the fluorous proteomics approach. It is an aqueous phosphate buffer (pH=6.5) containing β-mercaptoethanol – as reducing agent able to reduce papain disulfide bonds – and EDTA – as chelating agent. Notably, the diazomethyl ketone group does not react with β-mercaptoethanol, as reported in the literature.[30] Moreover, it is stable at pH=6.5.

Therefore, we synthesized intermediate **2-8** and tested its stability in the phosphate buffer before moving on the more tedious synthesis of compound **2-2**. With this aim, a solution of intermediate **2-8** in DMF was mixed with the buffer and then vigorously shaken at rt, reproducing the same conditions performed for papain inhibition. Then, the mixture was extracted with DCM to allow the separation of intermediate **2-8** from inorganic salts. The organic phase was dried over $MgSO_4$, filtered and concentrated under reduced pressure. The obtained residue was then analyzed by mass spectrometry. **Figure 2.23** shows the mass spectrum of this residue.

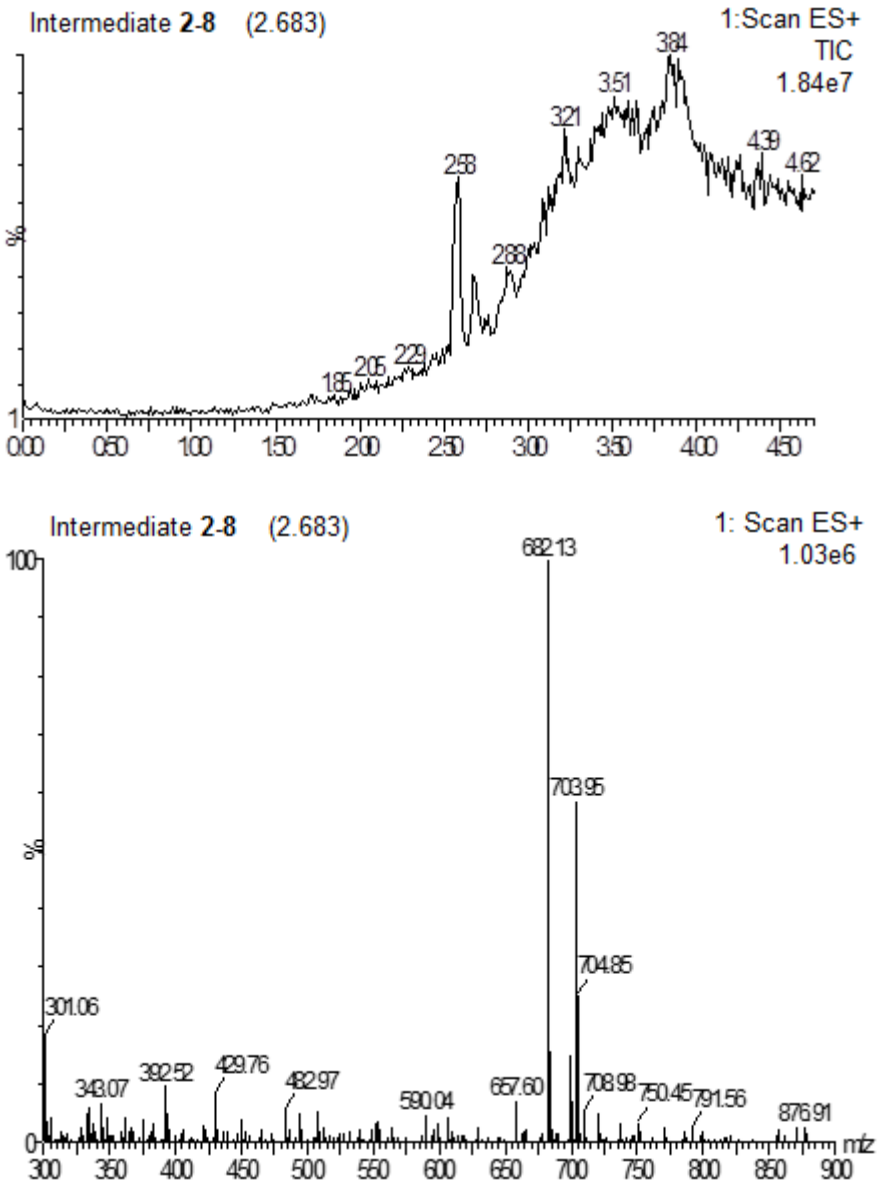

Figure 2.23 Mass spectrum of intermediate **2-8** after incubation in the aqueous buffer. Calculated *m/z*: 681.15. Found *m/z*: 682.13 $[M+H]^+$; 703.95 $[M+Na]^+$.

The mass spectrum showed the molecular peak of intermediate **2-8**, suggesting that this molecule is stable under incubation conditions.

2.7 UV Spectroscopy Studies

The activation of papain as well as its inhibition by diazomethyl ketone derivative was tested by UV spectroscopy assays, as described in the following paragraphs.

2.7.1 Papain Activation Assay

Since papain is commercialized in an inactive and more stable form, it must be activated before use by reducing disulfide bonds. Papain activation was carried out by incubating the protein for 1 hour at rt in phosphate buffer (pH=6.5) containing β-mercaptoethanol and EDTA. The actual protein activation was demonstrated by UV spectroscopy, taking advantage of the ability of papain to hydrolyze 4-nitrophenyl((benzyloxy)carbonyl)glycinate (compound **2-1**). UV assay was performed at 340 nm since the absorption of 4-nitrophenol does not depend on pH at this wavelength. **Figure 2.24** illustrates the hydrolysis of compound **2-1**.

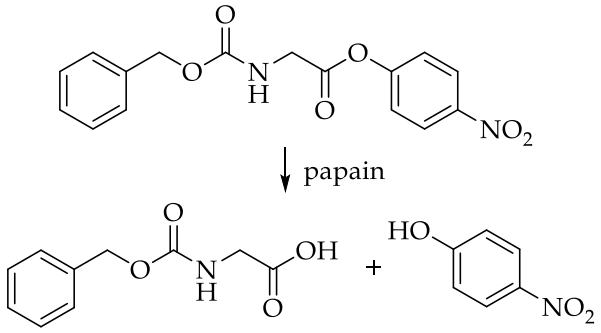

Figure 2.24 Hydrolysis of compound **2-1**.

The entity of spontaneous hydrolysis of compound **2-1** in the aqueous medium was also evaluated. Spontaneous hydrolysis of compound **2-1** was

monitored for 25 minutes both at rt and at 0 °C. As expected, spontaneous hydrolysis was greater at rt (**Figure 2.25**).

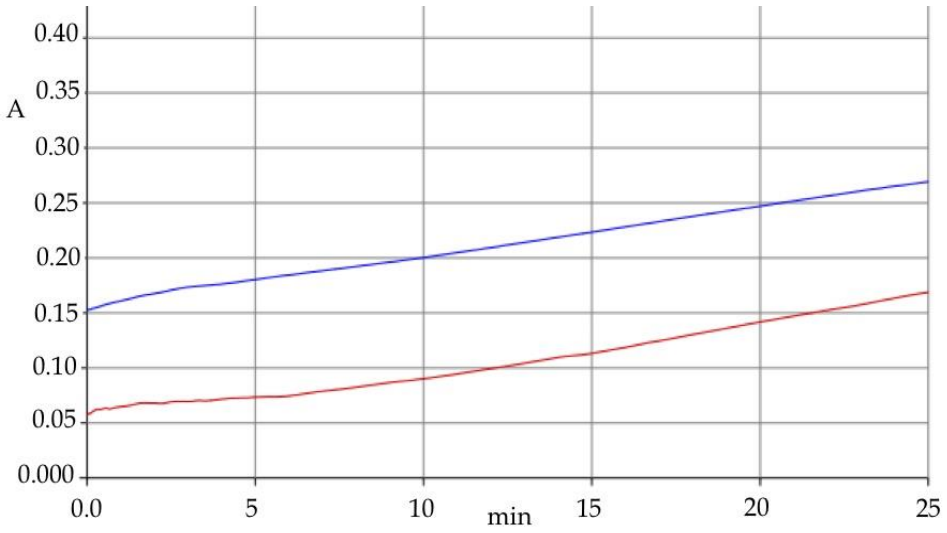

Blue curve: room temperature	**Red curve: 0 °C**
Reference: buffer w/o papain	Reference: buffer w/o papain
Sample: buffer w/o papain + compound **2-1** ($2.5 * 10^{-5}$)	Sample: buffer w/o papain + compound **2-1** ($2.5 * 10^{-5}$)

Figure 2.25 UV spectrum of spontaneous hydrolysis of compound **2-1** carried out at rt (blue curve) and at 0 °C (red curve).

Then, a new experiment was set up to evaluate the enzymatic activity of papain taking into account the spontaneous hydrolysis of compound **2-1** (**Figure 2.26**).

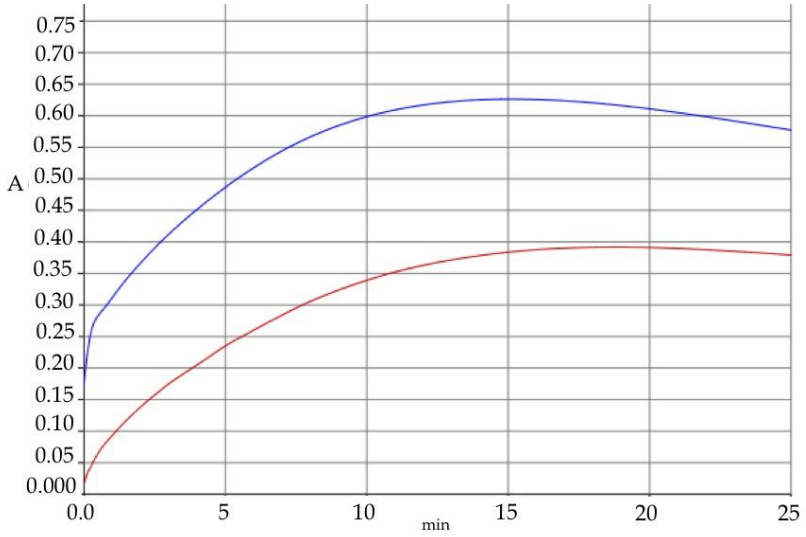

Blue curve: room temperature	**Red curve: 0 °C**
Reference: buffer w/o papain + compound **2-1** ($2.5 * 10^{-5}$)	Reference: buffer w/o papain + compound **2-1** ($2.5 * 10^{-5}$)
Sample: buffer with papain ($1.45 * 10^{-5}$ M) + compound **2-1** ($2.5 * 10^{-5}$)	Sample: buffer with papain ($1.45 * 10^{-5}$ M) + compound **2-1** ($2.5 * 10^{-5}$)

Figure 2.26 Enzymatic activity of papain taking into account the spontaneous hydrolysis of compound **2-1.** Blue curve was obtained at rt while red curve at 0 °C.

As shown in **Figure 2.26**, red and blue curves reached the plateau after 10 and 15 minutes respectively. As expected, the enzymatic activity is greater at rt than at 0 °C.

These experiments demonstrated papain activation under the previously described incubation conditions.

2.7.2 Papain Inhibition Assay

The ability of diazomethyl ketones to inhibit cysteine proteases like papain has already been described in the literature. However, the modification of the inhibitor by introducing a fluorinated alkyl chain leads to a new entity whose

ability to inactivate papain must be proved. Papain inactivation performed by fluorinated diazomethyl ketone derivative was tested before carrying out the fluorous proteomics approach. Indeed, papain inhibition arises from the alkylation of Cys25 in the catalytic site by the diazomethyl ketone derivative and therefore the inhibitor is covalently bound to the protein. Consequently, the success of the fluorinated proteomics approach depends mainly on fluorine-fluorine interactions between the fluorous alkyl chain borne by the inhibited papain and the fluorinated stationary phase.

To verify the papain inhibition, compound **2-2** was taken into account to perform UV spectroscopy assay. After papain activation, compound **2-2** was incubated with the buffer solution of the enzyme at rt for 15 minutes, keeping the solution vigorously shaken. Noteworthy, the purification of the activated papain is not required. Actually, diazomethyl ketones do not react with low-molecular-weight thiols and therefore β-mercaptoethanol does not affect the ability of diazomethyl ketone to bind papain.[28,31] Moreover, the presence of β-mercaptoethanol might be helpful, since it keeps the papain in the active form.

As shown in **Figure 2.27**, compound **2-2** was actually able to inhibit papain. In fact, the inhibition curve was flat, meaning that the hydrolysis of compound **2-1** catalyzed by papain did not occur.

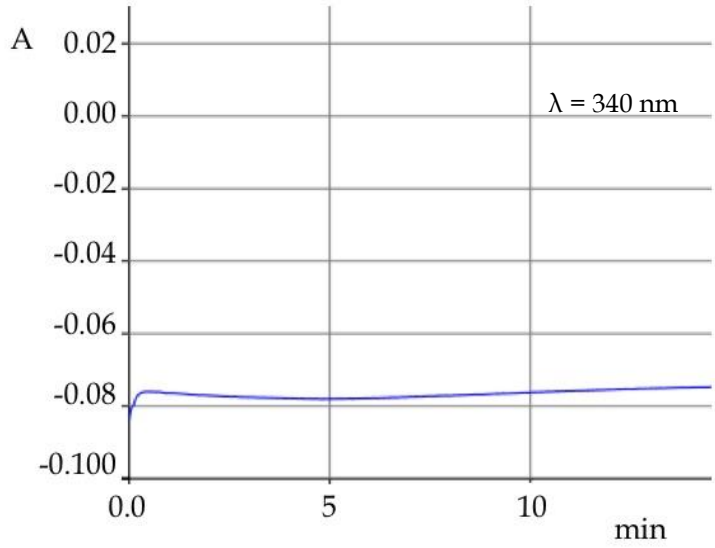

Reference: buffer containing papain ($1.45 * 10^{-5}$) + compound **2-1** ($4.4 * 10^{-3}$)

Sample: buffer containing papain ($1.45 * 10^{-5}$) + compound **2-1** ($4.4 * 10^{-3}$) + compound **2-2** ($4.4 * 10^{-3}$)

Figure 2.27 UV spectrum of papain inhibition.

2.8 Fluorous Proteomics Study

2.8.1 Affinity Purification

Affinity purification allows the separation of non-fluorinated components from fluorinated species, inhibited papain among them. First, a fluorophobic washing carried out with water is required to elute non-fluorinated molecules, such as salts as well as the fraction of papain that did not react with the fluorinated inhibitor and therefore was not retained in the column. The following fluorophilic elution performed with methanol allows the collection of fluorinated components, which were able to anchor the stationary phase. Then, the resin is recycled by washing with acetone. It is crucial to investigate how many column volumes of solvents are needed to completely elute non-fluorinated and fluorinated species. With this aim,

affinity chromatography of non-inhibited papain as well as papain inhibited by compound **2-4** was performed. In particular, 5 column volumes of water and 5 more of methanol were collected. These samples were reacted with Coomassie Brilliant Blue dye and then analyzed by UV assay. Indeed, Coomassie Brilliant Blue binds to proteins through ionic interactions between dye sulfonic acid groups and positive protein amide functions as well as through van der Waals interactions. Under acidic conditions, the dye has a brownish color, which turns blue when it is bound to the protein. The optical absorbance of the protein-bound dye is measured at a wavelength of 595 nm.

Figure 2.28 and **Figure 2.29** show the absorbance values of the elution with water and methanol for non-inhibited and inhibited papain respectively.

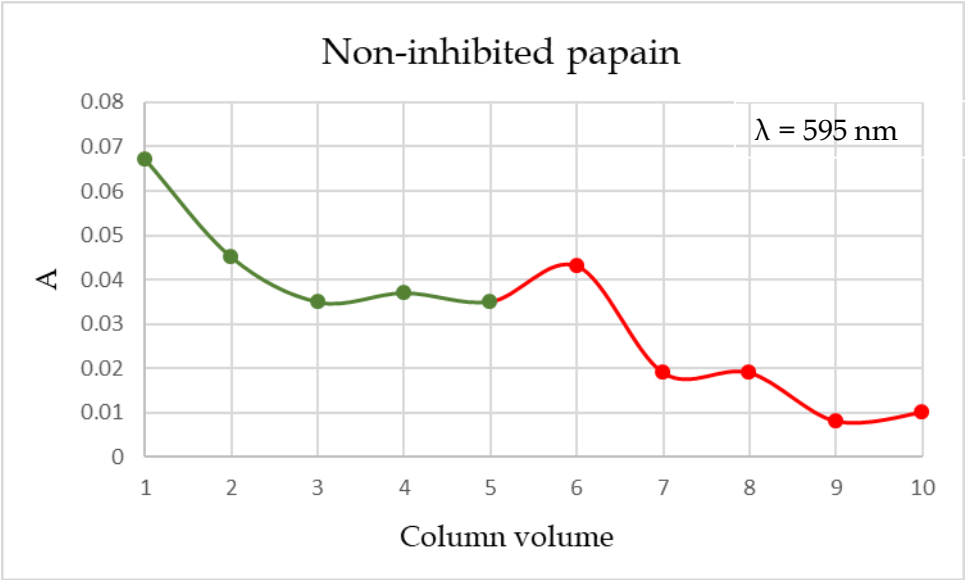

Figure 2.28 Plot absorbance value over column volume for non-inhibited papain (green line: elution with water; red line: elution with methanol).

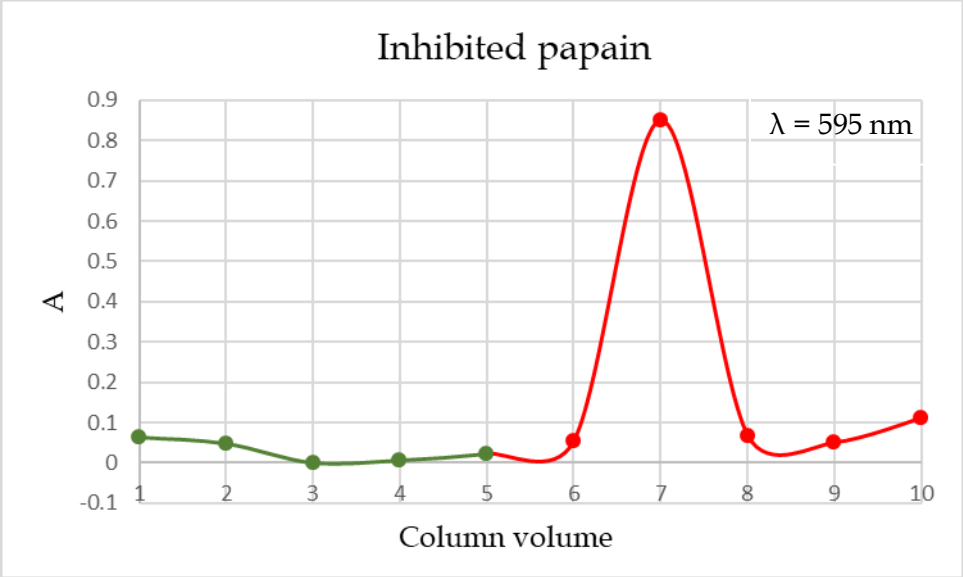

Figure 2.29 Plot absorbance value over column volume for inhibited papain (green line: elution with water; red line: elution with methanol).

Focusing on the fluorophobic elution for non-inhibited and inhibited papain (**Figure 2.30**), it is evident that papain was almost completely collected within two column volumes for the inhibited sample (**Figure 2.30**, orange curve). Indeed, the absorbance reduced after the elution with two column volumes of water, keeping the curve almost flat.

Despite the protein was collected mainly within two column volumes for the non-inhibited sample, it kept to be eluted in the following fluorophobic elutions (**Figure 2.30**, blue curve).

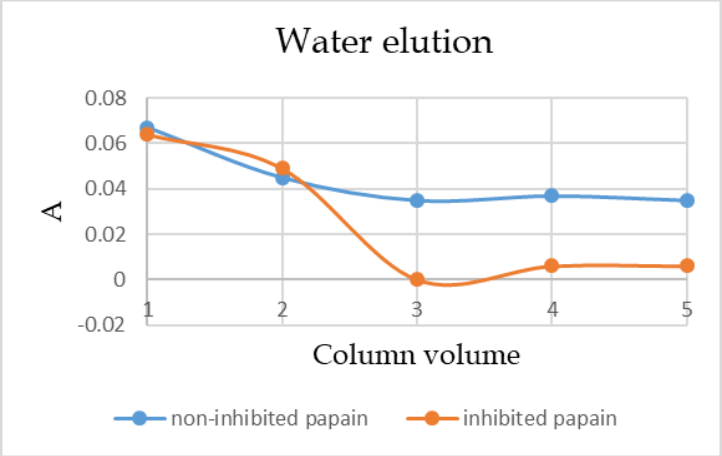

Figure 2.30 Comparison of water elutions for non-inhibited and inhibited papain.

As expected, the results obtained for the washings with methanol were different for the non-inhibited and the inhibited samples (**Figure 2.31**). Indeed, the absorbance kept very low for non-inhibited papain, with values near zero (**Figure 2.31**, blue curve), suggesting that the protein was not collected during the fluorophilic elutions. However, the absorbance incresed for the inhibited papain, reaching the highest value after one column volume of methanol and inhibited papain was collected completely within two column volumes of methanol (**Figure 2.31**, orange curve). This means that methanol was actually able to elute the inhibited protein.

Potentially, the excess of compound **2-4** which did not bind the protein but interacted with the stationary phase – because of the fluorinated alkyl chain – was eluted with methanol as well. To exclude any possible interference due to the presence of amide bonds, we analyzed a methanolic solution containing compound **2-4** and Coomassie Brilliant Blue by UV assay. The same experiment was performed with a negative control composed by only methanol and the dye. The absorbance values of these two samples were the same (0.14), proving that the presence of unbound compound **2-4** in the methanol washings did not interfere during UV assay.

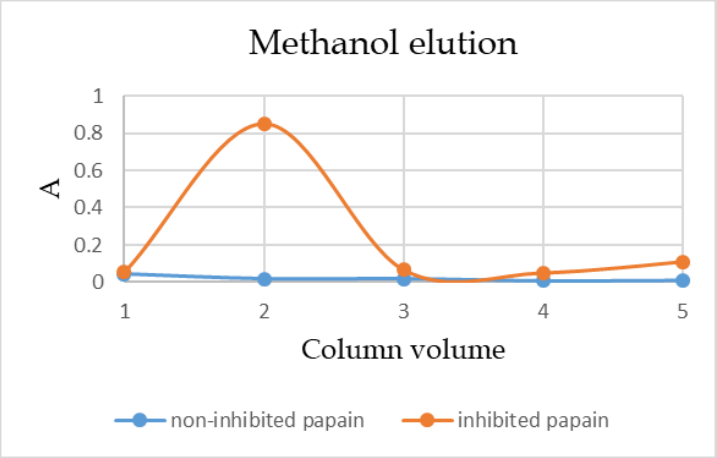

Figure 2.31 Comparison of methanol elutions for non-inhibited and inhibited papain.

Combined together, these results suggest that non-inhibited papain did not interact with the fluorinated stationary phase and therefore was completely eluted with water, as expected. Indeed, the protein was not detected in methanol fractions. In contrast, inhibited papain was actually able to interact with the fluorinated resin. In fact, papain was also collected with methanol. Methanol is a fluorophilic solvent able to overcome the fluorous-fluorous interactions between the fluorinated papain and the stationary phase, leading to the elution of fluorinated papain. Actually, papain was also collected with water. We hypothesized that the inibition of papain is a tedious reaction, in which the inhibitor must reach the binding pocket to block the enzyme. Consequently, the reaction between papain and compound **2-4** might not be completed. The fraction of protein collected with water is potentially represented by papain not bound to the fluorinated inhibitor and therefore not able to interact with the stationary phase.

In conclusion, a solvent-selective elution was observed. These results let us hypothesize that fluorinated papain might actually be anchored to the resin, making this approach suitable for the fluorous proteomics strategy.

2.8.2 SDS-PAGE

In order to prove the effectiveness of the fluorous proteomics approach, papain was incubated with compound **2-2** as well as with compound **2-3**. The samples were purified by affinity chromatography and the flurophilic elutions were analyzed by SDS-PAGE. **Figure 2.32** shows the electrophoresis results.

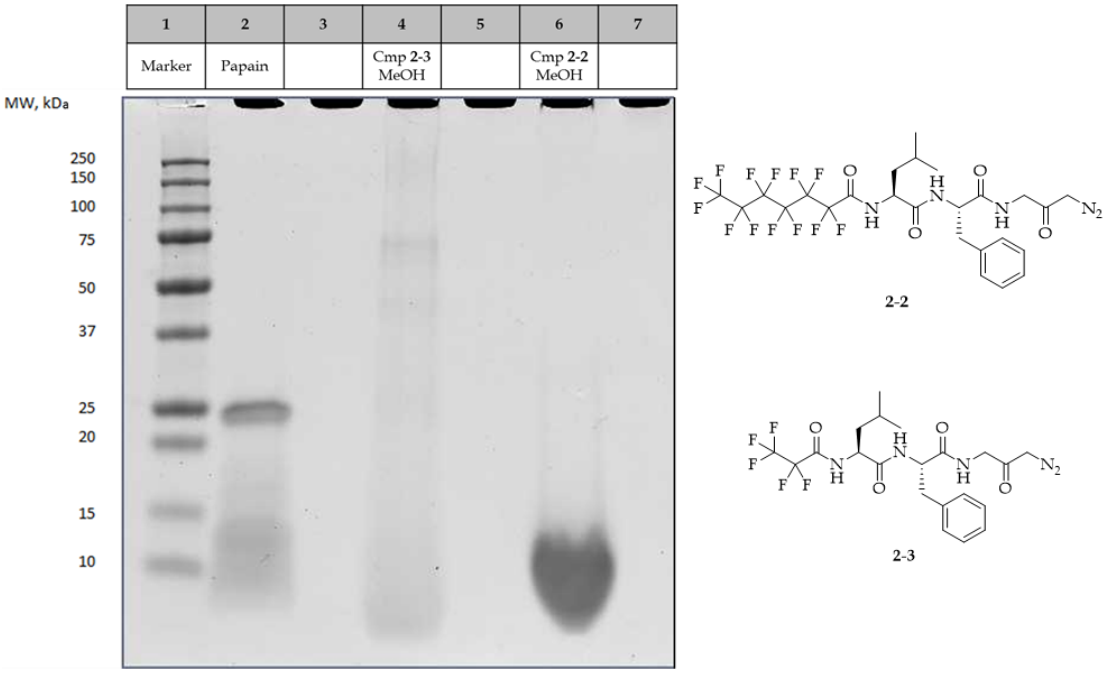

Figure 2.32 SDS-PAGE of fluorophilic elutions of papain previously incubated with compound **2-2** and **2-3**.

In lane 2, an aqueous solution of the commercially available papain was loaded (1 mg/ml; 25 µl). Papain has a molecular weight of 23,800 Dalton and actually, a band at about 24 kDa was observed by SDS-PAGE. However, a spot at lower molecular weights (<15 kDa) was also present. Therefore, to investigate the quality of papain provided by Sigma Aldrich and used for our purposes, we analyzed papain by mass analysis. Surprisingly, we found that the commercially available papain was a mixture of several proteins.

Among them, papaya proteinase, chymopapain and caricain were present. These proteins belong to the papain superfamily as they are papain-like cysteine proteases. They are found in *Carica papaya* latex – as papain – and act as endopeptidases. These papain-like enzymes have molecular weights ranging from 20 to 35 kDa and share a common fold. Indeed, Cys25 and His159 form the catalytic site as for papain. Consequently, diazomethyl ketone derivatives are able to inhibit all papain-like cysteine proteases.[32] Since these proteins are endopeptidases, we hypothesized they might auto-digested as well as be involved in the hydrolysis of papain, leading to peptides responsible for the spot at molecular weights lower than 15 kDa. The methanol elution of papain previously incubated with compound **2-3** was loaded in lane 4. As expected, no significant band or spot was observed. Actually, compound **2-3** brings a fluorinated alkyl chain not long enough for the interaction with the stationary phase. Consequently, proteins bound to compound **2-3** were not retained in the column and potentially were eluted with water. In contrast, compound **2-2** has a longer fluorinated alkyl chain, able to interact with the resin during affinity chromatography. Indeed, protein inhibited by compound **2-2** were eluted with methanol, as demonstrated by SDS-PAGE (**Figure 2.32**, lane 6). The band referred to non-digested inhibited papain-like enzymes (expected at about 24 kDa) was not observed. However, there is a clear spot at molecular weights lower than 15 kDa, probably due to peptides derived from auto-digestion. The obtained results are consistent with the solvent-selective elution observed during affinity chromatography (**Figure 2.29**).

2.8.3 Protein Identification

The proteins eluted with methanol were investigated by mass analysis. With this aim, the spot observed by SDS-PAGE for the inhibited sample (**Figure**

2.32, lane 6) was excised and the proteins digested by trypsin and analyzed by LC-MS/MS. A bioinformatics analysis was performed matching the obtained mass results with *Carica papaya* proteome. Four proteins belonging to the papain superfamily were detected: papain, chymopapain, papaya proteinase, and caricain. The isolated proteins are cysteine endopeptidases, which might auto-digest as well as digest each other. Consequently, proteins were also present as peptides, as demonstrated by SDS-PAGE (**Figure 2.32**). Therefore, the following tryptic digestion led to the formation of shorter peptides. This might have complicated the mass analysis and the target identification as well.

Some of the isolated peptides presented an unmodified cysteine. However, the peptide bearing the catalytic cysteine (Cys25) was not recovered. Actually, diazomethyl ketone derivatives can react only with Cys25, since the mechanism of this reaction involves the formation of a complex with His159, which is part of the catalytic triad. The fact that the peptide carrying Cys25 bound to the fluorinated inhibitor was not observed do not compromise the success of the fluorous proteomics approach. Indeed, it is usual not to find all peptides of a digested protein in a proteomic mass analysis. Furthermore, papain inhibition actually occurred as previously demonstrated by UV assay (**Figure 2.27**), suggesting that the diazomethyl ketone inhibitor bound the protein. In addition, the ability of the fluorinated stationary phase to retain only the inhibited papain (**Figure 2.30** and **Figure 2.31**) implies that the fluorinated inhibitor interacted with papain. The obtained results suggested successful interaction of compound **2-2** with the protein sample, allowing the anchor to the stationary phase.

2.9 Conclusions

Chemical proteomics is a useful tool for target identification. However, it suffers from several disadvantages. In particular, the aspecific binding observed using agarose beads covalently bound to streptavidin as stationary phase is the main issue in traditional chemical proteomics approach. Indeed, proteins that interact aspecifically with the resin are often eluted with the biological target complicating the mass analysis. Therefore, we investigated a new recognition system able to afford a greater selectivity. With this aim, we designed an innovative fluorous proteomics technique based on the strong and noncovalent fluorous-fluorous interactions. In order to validate this new approach, papain was considered as target protein. Fluorinated diazomethyl ketone inhibitors were successfully synthesized and used as probes for applying the fluorous proteomics strategy. Only cysteine proteases belonging to the papain superfamily were selectively isolated by fluorophilic washings during affinity chromatography, demonstrating the effectiveness of the fluorous proteomics approach. Interestingly, papain provided by Sigma Aldrich was a crude *Carica papaya* extract (enzymatic activity ≥ 3 U/mg), containing several proteins, papain-like cysteine proteases among them. The strength of the fluorous proteomics approach was demonstrated by the isolation of proteins showing high homology with papain and belonging to the papain superfamily while proteins with different structures were not be retained by the perfluorinated stationary phase. Therefore, the fluorous proteomics methodology can be successfully applied for target identification.

2.10 Experimental Section

2.10.1 Materials

All reagents were purchased from Sigma-Aldrich and Acros Organics. All solvents were of ACS grade or higher and were obtained from Sigma-Aldrich or Acros Organics. Columns for affinity purification were purchased from Fisher Scientific. All disposal materials and reagents for electrophoresis were purchased from Bio-Rad. Dry reactions were performed under argon using dry solvents and reagents. Reactions were monitored by thin-layer chromatography carried out on 0.25 mm Merck silica gel plates (60F-254) with UV light as the visualizing agent and potassium permanganate or phosphomolibdic acid stains as developing agents. Chromatographic separation was performed using Silicycle 60 Å SiO_2 or Waters 2525 Binary Gradient Module HPLC. Purity was analyzed by HPLC VWR Hitachi Pump L2130. NMR spectra were recorded on Varian Mercury 300 VX (Department of Pharmaceutical Sciences, University of Milan) using appropriate deuterated solvents. Mass spectra were acquired on API 2000 LC/MS/MS System Package Applied Biosystem (University of Milan) and MALDI TOF-TOF AUTOFLEX III Bruker Daltonics (Centro Interdipartimentale Grandi Apparecchiature, University of Milan). Protein separation was performed using electrophoresis cell Mini-PROTEAN® Tetra System Power PAC 300, Mini-PROTEAN® TGX™ Precast gel Any KD™, Laemmli Sample Buffer 4X, Precision Plus Protein Standard, 10X Tris/Glycine/SDS Electrophoresis Buffer, Coomassie Brilliant Blue R-250. Nano LC-MS/MS analysis was performed using Thermo Scientific Q-Exactive mass spectrometer equipped with a nano-electrospray ion source (Proxeon Biosystems) and a nUPLC Easy

nLC 1000 (Proxeon Biosystems). (Protein Microsequencing Facility, San Raffaele Scientific Institute, Milan).

2.10.2 Methods

Purity was measured by reverse phase HPLC according to the method described below:

Time (min)	% A	% B	Flow (ml/min)
0	100	0	0
1	100	0	1
18	0	100	1
22	0	100	1
24	100	0	1
30	100	0	1
31	100	0	0

- phase A: H_2O/CH_3CN/TFA 97:3:0.1
- phase B: H_2O/CH_3CN/TFA 30:70:0.1

Purification of compound **2-1** was performed using preparative HPLC, according to the method described below:

Time (min)	% A	% B	Flow (ml/min)	Gradient
0	95	5	1	linear
1	95	5	14	linear
20	0	100	14	linear
25	0	100	14	linear
26	95	5	14	linear
30	95	5	14	linear
31	95	5	0	linear

- phase A: H_2O/TFA (0.1%)
- phase B: CH_3CN/TFA (0.1%)

Protein identification was performed by desalting aliquots of the sample containing tryptic peptides using StageTip C18. The samples were analysed by nLC-MS/MS using a Q-Exactive mass spectrometer equipped with a nano-electrospray ion source and a nUPLC Easy nLC 1000. Peptide separations occurred on a homemade (75 µm i.d., 12 cm long) reverse phase silica capillary column, packed with 1.9 µm ReproSil-Pur 120 C18-AQ (Dr. Maisch GmbH, Germany). A gradient of eluents A (water with 0.1% v/v formic acid) and B (acetonitrile with 0.1% v/v formic acid) was used to achieve separation (300 nL/min flow rate), from 0% B to 45% B in 45 minutes. Full scan spectra were acquired with the lock-mass option, resolution set to 70,000 and mass range from m/z 300 to 2000 Da. The ten

most intense doubly and triply charged ions were selected and fragmented. All MS/MS samples were analysed using Mascot search engine (version 2.6, Matrix Science) to search the SwissProt Complete Proteome_2016_10 (552,884 sequences; 197,760,918 residues), taxonomy Viridiplantae. Searches were performed with the following settings: trypsin as proteolytic enzyme; 3-missed cleavages allowed; addition of 677.16 Da on cysteine, due to the addition of the fluorinated papain inhibitor compound **2-2**, as fixed modification; protein N-terminus-acetylation, methionine oxidation and carbamidomethylation on cysteine as variable modifications; mass tolerance was set to 5 ppm and to 0.02 Da for precursor and fragment ions, respectively.

2.10.3 General Synthetic Procedures

Procedure 1: Coupling Reaction

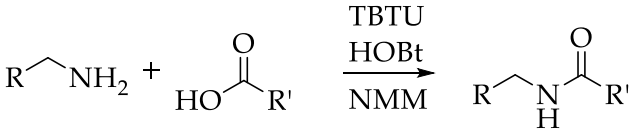

The carboxylic acid (1.1 eq) and the amine (1.0 eq) are dissolved in a suitable solvent (DMF or dichloromethane) (5 ml/mmol) under nitrogen. The mixture is cooled at 0 °C before adding HOBt (1.5 eq) and TBTU (1.2 eq). Then, NMM is added until pH=7-8. The mixture is allowed to react overnight at rt. The solvent is removed under reduced pressure. The residue is taken up in DCM and the organic phase is washed with HCl 1N, saturated aqueous $NaHCO_3$, water, and brine. The organic layer is dried over Na_2SO_4, filtered, and concentrated under reduced pressure.

Procedure 2: Hydrogenolysis

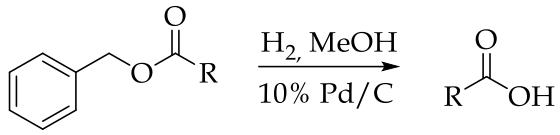

Benzyl-protected compound is dissolved in methanol (10 ml/mmol) and then 10% Pd/C (80 mg/mmol) is added. The mixture is reacted under hydrogen at rt and atmospheric pressure for 1 day. The mixture is filtered and the solvent removed under reduced pressure. The deprotected product is used in the following step without further purification.

Procedure 3: Boc-Deprotection

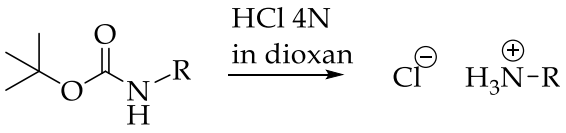

Boc-protected compound is cooled to 0 °C before adding HCl 4N in dioxane (10 ml/g of Boc-protected compound). The mixture is stirred for 30 minutes at rt, then the solvent is evaporated under reduced pressure and the residue is washed three times with ethyl ether. The deprotected product is used in the following step without further purification.

Procedure 4: p-Tolylsulfonylmethylnitrosamine (Diazald®) Synthesis

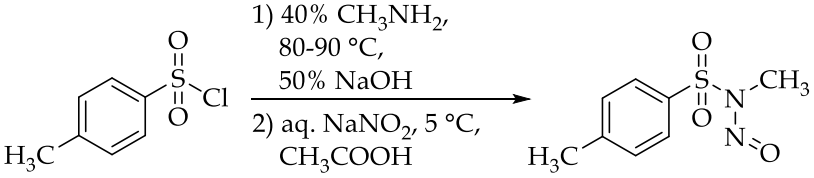

A total of 100 g (0.53 mmol) of p-toluenesulfonyl chloride is divided into three portions of 59.4 g, 28.1 g, and 12.5 g. The first portion is added during about 5 minutes to 52.8 ml (0.63 mmol) of 40% aqueous methylamine contained in a round-bottomed flask. The mixture is allow to heat to 80-90 °C in order to maintain the sulfonylmethylamide in a molten condition. As soon as the mixture has become acidic, as indicated by testing a drop on litmus paper, 15.6 ml of 50% aqueous NaOH (23.5 g NaOH dissolved in 47 ml of H_2O) is added carefully. This is followed immediately by gradual addition of the second portion of the p-toluenesulfonyl chloride as before. When the mixture has become acidic again, 7.8 ml of the aqueous NaOH solution is added, followed by the final portion of p-toluenesulfonyl chloride. After the mixture has again become acidic, the remainder of the aqueous NaOH solution is added. The liquid phase of the final mixture should be alkaline, otherwise methylamine is added to render the mixture basic. The mixture is stirred vigorously for 15 minutes. The hot reaction mixture is poured into 470 ml of glacial acetic acid and the flask is rinsed clean with 80 ml of acetic acid. The solution is cooled in an ice bath to about 5 °C and an aqueous solution of $NaNO_2$ (39.1 g dissolved in 78 ml of H_2O) is added from a dropping funnel during about 45 minutes. The temperature of the mixture must be kept below 10 °C, and stirring is continued for 15 minutes after addition is completed. During the reaction, the nitroso compound separates as a yellow crystalline product. 315 ml of H_2O are added to the mixture. Then, the precipitate is separated by filtration, pressed on the funnel, and washed with about 155 ml of H_2O. The product is transferred to a beaker, stirred well with about 125 ml of H_2O, then filtered and washed again on the funnel. This process is repeated if necessary to remove the odor of acetic acid. After drying to constant weight under vacuo, the product melts in the range between 55 and 60 °C.

Procedure 5: Diazomethane Synthesis

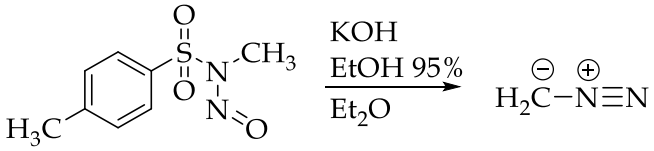

In a round-bottom flask equipped with graduated dropping funnel and Claisen condenser, KOH aqueous solution (3 g dissolved in 5 ml of water), EtOH 95% (5 ml) and Et_2O (5 ml) are added and stirred vigorously. The mixture is heated to 70 °C. The solvents evaporates, vapours are condensated and collected in a round-bottom flask kept at -20 °C. When the condensation starts, a solution of Diazald® (11.25 g dissolved in 65 ml of Et_2O) is added dropwise to the evaporating mixture. Be careful during addition of Diazald® because explosions can occur. Diazomethane is formed and collected as diethyl ether solution in the round-bottom flask at -20 °C. When the reaction is finished, the diethyl ether solution of diazomethane (~ 50 ml) is ready to be used in the following step without further purification. All glassware is neutralized with acetic acid.

Procedure 6: Diazomethyl Ketone Synthesis

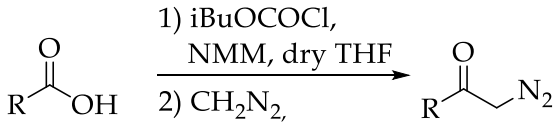

A solution of carboxylic acid (1 eq) and NMM (1.1 eq) in dry THF (4.7 ml/mmol of carboxylic acid) is cooled to -15 °C before adding iBuOCOCl (1.1 eq). Then, the reaction is stirred for 15 minutes at rt. The mixture is filtered and the liquid is cooled to -70 °C before adding the diethyl ether solution of

diazomethane. The mixture is allowed to cool at rt and react overnight. The solvent is evaporated under reduced pressure and the residue is taken up in Et_2O. The organic layer is washed once with saturated aqueous $NaHCO_3$ and once with brine. The organic phase is dried over Na_2SO_4, filtered, and evaporated under reduced pressure.

Procedure 7: Nucleophilic Substitution of Alkoxide

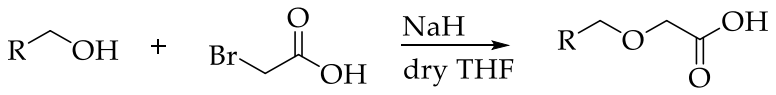

A solution of alcohol (0.5 eq) in dry THF (8.8 ml) is added dropwise to a mixture of NaH (3 eq) in dry THF (8.8 ml) under argon and the mixture is stirred for 1 hour at rt. Then, a solution of bromoacetic acid (1 eq) in dry THF (8.8 ml) is added dropwise. The mixture is stirred for 24 hours, monitoring the reaction by TLC. Once the reaction is completed, the excess of NaH is destroyed by dropwise addition of water. THF is evaporated in vacuo, and HCl 2M is added to the residue prior to extraction with DCM. The organic layer is washed with water, dried over Na_2SO_4, filtered and evaporated under reduced pressure.

2.10.4 General Procedures for Fluorous Proteomics

Procedure 8: Papain Activation

EDTA (263 mg, 0.9 mmol) and papain (334 mg) are dissolved in 100 ml phosphate buffer 85 mM (pH=6.5). Then, β-mercaptoethanol (148 µl, 2.1 mmol) is added and the solution is shaken vigorously for 1 hour. Activated papain is used without further purification.

Procedure 9: Papain Inhibition

Activated papain in phosphate buffer (500 µl) is incubated with a solution of the inhibitor in DMF (56 mM, 45 µl). Papain inhibition is completed after 15 minutes.

Procedure 10: Affinity Chromatography Procedure

The fluorinated stationary phase (1 g) is placed in a Pierce Centrifuge column and washed with Milli-Q water (6 CV). The protein sample is loaded and then incubated for 10 minutes to promote the interaction with the fluorinated resin. Non-fluorinated components are then gravity eluted with Milli-Q water (4 CV) and discarded. Then, the fluorinated components are selectively gravity eluted using MeOH (4 CV). The combined methanolic washings are dried under reduced pressure. The stationary phase can be recycled by washing with acetone (6 CV).

Procedure 11: SDS-PAGE Purification

Laemmli sample buffer 4X (12.5 µl) and DTT 200 mM (12.5 µl) are added to the eluted sample (25 µl) and then heated at 99 °C for 5 minutes.
The electrophoresis cell is filled with an aqueous solution of running buffer (25 mM Tris, 192 mM Gly, 0.1% SDS; pH=8.3. Prepare the electrophoresis buffer by mixing 70 ml of the running buffer with 630 ml of fresh Milli-Q water).
Polyacrylamide gel is put inside the electrophoresis tank before loading denaturated samples and marker into the gel wells. The tank is covered and the power supply is turned on to start the separation. The running voltage is 200 V and the run time is about 30 minutes. When bromophenol blue

tracking dye reaches the gel bottom, the separation must be stopped. The gel is put in Milli-Q water and gently shaken. The Milli-Q water is then discarded and fresh Milli-Q water is added, keeping the gel shaken.

Procedure 12: Gel Staining

Coomassie Brilliant Blue is added to completely cover the gel. Then, the gel is gently shaken until protein bands can be observed. Coomassie staining is discarded and Milli-Q water is added to the gel. Milli-Q water is replenished several times until background of the gel is fully destained.

Procedure 13: Protein Digestion

Gel band is excised using a scalpel as closely to the staining boundary as possible. The gel band is cut and the size of gel pieces must be reduced to 1-2 mm in each dimension to promote the peptide recovery. Gel pieces are put into an eppendorf and destained with 0.1 ml of destaining solution (50% 25 mM NH_4CO_3/50% CH_3CN). The destaining solution becomes light blue and can be discarded. This operation must be repeated. 0.3 ml of reducing solution (10 mM DTT in 50 mM NH_4HCO_3) are added to reduce disulfide bonds. The mixture is centrifuged for 45 minutes at 56 °C to 1000 rpm, then the reducing solution is discarded. To remove completely the reducing solution, gel pieces are washed with digestion buffer (50 mM NH_4HCO_3 in Milli-Q water). Then, 0.3 ml of alkylating solution (55 mM 2-iodoacetamide in 50 mM NH_4HCO_3) are added to alkylate the free thiol groups. The sample must be kept in the dark for 30 minutes and then is incubated with 0.9 ml CH_3CN at rt. Gel pieces become tough and white. CH_3CN is removed and gel pieces are allowed to dry under air. Gel pieces are treated with trypsin

V5111A Promega (0.21 ml) previously diluted with buffer digestion. The sample is shaken overnight at 37 °C.

Procedure 14: Peptides Extraction

TFA 50% (0.002 ml) is added to the sample to stop the protein digestion. The solution is collected in a new eppendorf. 0.1 ml of extraction solution (3% TFA/30% CH_3CN in Milli-Q water) are added to the gel pieces and then are centrifuged at rt to 1400 rpm. The extraction solution is pipetted in the eppendorf containing the digested protein. Gel pieces are treated again with the extraction solution as described above. CH_3CN (0.2 ml) is added to the gel pieces and are incubated for 10 minutes at rt until they become tough and white. CH_3CN is pipetted in the same eppendorf and this operation is repeated. Peptides are dried under vacuum. The formation of a white or light blue pellet might be observed.

2.10.5 Specific Synthetic Procedures

Intermediate 2-6

Benzyl (tert-butoxycarbonyl)-L-phenylalanylglycinate

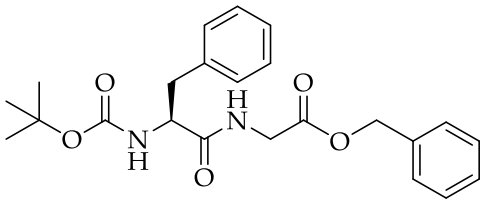

Boc-L-Phe-OH and Gly benzyl ester were coupled according to general procedure **1** and using the following reactants:

- 2.59 g Boc-Phe-OH, 9.78 mmol (1.1 eq)
- 3.00 g Gly benzyl ester p-toluenesulfonate salt, 8.89 mmol (1 eq)
- 3.42 g TBTU, 10.7 mmol (1.2 eq)
- 1.80 g HOBt, 13.3 mmol (1.5 eq)
- 4.9 ml NMM, 44.4 mmol (5 eq)
- 11 ml dry DMF

The reaction was monitored by TLC and then extracted with DCM. Intermediate **2-6** was isolated as white solid (3.28 g, 7.95 mmol, 89%).

R_f = 0.81 (DCM/MeOH 9:1)

^{1}H NMR (300 MHz, Chloroform-d) δ 7.45 – 7.14 (m, 10H), 6.41 (t, *J* = 5.4 Hz, 1H), 5.16 (s, 2H), 4.96 (bs, 1H), 4.40 (t, *J* = 7.4 Hz, 1H), 4.08 (dd, *J* = 18.3, 5.4 Hz, 1H), 3.96 (dd, *J* = 18.4, 5.1 Hz, 1H), 3.09 (d, *J* = 7.5 Hz, 2H), 1.39 (s, 9H).

ESI-MS, *m/z*: 411.22 $[M-H]^-$

Intermediate 2-7

Benzyl (tert-butoxycarbonyl)-L-leucyl-L-phenylalanylglycinate

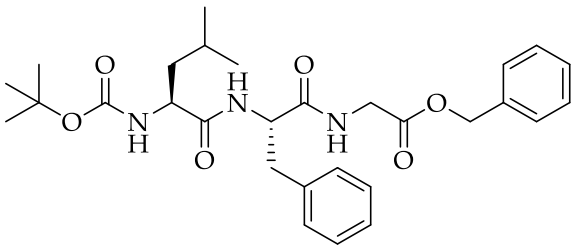

Intermediate **2-7** was obtained by coupling (general procedure **1**) Boc-L-Leu-OH and intermediate **2-6**, previously deprotected according to general procedure **3**.

For the deprotection reaction, the following reagents were used:

- 32.8 ml HCl 4N in dioxan
- 3.28 g intermediate **2-6**, 7.95 mmol

For the coupling reaction, the following reagents were used:

- 2.18 g Boc-L-Leu-OH, 8.75 mmol (1.1 eq)
- 3.06 g TBTU, 9.54 mmol (1.2 eq)
- 1.61 g HOBt, 11.9 mmol (1.5 eq)
- 3.50 ml NMM, 31.8 mmol (4 eq)
- 23 ml dry DMF

The reaction was monitored by TLC and then extracted with DCM. The crude product was purified by silica gel column chromatography (DCM/MeOH, from 100:0 to 98:2). Intermediate **2-7** was isolated as white solid (2.78 g, 5.29 mmol, 67%).

R_f = 0.88 (DCM/MeOH 9:1)

^{1}H NMR (300 MHz, Chloroform-*d*) δ 7.43 – 7.16 (m, 11H), 6.68 (bs, 1H), 6.48 (d, *J* = 8.1 Hz, 1H), 5.15 (s, 2H), 4.79 – 4.62 (m, 2H), 4.08 (dd, *J* = 18.0, 6.0 Hz, 1H), 3.91 (dd, *J* = 18.0, 6.0 Hz, 1H), 3.14 (d, *J* = 4.7 Hz, 2H), 1.68 – 1.48 (m, 3H), 1.38 (s, 9H), 0.89 (t, *J* = 6.4 Hz, 6H).

ESI-MS, *m/z*: 524.21 $[M-H]^-$

Intermediate 2-8

(2,2,3,3,4,4,5,5,6,6,7,7,7-tridecafluoroheptanoyl)-L-leucyl-L-phenylalanylglycine

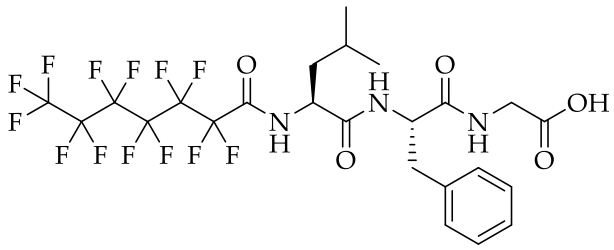

Intermediate **2-8** was prepared by coupling (general procedure **1**) perfluoroheptanoic acid and intermediate **2-7**, previously deprotected according to general procedure **3**. The resulting product was then deprotected according to general procedure **2**.

For the Boc-deprotection, the following reagents were used:

- 5 ml HCl 4N in dioxan
- 500 mg intermediate **2-7**, 0.95 mmol

For the coupling reaction, the following reagents were used:

- 484.2 mg perfluoroheptanoic acid, 1.33 mmol (1.4 eq)
- 293.0 mg DCC, 1.42 mmol (1.5 eq)
- 6.0 mg DMAP, 0.05 mmol (1/20 eq)
- 0.21 ml NMM, 1.9 mmol (2 eq)
- 5 ml DCM

For the hydrogenolysis, the following reagents were used:

- 9.5 ml MeOH
- 76.0 mg 10% Pd/C

The coupling reaction was monitored by TLC and the mixture extracted with DCM. The crude product was purified by silica gel column chromatography (DCM/MeOH, from 100:0 to 98:2) before hydrogenolysis. Intermediate **2-8** was isolated as white solid (115.8 mg, 0.17 mmol, 18%).

R_f = 0.51 (DCM/MeOH 9:1)

^{1}H NMR (300 MHz, Methanol-d_4) δ 9.26 (d, *J* = 8.1 Hz, 1H), 8.30 (d, *J* = 8.1 Hz, 1H), 8.21 (t, *J* = 5.8 Hz, 1H), 7.30 – 7.13 (m, 5H), 4.72 – 4.61 (m, 1H), 4.58 – 4.47 (m, 1H), 3.92 – 3.88 (m, 2H), 3.18 (dd, *J* = 13.9, 5.5 Hz, 1H), 2.94 (dd, *J* = 13.9, 8.8 Hz, 1H), 1.72 – 1.48 (m, 3H), 0.93 (d, *J* = 5.8 Hz, 3H), 0.89 (d, *J* = 5.8 Hz, 3H).

^{19}F NMR (282 MHz, Methanol-d_4) δ -82.08 – -82.60 (m, 3F), -120.36 – -120.55 (m, 2F), -120.64 – -120.88 (m, 2F), -122.52 – -122.90 (m, 2F), -123.50 – -124.11 (m, 2F), -127.23 – -127.51 (m, 2F).

ESI-MS, *m/z*: 680.25 $[M-H]^-$

Intermediate 2-9

Benzyl (2,2,3,3,3-pentafluoropropanoyl)-L-leucyl-L-phenylalanylglycinate

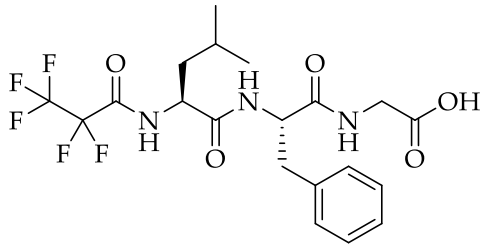

Intermediate **2-7** (0.95 mmol, 1 eq) was Boc-deprotected according to general procedure **3**, using the following reagents:

- 5 ml HCl 4N in dioxan
- 500 mg intermediate **2-7**, 0.95 mmol

Deprotected intermediate **2-7** was dissolved in DCM (3 ml) and cooled to 0 °C. Then, TEA (0.66 ml, 4.75 mmol, 5 eq) was added to get pH=8. Pentafluoropropionic anhydride (0.23 ml, 1.14 mmol, 1.2 eq) was added dropwise and the mixture was allowed to react overnight at rt. The reaction was monitored by TLC. The solvent was removed under reduced pressure and the residue was taken up in DCM. The organic layer was washed three times with HCl 1N, three times with saturated aqueous $NaHCO_3$, twice with water and with brine. The organic layer was dried over $MgSO_4$, filtered and the solvent evaporated under reduced pressure. The crude product was purified by silica gel column chromatography (DCM/MeOH, from 100:0 to 96:4). The resulting product was deprotected according to general procedure **2** using the following reagents:

- 8.5 ml MeOH
- 68 mg 10% Pd/C

Intermediate **2-9** was isolated as white solid (317.0 mg, 0.66 mmol, 69%).

R_f = 0.15 (DCM/MeOH 9:1)

^{1}H NMR (300 MHz, Methanol-d_4) δ 8.28 (d, *J* = 8.1 Hz, 1H), 8.20 (s, 1H), 7.40 – 7.11 (m, 6H), 4.70 – 4.58 (m, 1H), 4.51 (dd, *J* = 10.6, 4.0 Hz, 1H), 3.92 – 3.84 (m, 2H), 3.17 (dd, *J* = 14.1, 5.6 Hz, 1H), 2.93 (dd, *J* = 14.1, 8.8 Hz, 1H), 1.71 – 1.42 (m, 3H), 0.93 (d, *J* = 6 Hz, 3H), 0.88 (d, *J* = 6 Hz, 3H).

^{19}F NMR (282 MHz, Chloroform-*d*) δ -81.98 – -83.14 (m, 3F), -122.15 – -123.74 (m, 2F).

ESI-MS, *m/z*: 480.13 $[M-H]^-$

Intermediate 2-10

2-((2,2,3,3,4,4,5,5,6,6,7,7,8,8,8-pentadecafluorooctyl)oxy)acetic acid

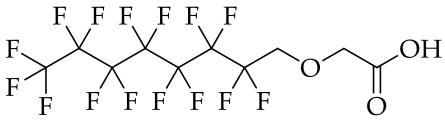

Intermediate **2-10** was prepared according to general procedure **7**.
The following reagents were used:

- 700.0 mg 1H,1H-pentadecafluoroheptanol (1.75 mmol, 0.5 eq) in dry THF (8.8 ml)
- 252.0 mg NaH (10.5 mmol, 3 eq) in dry THF (8.8 ml)
- 486.3 mg bromoacetic acid (3.5 mmol, 1 eq) in dry THF (8.8 ml)

Intermediate **2-10** was isolated as white solid (723.8 mg, 1.58 mmol, 90%) and used in the following step without further purification.

R_f = 0.38 (DCM/MeOH 9:1)

^{1}H NMR (300 MHz, Chloroform-*d*) δ 4.33 (s, 2H), 4.13 (t, *J* = 13.6 Hz, 2H).

^{19}F NMR (282 MHz, Chloroform-*d*) δ -80.78 (t, *J* = 9.9 Hz, 3F), -119.68 – -120.07 (m, 2F), -121.85 – -122.42 (m, 4F), -122.64 – -123.09 (m, 2F), -123.20 – -123.49 (m, 2F), -125.96 – -126.34 (m, 2F).

ESI-MS, *m/z*: 457.00 $[M-H]^-$

Intermediate 2-11

Benzyl (2-((2,2,3,3,4,4,5,5,6,6,7,7,8,8,8-pentadecafluorooctyl)oxy)acetyl)-L-leucyl-L-phenylalanylglycinate

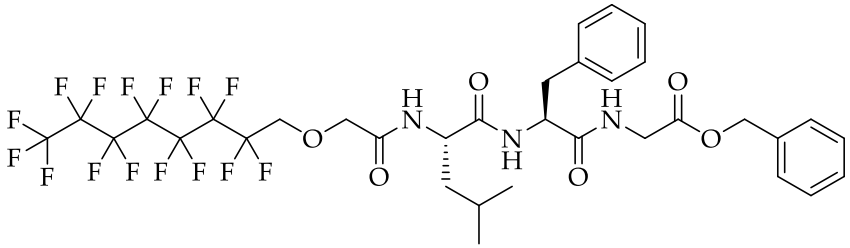

Intermediate **2-11** was obtained by coupling (general procedure **1**) intermediate **2-10** and intermediate **2-7**, previously deprotected according to general procedure **3**.

For the deprotection reaction, the following reagents were used:

- 0.6 ml HCl 4N in dioxan
- 58.3 mg intermediate **2-7**, 0.11 mmol

For the coupling reaction, the following reagents were used:

- 71.5 mg intermediate **2-10**, 0.16 mmol (1.4 eq)
- 0.027 ml DIC, 0.17 mmol (1.5 eq)
- 0.7 mg DMAP, 0.006 mmol (1/20 eq)
- 0.024 ml NMM, 0.22 mmol (2 eq)
- 2.2 ml DCM

The reaction was monitored by TLC and then extracted with DCM. The crude product was purified by silica gel column chromatography (DCM/MeOH, from 100:0 to 97:3). Intermediate **2-11** was isolated as white solid (53.1 mg, 0.061 mmol, 55%).

R_f = 0.88 (DCM/MeOH 9:1)

^{1}H NMR (300 MHz, Chloroform-*d*) δ 7.44 – 7.14 (m, 11H), 6.60 (d, *J* = 7.7 Hz, 1H), 6.52 (t, *J* = 5.5 Hz, 1H), 5.16 (s, 2H), 4.41 – 4.28 (m, 2H), 4.17 – 3.87 (m, 6H), 3.16 (dd, *J* = 14.2, 6.5 Hz, 1H), 3.07 (dd, *J* = 14.2, 7.6 Hz, 1H), 1.75 – 1.38 (m, 3H), 0.90 (d, *J* = 6.0 Hz, 3H), 0.87 (d, *J* = 6.0 Hz, 3H).

^{19}F NMR (282 MHz, Chloroform-*d*) δ -80.72 (t, *J* = 10.0 Hz, 3F), -119.45 – -119.60 (m, 2F), -121.78 – -122.18 (m, 4F), -122.63 – -122.89 (m, 2F), -122.97 – -123.42 (m, 2F), -125.94 – -126.19 (m, 2F).

ESI-MS, *m/z*: 864.34 $[M-H]^-$

Intermediate 2-12

1,3-bis(2,2,3,3,3-pentafluoropropoxy)propan-2-ol

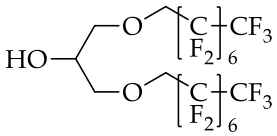

2,2,3,3,4,4,5,5,6,6,7,7,8,8,8-pentadecafluoro-1-octanol (700.0 mg, 1.75 mmol, 3.5 eq) was heated to 120 °C before adding crushed NaOH (40.0 mg, 1 mmol, 2 eq) under argon. The mixture was kept at 120 °C for 30 minutes. Then, epichlorohydrin (0.04 ml, 0.5 mmol, 1 eq) was added and the mixture was allowed to react overnight at this temperature. The mixture was cooled to rt, diluted with 180 ml distilled water and the aqueous layer was extracted with DCM. The organic phase was dried over Na_2SO_4, filtered and evaporated under reduced pressure.

Intermediate **2-12** was isolated as oily residue (300.0 mg, 0.35 mmol, 70%) and used in the following step without further purification.

R_f= 0.36 (cyclohexane/EtOAc 7:3)

^{1}H NMR (300 MHz, Chloroform-*d*) δ 4.08 – 3.86 (m, 5H), 3.70 (d, *J* = 4.9 Hz, 4H), 2.28 (s, 1H).

^{19}F NMR (282 MHz, Chloroform-*d*) δ -80.95 (t, *J* = 10.1 Hz, 6F), -119.55 – -120.09 (m, 4F), -121.94 – -122.63 (m, 8F), -122.68 – -123.22 (m, 4F), -123.32 – -123.80 (m, 4F), -126.07 – -126.59 (m, 4F).

ESI-MS, *m/z*: 901.10 $[M+HCOO]^-$

Intermediate 2-13

2-((1,3-bis(2,2,3,3,3-pentafluoropropoxy)propan-2-yl)oxy)acetic acid

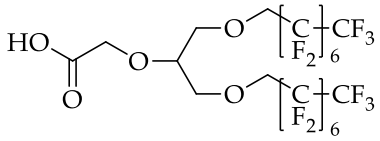

Intermediate **2-13** was prepared according to general procedure **7**.
The following reagents were used:

- 502.7 mg intermediate **2-12** (0.59 mmol, 0.5 eq) in dry THF (6.3 ml)
- 85.0 mg NaH (3.54 mmol, 3 eq) in dry THF (6.3 ml)
- 164.1 mg bromoacetic acid (1.18 mmol, 1 eq) in dry THF (6.3 ml)

Intermediate **2-13** was isolated as yellow oil (468.8 mg, 0.51 mmol, 86%) and used in the following step without further purification.

R_f= 0.41 (cyclohexane/EtOAc 7:3)

^{1}H NMR (300 MHz, Chloroform-*d*) δ 4.31 – 4.24 (m, 1H), 4.09 – 3.95 (m, 6H), 3.71 (d, *J* = 4.4 Hz, 4H).

^{19}F NMR (282 MHz, Chloroform-*d*) δ -80.67 – -81.15 (m, 6F), -119.48 – -120.05 (m, 4F), -121.83 – -122.54 (m, 8F), -122.59 – -123.20 (m, 4F), -123.30 – -123.80 (m, 4F), -125.97 – -126.49 (m, 4F).

ESI-MS, *m/z*: 456.99 $[(M-2H)/2]^{2-}$

Intermediate 2-14

benzyl (2-((1,3-bis((2,2,3,3,4,4,5,5,6,6,7,7,8,8,8-pentadecafluorooctyl)oxy)propan-2-yl)oxy)acetyl)-L-leucyl-L-phenylalanylglycinate

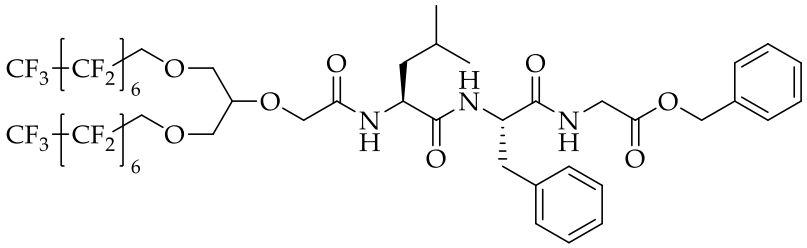

Intermediate **2-14** was prepared by coupling (general procedure **1**) intermediate **2-13** and intermediate **2-7**, previously deprotected according to general procedure **3**.

For the deprotection reaction, the following reagents were used:

- 1.92 ml HCl 4N in dioxan
- 191.8 mg intermediate **2-7**, 0.36 mmol

For the coupling reaction, the following reagents were used:

- 468.8 mg intermediate **2-13**, 0.51 mmol (1.4 eq)
- 0.085 ml DIC, 0.54 mmol (1.5 eq)
- 2.44 mg DMAP, 0.02 mmol (1/20 eq)
- 0.08 ml NMM, 0.72 mmol (2 eq)
- 3.6 ml dry DMF

The reaction was monitored by TLC and then extracted with DCM. The crude product was purified by silica gel column chromatography (DCM/MeOH, from 100:0 to 98:2). Intermediate **2-14** was isolated as yellow oil (43.8 mg, 0.033 mmol, 9%).

R_f= 0.96 (DCM/MeOH 9:1)

^{1}H NMR (300 MHz, Chloroform-*d*) δ 7.42 – 7.15 (m, 10H), 6.65 (d, *J* = 7.7 Hz, 1H), 6.59 (d, *J* = 7.6 Hz, 1H), 6.51 (t, *J* = 7.0 Hz, 1H), 5.16 (s, 2H), 4.78 – 4.62 (m, 1H), 4.42 – 4.27 (m, 1H), 4.24 – 3.83 (m, 9H), 3.82 – 3.55 (m, 4H), 3.11 (dd, *J* = 14.2, 7.1 Hz, 2H), 1.78 – 1.40 (m, 3H), 0.97 – 0.76 (m, 6H).

^{19}F NMR (282 MHz, Chloroform-*d*) δ -80.62 – -80.96 (m, 6F), -119.29 – -120.04 (m, 4F), -121.87 – -122.26 (m, 8F), -122.67 – -123.01 (m, 4F), -123.06 – -123.56 (m, 4F), -126.03 – -126.28 (m, 4F).

ESI-MS, *m/z*: 1322.01 $[M+H]^+$

Compound 2-1

4-nitrophenyl((benzyloxy)carbonyl)glycinate

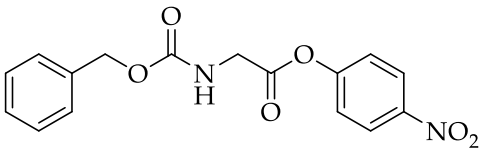

Compound **2-1** was synthesized by coupling (general procedure **1**) p-nitrophenol and Z-Gly-OH. The following reagents were used:

- 0.61 g Z-Gly-OH, 2.9 mmol (1.1 eq)
- 0.36 g p-nitrophenol, 2.6 mmol (1 eq)
- 1.48 g HBTU, 3.9 mmol, (1.5 eq)
- 0.35 g DMAP, 2.9 mmol (1.1 eq)
- 11 ml DCM

The reaction was monitored by TLC and then extracted with DCM. The crude product was purified by HPLC. Compound **2-1** was isolated as white solid (0.54 g, 1.64 mmol, 63%).

R_f = 0.72 (DCM/MeOH 9:1)

^{1}H NMR (300 MHz, Chloroform-*d*) δ 8.28 (d, *J* = 8.7 Hz, 2H), 7.42 – 7.28 (m, 7H), 5.28 (bs, 1H), 5.17 (s, 2H), 4.28 (d, *J* = 5.5 Hz, 2H).

ESI-MS, *m/z*: 329.35 $[M-H]^-$

Compound 2-2

N-((S)-1-(((S)-1-((3-diazo-2-oxopropyl)amino)-1-oxo-3-phenylpropan-2-yl)amino)-4-methyl-1-oxopentan-2-yl)-2,2,3,3,4,4,5,5,6,6,7,7,7-tridecafluoroheptanamide

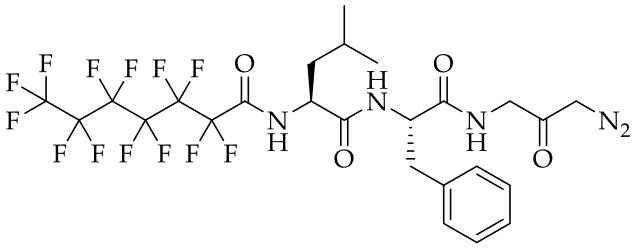

Compound **2-2** was synthesized following general procedure **6** from intermediate **2-8** and diazomethane previously prepared according to general procedures **4** and **5**.

The reagents listed below were used:

- 84.0 mg intermediate **2-8**, 0.13 mmol (1 eq)
- 0.018 ml iBuOCOCl, 0.14 mmol (1.1 eq)
- 0.015 ml NMM, 0.14 mmol (1.1 eq)
- 50 ml CH_2N_2
- 0.6 ml dry THF

Compound **2-2** was isolated as yellow oil (77.7 mg, 0.11 mmol, 85%) and used for fluorous proteomics without further purification.

ESI-MS, *m/z*: 678.06 [M-N_2]

Compound 2-3

(S)-N-((S)-1-((3-diazo-2-oxopropyl)amino)-1-oxo-3-phenylpropan-2-yl)-4-methyl-2-(2,2,3,3,3-pentafluoropropanamido)pentanamide

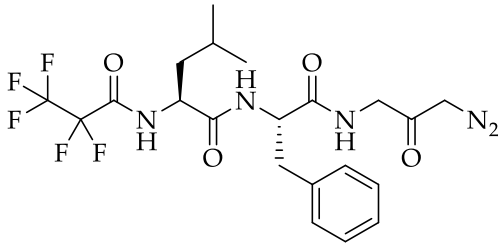

Compound **2-3** was synthesized following general procedure **6** from intermediate **2-9** and diazomethane prepared according to general procedures **4** and **5**.

The reagents listed below were used:

- 51.0 mg intermediate **2-9**, 0.11 mmol (1 eq)
- 0.016 ml iBuOCOCl, 0.12 mmol (1.1 eq)
- 0.013 ml NMM, 0.12 mmol (1.1 eq)
- 50 ml CH_2N_2
- 0.52 ml dry THF

Compound **2-3** was isolated as yellow oil (45.7 mg, 0.09 mmol, 82%) and used for fluorous proteomics without further purification.

ESI-MS, *m/z*: 478.03 [M-N_2]

Compound 2-4

(S)-N-((S)-1-((3-diazo-2-oxopropyl)amino)-1-oxo-3-phenylpropan-2-yl)-4-methyl-2-(2-((2,2,3,3,4,4,5,5,6,6,7,7,8,8,8-pentadecafluorooctyl)oxy)acetamido)pentanamide

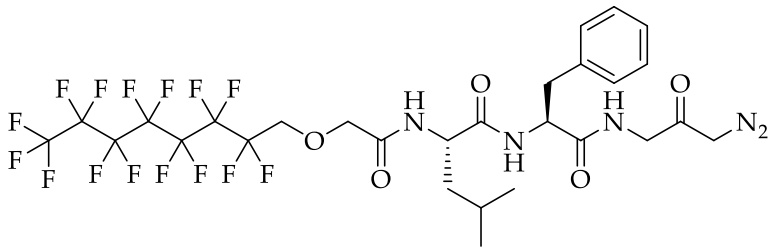

Compound **2-4** was synthesized following general procedure **6** from intermediate **2-11**, previously deprotected according to procedure **2**, and diazomethane prepared according to procedures **4** and **5**.

For the deprotection of intermediate **2-11**, the following reagents were used:

- 126.1 mg intermediate **2-11**, 0.15 mmol (1 eq)
- 28.0 mg 10% Pd/C
- 3.5 ml MeOH

For the synthesis of compound **2-4**, the reagents listed below were used:

- 0.022 ml iBuOCOCl, 0.17 mmol (1.1 eq)
- 0.019 ml NMM, 0.17 mmol (1.1 eq)
- 50 ml CH_2N_2
- 0.71 ml dry THF

Compound **2-4** was isolated as yellow oil (104.1 mg, 0.13 mmol, 87%) and used for fluorous proteomics without further purification.

ESI-MS, *m/z*: 771.94 [M-N_2]

Compound 2-5

(S)-2-(2-((1,3-bis((2,2,3,3,4,4,5,5,6,6,7,7,8,8,8-pentadecafluorooctyl)oxy)propan-2-yl)oxy)acetamido)-N-((S)-1-((3-diazo-2-oxopropyl)amino)-1-oxo-3-phenylpropan-2-yl)-4-methylpentanamide

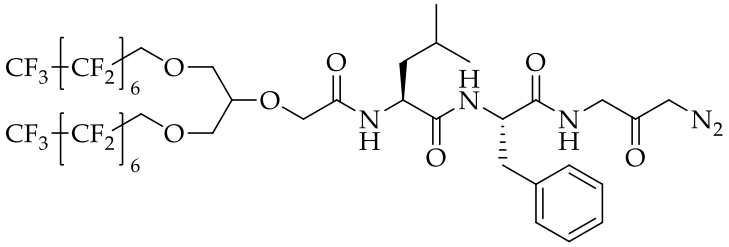

Compound **2-5** was synthesized following general procedure **6** from intermediate **2-14**, previously deprotected according to procedure **2**, and diazomethane prepared according to procedures **4** and **5**.

For the deprotection of intermediate **2-14**, the following reagents were used:

- 42.5 mg intermediate **2-14**, 0.032 mmol (1 eq)
- 16 mg 10% Pd/C
- 2 ml MeOH

For the synthesis of compound **2-5**, the reagents listed below were used:

- 4.54 µl iBuOCOCl, 0.035 mmol (1.1 eq)
- 3.60 µl NMM, 0.035 mmol (1.1 eq)
- 50 ml CH_2N_2
- 0.15 ml dry THF

Compound **2-5** was isolated as yellow oil (37.7 mg, 0.03 mmol, 94%) and used for fluorous proteomics without further purification.

ESI-MS, *m/z*: 629.23 $[(M+2H)/2]^{2+}$

2.11 References

1. Bantscheff, M., Scholten, A. & Heck, A. J. R. Revealing Promiscuous Drug-Target Interactions by Chemical Proteomics. *Drug Discov. Today* **14,** 1021–1029 (2009).
2. Rix, U. & Superti-Furga, G. Target Profiling of Small Molecules by Chemical Proteomics. *Nat. Chem. Biol.* **5,** 616–624 (2009).
3. Huang, F. *et al.* Chemical Proteomics: Terra Incognita for Novel Drug Target Profiling. *Chin J Cancer* **31,** 507–518 (2012).
4. Park, K. D., Liu, R. & Kohn, H. Useful Tools for Biomolecule Isolation, Detection, and Identification: Acylhydrazone-Based Cleavable Linkers. *Chem. Biol.* **16,** 763–772 (2009).
5. Speers, A. E. & Cravatt, B. F. A Tandem Orthogonal Proteolysis Strategy for High-Content Chemical Proteomics. *J. Am. Chem. Soc.* **127,** 10018–10019 (2005).
6. van der Veken, P. *et al.* Development of a Novel Chemical Probe for the Selective Enrichment of Phosphorylated Serine- and Threonine-Containing Peptides. *ChemBioChem* **6,** 2271–2280 (2005).
7. Piggott, A. M. & Karuso, P. Synthesis of a New Hydrophilic o -Nitrobenzyl Photocleavable Linker Suitable for Use in Chemical Proteomics. *Tetrahedron Lett.* **46,** 8241–8244 (2005).
8. Koopmans, T., Dekker, F. J. & Martin, N. I. A Photocleavable Affinity Tag for the Enrichment of Alkyne-Modified Biomolecules. *RSC Adv.* **2,** 2244–2246 (2012).
9. Steen, H. & Mann, M. A New Derivatization Strategy for the Analysis of Phosphopeptides by Precursor Ion Scanning in Positive Ion Mode. *J. Am. Soc. Mas Spec.* **13,** 996–1003 (2002).
10. Oda, Y., Nagasu, T. & Chait, B. T. Enrichment Analysis of Phosphorylated Proteins as a Tool for Probing the Phosphoproteome.

Nat. Biotechnol. **19,** 379–382 (2001).

11. Brittain, S. M., Ficarro, S. B., Brock, A. & Peters, E. C. Enrichment and Analysis of Peptide Subsets Using Fluorous Affinity Tags and Mass Spectrometry. *Nat. Biotechnol.* **23,** 463–468 (2005).
12. Curran, D. P., Hadida, S. & He, M. Thermal Allylations of Aldehydes with a Fluorous Allylstannane. Separation of Organic and Fluorous Products by Solid Phase Extraction with Fluorous Reverse Phase Silica Gel. *J. Org. Chem.* **62,** 6714–6715 (1997).
13. Zhang, W. & Curran, D. P. Synthetic Applications of Fluorous Solid-Phase Extraction (F-SPE). *Tetrahedron* **62,** 11837–11865 (2006).
14. Dell' Agli, M. P. *et al.* High Antiplasmodial Activity of Novel Plasmepsins I and II Inhibitors. *J. Med. Chem.* **49,** 7440–7449 (2006).
15. Romeo, S. *et al.* Plasmepsin II Inhibition and Antiplasmodial Activity of Primaquine–Statine 'double-drugs'. *Bioorg. Med. Chem. Lett.* **14,** (2004).
16. Philip, A., Kepler, J. A., Johnson, B. H. & Carroll, F. I. Peptide Derivatives of Primaquine as Potential Antimalarial Agents. *J. Med. Chem.* **31,** 870–874 (1988).
17. Mok, S. *et al.* Artemisinin Resistance in Plasmodium Falciparum Is Associated with an Altered Temporal Pattern of Transcription. *BMC Genomics* **12,** 391 (2011).
18. Trape, J. F. The Public Health Impact of Chloroquine Resistance in Africa. *Am. J. Trop. Med. Hyg.* **64,** 12–17 (2001).
19. Karen, I. B. *Milestones in Drug Therapy.* (2012).
20. Dandapani, S. Recent Applications of Fluorous Separation Methods in Organic and Bioorganic Chemistry. *QSAR Comb. Sci.* **25,** 681–688 (2006).
21. Dreuth, J., Jansonius, J., Koekoek, R., Swen, H. & Wolters, B. Stucture of Papain. *Nature* **218,** 929 (1968).
22. Alecio, M. R., Dann, M. L. & Lowe, G. The Specificity of the S1 Subsite

of Papain. *Biochem. J.* **141,** 495–501 (1974).

23. Janowski, R., Kozak, M., Janowska, E., Grzonka, Z. & Jaskolski, M. Two Polymorphs of a Covalent Complex between Papain and a Diazomethylketone Inhibitor. *J. Pept. Res.* **64,** 141–150 (2004).
24. Haquette, P. *et al.* Cysteine-Specific, Covalent Anchoring of Transition Organometallic Complexes to the Protein Papain from Carica papaya. *ChemBioChem* **8,** 224–231 (2007).
25. Elshani, S., Kobzar, E. & Bartsch, A. R. Macrocyclic Ligands with Partially Fluorinated Sidearms: Synthesis and Metal Ion Complexation. *Tetrahedron* **56,** 3291–3301 (2000).
26. Albericio, F., Chinchilla, R., Dodsworth, D. & Najera, C. New Trends in Peptide Coupling Reagents. *Org. Prep. Proced. Int.* **33,** 203–313 (2001).
27. Valeur, E. & Bradley, M. Amide Bond Formation: beyond the Myth of Coupling Reagents. *Chem. Soc. Rev.* **38,** 606–631 (2009).
28. Brocklehurst, K. & Malthouse, J. P. G. Mechanism of the Reaction of Papain with Substrate-Derived Diazomethyl Ketones. *Biochem. J.* **175,** 761–764 (1978).
29. Parlato, M. C., Jee, J. P., Teshite, M. & Mecozzi, S. Synthesis, Characterization, and Applications of Hemifluorinated Dibranched Amphiphiles. *J. Org. Chem.* **76,** 6584–6591 (2011).
30. Green, G. D. J. & Shaw, E. Peptidyl Diazomethyl Ketones are Specific Inactivators of Thiol Proteinases. *J. Biol. Chem.* **256,** 1923–1928 (1981).
31. Leary, R., Larsen, D., Watanabe, H. & Shaw, E. Diazomethyl Ketone Substrate Derivatives as Active-Site-Directed Inhibitors of Thiol Proteases. Papain. **16,** 5857–5861 (1977).
32. Turk, D., Guncar, G., Podobnik, M. & Turk, B. Revised Definition of Substrate Binding Sites of Papain-Like Cysteine Proteases. *Biol. Chem.* **379,** 137–147 (1998).

Chapter 3

Noncovalent Fluorous Interactions: New Approaches for Drug Delivery

3.1 Fluorinated Amphiphiles for Drug Delivery

Colloidal carrier systems composed of amphiphilic block copolymers represent an attractive route for delivery of hydrophobic drugs.[1,2] Cancer therapy is the main field of application of these delivery systems.[2,3,4] According to estimates from the International Agency for Research on Cancer (IARC), by 2030 cancer is expected to grow up to 21.4 million new cancer cases and 13.2 million cancer deaths.[5] The large majority of currently used anti-cancer agents are extremely toxic and a non-specific delivery is responsible for severe side effects. Moreover, anti-cancer drugs are highly hydrophobic and low soluble in aqueous, biological tissues. Due to their intrinsic hydrophobicity, intravenous injection of chemotherapic agents might lead to embolization of blood capillaries (≤ 5 µm) before reaching the tumor site.[6] Furthermore, low solubility – coupled with metabolic degradation and excretion – results in poor systemic drug concentrations. For example, Paclitaxel (PTX) is one of the most effective chemotherapeutic drugs and is active against a broad range of cancers, such as lung, breast, ovarian, neck and head cancers as well as advanced forms of Kaposi's sarcoma.[7,8] However, it shows a poor water solubility (less than 0.03 mg/ml),[9] which greatly limits its widespread application in the clinical setting. In order to reduce the side effects of anticancer agents as well as increase their bioavailability, several colloidal systems have been investigated. Among them, polymeric micelles and nanoemulsions are the most promising for targeted drug delivery.

Polymeric micelles are characterized by amphiphilic moieties that can self-assemble into structures with hydrophobic cores and hydrophilic surfaces (**Figure 3.1**).[2,10,11,12,13] Micelles are dynamic equilibrium system and are thermodynamically stable. The non-covalent, self-assembly occurs above the critical micellar concentration (CMC).[6] The hydrophobic anticancer drug is

solubilized in the micelle core while the hydrophilic surface of the micelle ensures water solubility. This colloidal system has diameter in the range of 10-100 nm.[6] Because of their small sizes, polymeric micelles can reach solid tumor by extravasation.[14,15,16]

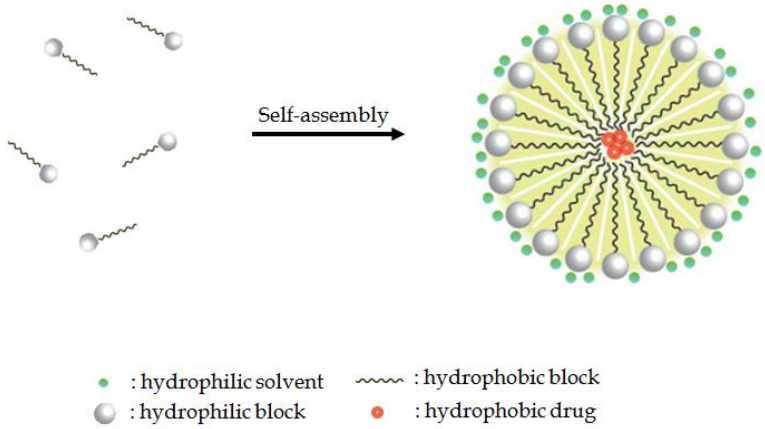

Figure 3.1 Schematic representation of drug-loaded polymeric micelles formed from self-assembly of amphiphilic block copolymers in aqueous media above CMC.

In contrast, nanoemulsions are heterogeneous dispersions of two immiscible liquids with a mean droplet diameter in the nanometric scale. Nanoemulsions are non-equilibrium colloidal systems. They are kinetically stable and energy input is required to form nanoemulsions, as shown in **Figure 3.2**.

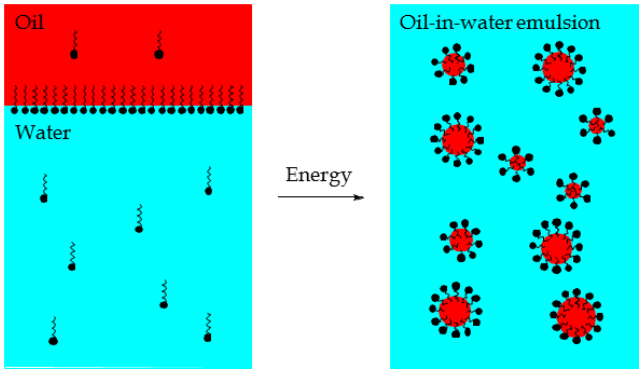

Figure 3.2 Schematic representation of oil-in-water emulsion formation.

Due to the greater size of nanoemulsions compared to micelles, a larger amount of drug can be loaded into nanoemulsions, making them more attractive for targeted drug delivery.[17]

The colloidal formulations of PTX currently in clinical use are Taxol®, Abraxane® and Genexol-PM®. Taxol® contains Cremophor EL, a polyoxyethylated castor oil, as vehicle used to solubilize PTX. After intravenous injection of Taxol®, side effects ascribed to Cremophor EL have been reported.[9] Indeed, severe anaphylactoid hypersensitivity reactions, hyperlipidaemia, abnormal lipoprotein patterns, aggregation of erythrocytes and peripheral neuropathy can be observed in patients treated with Taxol®.[9] Abraxane® is a nanoparticle albumin-bound PTX formulation approved by the FDA in 2005.[18] Although Abraxane® mitigates some side effects of solvent-bound PTX, anemia and thrombocytopenia have still being reported.[19] Genexol-PM® is a Cremophor EL-free polymeric micelle formulation of PTX with poly(ethylene glycol) (PEG) and poly(D,L-lactic acid).[7] Although the *in vivo* efficacy of Genexol-PM® is 3-fold higher than Taxol® efficacy, its biodistribution is 2-3-fold higher in the liver, spleen, kidney, lung, heart and tumor cells.[20,21] In the recent years, researchers have made efforts to develop nanocarriers with less side effects. The advantages of nanomedicines include their ability to protect drugs from degradation increasing the drug stability, improved pharmacokinetic features and biodistribution, tunable payload release, the ability to specifically deliver the drug to targeted diseased tissues and cells, and their ability to respond to internal and external stimuli to achieve spatial and temporal control over the release of therapeutic payloads.[6,7,22,23,24,25] After intravenous injection, reticuloendothelial system (RES) – represented by monocytes and macrophages located in lymph nodes, spleen and liver – and renal clearance compete with the tumor for nanosystems.[26,27] Nanosystems that escape the RES organs and the kidneys are able to reach the tumor. The percentage of

injected nanocarriers that interact with the tumor tissue is defined as the nanoparticle delivery efficiency.[14] It has been estimated that only 0.7% of the injected dose (ID) of nanosystems reach the solid tumor.[14] However, this percentage is still 10- to 100-fold higher than that of naked drug molecules.[28] Nanocarriers can get the tumor by passive or active targeting. Passive targeting is based on the enhanced permeability and retention (EPR) effect.[26] The tumor vasculature is abnormal and chaotic, exhibiting areas characterized by increased and sparse vascular density, hierarchical disorganization, serpentine structure and irregular branching, lack of innervation and smooth muscle cells, wide lumen, and includes vascular malformations that form arteriovenous shunts.[14,29] Tumor vasculature develops irregularly in order to supply nutrients and oxygen needed in larger amount in the growing cancer. The endothelial tumor cells are poorly aligned, displaying large fenestrations between them. The size of these gaps ranges from 200 nm to 800 nm, depending on the tumor type and stage.[6,30,31] Moreover, they show disrupted basement membranes and little pericyte coverage.[14] Blood flow behavior is unusual in cancer vessels. It has been observed that tumor blood flows only once in 15-20 minutes and then stops for a while. Moreover, blood often flows in the opposite direction.[29] These factors combined with the increased release of vascular permeability factors – such as nitric oxide, bradykinin, matrix metalloproteinases (MMPs) and vascular endothelial growth factor (VEGF) – lead to an abnormal hyperpermeability, making the tumor blood vessels leaky.[6,14,26] Consequently, nanocarriers inside tumor blood vessels move slowly and this allows the nanosystems to diffuse out into the extracellular matrix.[14] Interestingly, major RES organs such as liver and spleen display a fenestrated endothelium and circulating small particles can be sequestered by EPR mechanism. Therefore, a large amount of systemically injected nanocarriers accumulates in the RES organs.[27] Furthermore, the rapid cancer cell growth

compresses the lymph vessels, causing them to collapse, leading to a poor lymphatic drainage. Both the increased vascular permeability and the defective lymphatic drainage are responsible for the extravasation of blood proteins and nanosystems as well as their retention at the tumor site. **Figure 3.3** illustrates the EPR effect.

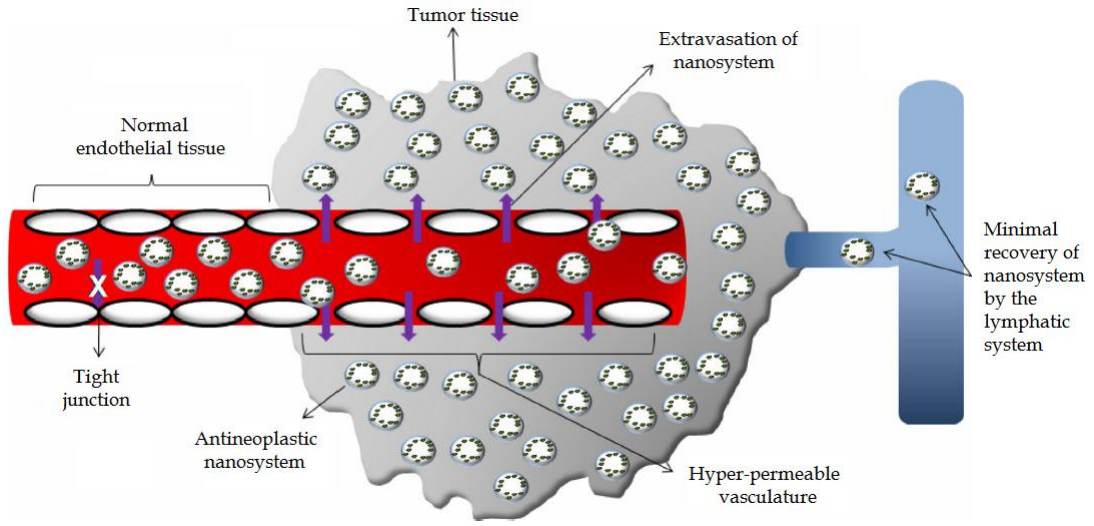

Figure 3.3 Enhanced permeability and retention (EPR) effect and passive targeting.[32]

Although the EPR effect plays an important role in the accumulation of nanocarriers in solid tumors, it shows some limitations.[6] Cancer types are heterogeneous, being characterized by different degree of vascularization and vascular permeability. It is known that the central area of metastatic cancers is not characterized by the EPR effect and therefore the accumulation of macromolecules in this site is more difficult.[29] Furthermore, the size of the gaps of the endothelial blood vessels varies within the same tumor, leading to areas that do not display the EPR effect. The leaky vasculature only allows the extravasation of nanocarriers with appropriate size and surface characteristics.[29] Otherwise, nanocarriers might leak back into the systemic bloodstream and be removed from the body.

Since cancer cells overexpress antigens and receptors, which are absent or low abundant in healthy tissues, an active targeting can be used to address nanosystems to the tumor site allowing a selective accumulation.[6,33] Epidermal growth factor, somatostatin, transferrin, and folate receptors have been investigated for active targeting.[6,22] Recently, peptides have been taken into account as targeting ligands because of their small size, lower immunogenicity compared to proteins, better *in vivo* stability, and lower cost.[6] In particular, the arginine-glycine-aspartic acid (RGD) tripeptide has been widely investigated as target for integrin receptors.

The main challenge in the development of nanosystems is their stability in the body. Nanocarriers should be stable for enough time in order to reach the cancer cells and then release the payload drug. A longer circulation lifetime of nanosystems is desired, since it would increase the possibility of nanosystems to accumulate within the tumor. Moreover, nanocarriers interact with blood proteins to form new biological entities called "protein corona" that can aggregate.[14] It has been demonstrated that particles with cationic surfaces show the strongest macrophage uptake. Neutral polymers such as PEG are often conjugate to nanocarriers with the aim of masking these particles from macrophages and increasing their circulation lifetime. In fact, the coating of nanosystems with PEG leads to the formation of stealth particles characterized by a hydrated layer. This provides steric hindrance which prevents phagocytosis.[29] Most importantly, the drug must remain confined inside the nanosystems and released only after nanocarriers have reached the tumor. A slower and sustained release of the drug from the nanocarriers might lead to a prolonged effect period against tumor cells, reduce the required amount of drug and decrease the systemic side effects.[34]

3.2 Background and Project Aim

Amphiphilic polymers that can assembly in aqueous solution have found several applications in drug delivery. Among them, nanoemulsions are attractive drug carriers because of their kinetic stability over time as well as their larger oil droplet core, perfect for the shielding of hydrophobic drugs. However, drug release from these colloidal systems is often too fast, leading to burst release of drug and toxicity concerns.

It has been demonstrated that the introduction of fluorous block to traditional hydrophilic-lipophilic block copolymers allows the development of micelles with improved kinetic and thermodynamic stability. Also, these semifluorinated systems are able to modulate drug time-release.[35] We hypothesized that similar results might be achieved when semifluorinated polymers are used to prepare nanoemulsions.

A new class of triblock copolymers composed by hydrophilic, fluorophilic and lipophilic moieties were synthesized by Professor Mecozzi group. These semifluorinated copolymers were used to prepare nanoemulsions for the delivery of hydrophobic drugs. To test the drug release profile of these nanoemulsions, PTX was taken into account as hydrophobic drug. In particular, a triphilic, linear, and semifluorinated polymer called **M2F8H18** was synthesized (**Figure 3.4**).

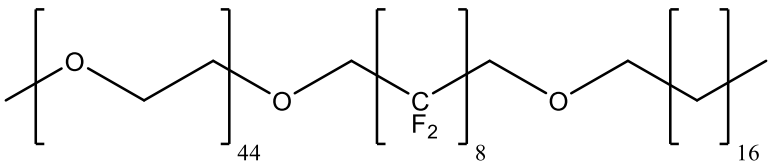

Figure 3.4 Chemical structure of **M2F8H18**.

M2F8H18 is characterized by a linear alkyl chain of eighteen carbon atoms (H18) that stabilizes an oil droplet core loaded with PTX. In fact, the long alkyl chains penetrate the large droplet core and interact with the hydrophobic drug providing particle stability. The hydrophilic moiety is represented by a PEG unit, which ensures water solubility and is biocompatible. mPEG with average molecular weight of 2,000 Daltons (M2) was selected as hydrophilic unit to allow the most efficient packing of the PEG groups. Indeed, the M2 moiety shows less hydrophilic-group steric repulsion if compared to larger PEGs. More efficient packing directly relates to smaller particle sizes. It is remarkable that PEG is a common choice as hydrophilic component of micelles and liposomes. It is one of the few polymers approved by FDA as a vehicle or base in food, pharmaceuticals and cosmetics.[36] PEG is not toxic, is eliminated intact by either the kidneys or the faeces and is known to lack immunogenicity. Pegylation – the process that binds polyethylene glycol chains to candidate molecules – has been exploited to prolong blood circulation time of liposomes. Indeed, pegylated liposomes show increased half-life, decreased plasma clearance due to the decreased uptake by RES organs, and a better distribution in diseased tissues. Moreover, it has been demonstrated that pegylated liposomes are less prone to leak drug before reaching the target tissue.[36]

M2F8H18 bears a fluorophilic moiety placed between the hydrophilic and the lipophilic units. The fluorophilic portion, represented by eight CF_2 residues (F8), provides enhanced particle stability due to the formation of the fluorous phase. Furthermore, the fluorous shell controls the drug release from the core and shields the internal drug-containing oil droplet core. Due to the lipophobic properties of the fluorocarbon segment, it is not involved in the encapsulation of hydrophobic drugs.[35] Oil-in-water nanoemulsions have been prepared using **M2F8H18** and PTX. The ability of medium chain triglycerides (MCT) and ionic liquids (IL), such as methyltrioctylammonium

bis(trifluoromethylsulfonyl)imide [N_{1888}][NTf_2], to dissolve PTX was investigated. Both MCT and IL were excellent media to solubilize high concentrations of PTX (**Figure 3.5**).

Media	Concentration solubilized PTX (mg/ml)
MCT	15
[N_{1888}][NTf_2]	44

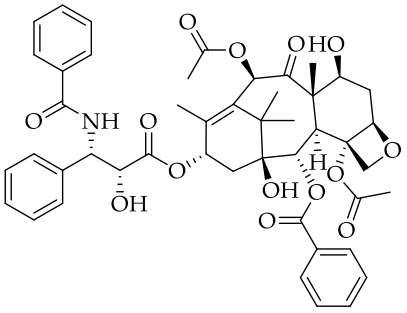

PTX

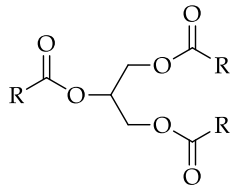

R = $(CH_2)_6CH_3$ 66%
$(CH_2)_8CH_3$ 32%

MCT

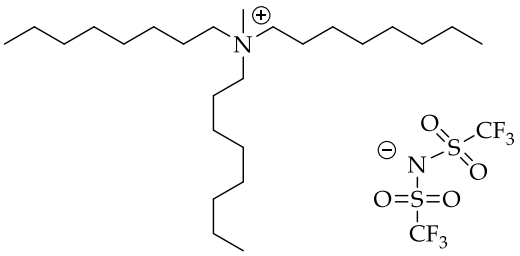

[N_{1888}][NTf_2]

Figure 3.5 Chemical structures of PTX, MCT (Neobee® M-5), [N_{1888}][NTf_2] and the concentration of solubilized PTX in each medium.

Particle size and growth of **M2F8H18** nanoemulsions were monitored by Dynamic Light Scattering (DLS) measurements. Nanoemulsions can destabilize by molecular diffusion or Ostwald ripening. By this mechanism, individual molecules leave the smallest droplets, in which the chemical potential is higher due to the higher curvature, and join larger droplets. It is characterized by a linear increase of the droplet volume over time and by a time-invariant size distribution.[37,38,39] Consequently, plotting particle size over time can give a good representation of emulsion stability. DLS study demonstrated that **M2F8H18** nanoemulsions exhibited excellent kinetic stability over long periods of time (**Figure 3.6**).

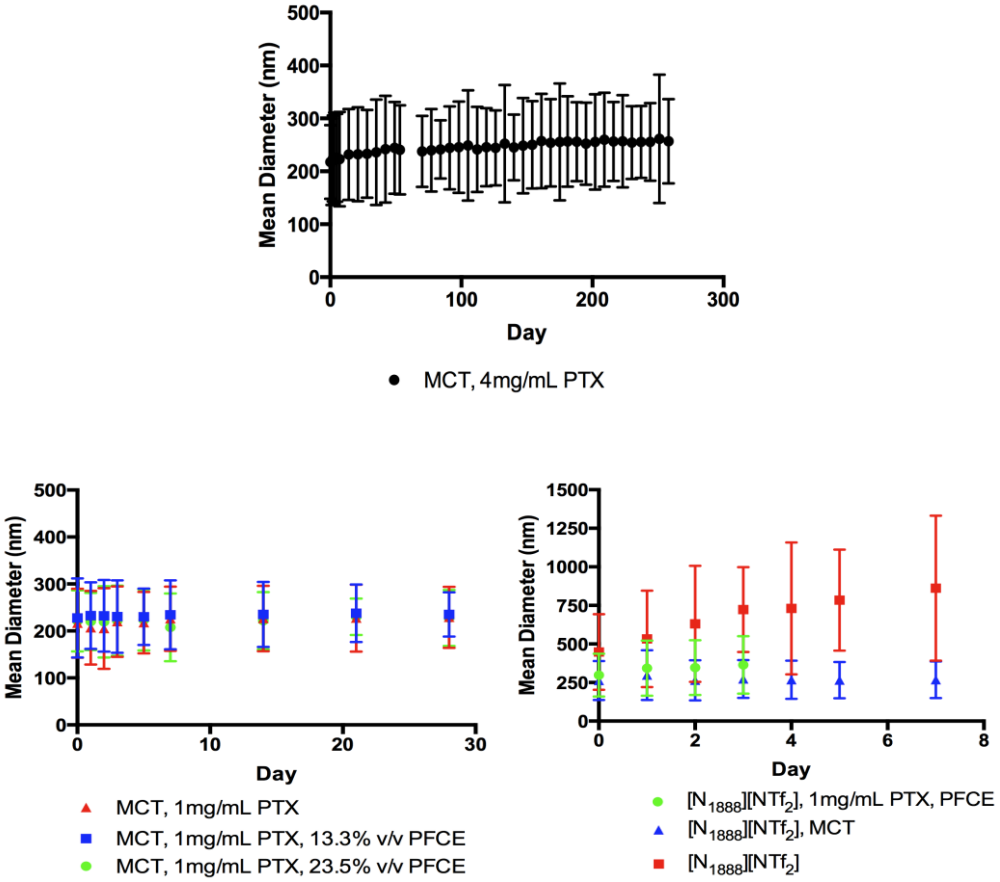

Figure 3.6 Plot of DLS measurements for nanoemulsions loaded with PTX. MCT and $[N_{1888}][NTf_2]$ were taken into account as media to dissolve PTX. The stability of nanoemulsions containing perfluoro-15-crown-5-ether (PFCE) as ^{19}F contrast agent for ^{19}F MRI studies was also evaluated.

In vitro drug release profile was also investigated. The linear **M2F8H18** nanoemulsion showed a $t_{1/2}$ of 69.5 hours (**Figure 3.7**). Interestingly, burst release of PTX was not observed. The controlled drug release of the **M2F8H18** nanoemulsion might be due both to the penetration of the long hydrocarbon chain of **M2F8H18** into the hydrophobic core in which the hydrophobic drug is loaded, and to the perfluorocarbon shell surrounding the oil droplet. The fluorous shell forms a barrier to control drug release from the core as well as provides particle stability. The effect of the fluorous shell is demonstrated by comparing drug release half-lives from **M2F8H18**

nanoemulsions to the **M2H18**-based nanoemulsions lacking of the fluorous moiety (69.5 h and 52.9 h respectively).

Moreover, addition of perfluroro-15-crown-5-ether (PFCE) imaging agent to **M2F8H18** nanoemulsions increased the drug release half-life even further ($t_{1/2}$=92.4 h) by stabilization of the hydrocarbon oil droplet (**Figure 3.7**). Therefore, PFCE shows a dual effect: it provides imaging potential to the nanoemulsions and enhances the modulation of drug release at the same time.

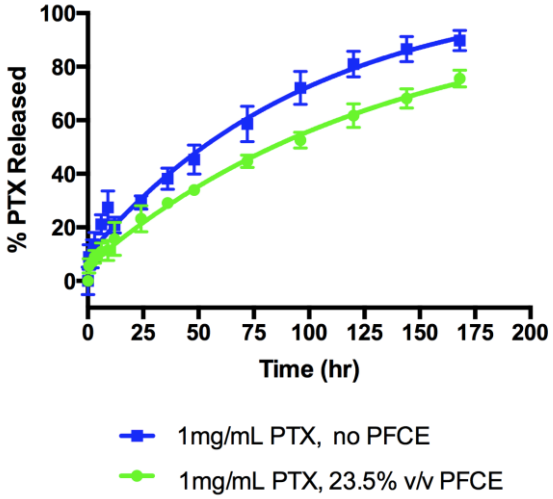

Polymer	Half-life (hrs)
M2F8H18	69.5
M2F8H18	92.4

Figure 3.7 Drug release profile of nanoemulsions prepared with or without PFCE.

A prolonged drug release and a long half-life are desired in order to avoid the release of the encapsulated drug before reaching the diseased tissues. It is known that intravenously-injected nanoemulsions are able to get the tumor by EPR effect and reach peak accumulation within 12-24 hours.[27] Therefore, a longer circulation lifetime increases the possibility for nanoemulsions to accumulate in the tumor and then release the drug.[14] This would reduce the systemic toxicity and side effects. The drug release rate and the pharmacokinetic behavior can be modulated based on the size of the fluorocarbon moiety introduced in the polymer.[35] In fact, the chemical

structure and the size of the fluorinated polymer affect the formation and stability of the nanoemulsions and consequently the drug release rate. Therefore, the aim of this project was designing and synthesizing two triphilic, dibranched, and semifluorinated polymers to prepare nanoemulsions. **Figure 3.8** shows the chemical structures of these dibranched polymers.

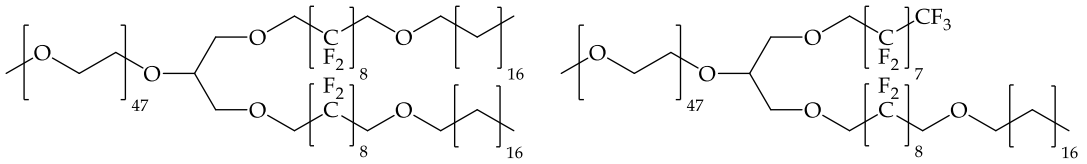

Figure 3.8 Chemical structures of the triphilic, dibranched, and semifluorinated **M2diF8H18** and **M2F8H18/F8** polymers.

If compared with the linear **M2F8H18**, the dibranched and symmetric **M2diF8H18** is bulkier where the hydrophobic block is represented by two alkyl chains of eighteen carbon atoms each and two fluorous chains of eight CF_2 residues each. In contrast, **M2F8H18/F8** is an asymmetric and triphilic polymer in which one branch is shorter than the other one, being composed only by the fluorinated block. Since the alkyl chains are involved in the stabilization of oil droplet core while the fluorous shell gives stability to the colloidal system by formation of the fluorous phase, it is expected that these new polymers will lead to nanoemulsions with a different design that display differences in term of stability and drug release profile. The rationale is to reach a better control of the drug release by a different polymer design, improving the drug release half-life.

Figure 3.9 compares the nanoemulsions design achieved with linear and dibranched polymers.

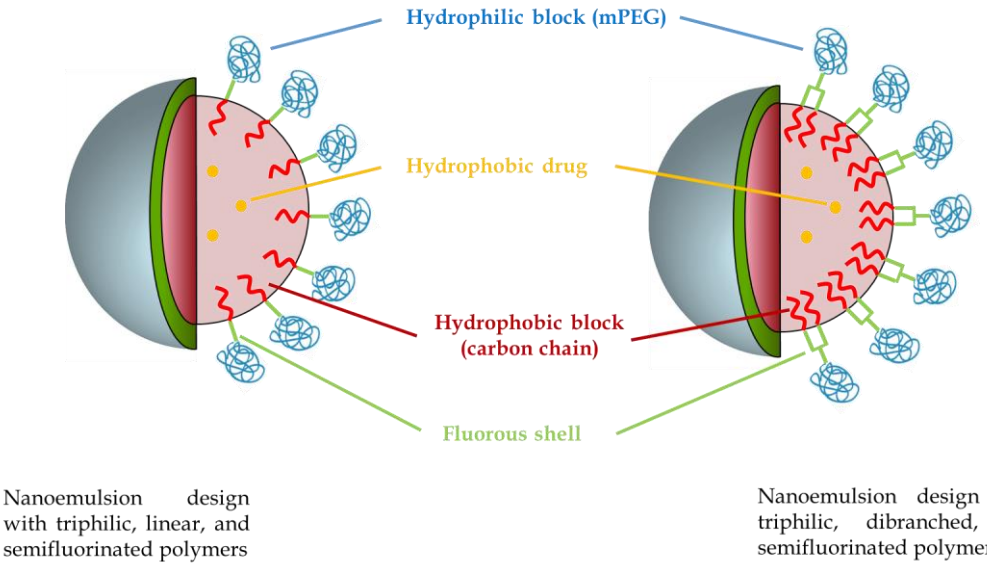

Figure 3.9 Comparison of nanoemulsions design obtained with triphilic, linear, and semifluorinated polymers such as **M2F8H18** (left-handed) and with triphilic, dibranched, and semifluorinated polymers such as **M2diF8H18** (right-handed).

This chapter will describe the synthesis of **M2diF8H18** and **M2F8H18/F8**. The preparation and purification of fluorinated molecules can be very difficult because of their unique chemical properties and reactivity, poor solubility in common organic solvents, hydrophobicity and lipophobicity, leading to difficulties in handling, solubilization and purification of fluorinated compounds.[40,41] Moreover, the reactivity of fluorocarbons is greatly reduced when the fluorous moiety is directly bound to the reactive functional group. This can be explained taking into account the strong electron-withdrawing effect of fluoroalkyl chains.[40] For these reasons, the synthesis of **M2diF8H18** and **M2F8H18/F8** has been optimized in order to find the best reaction conditions and increase the final yield.

3.3 Polymers Synthetic Scheme

The synthesis of **M2diF8H18** and **M2F8H18/F8** is represented in **Scheme 3.1**.

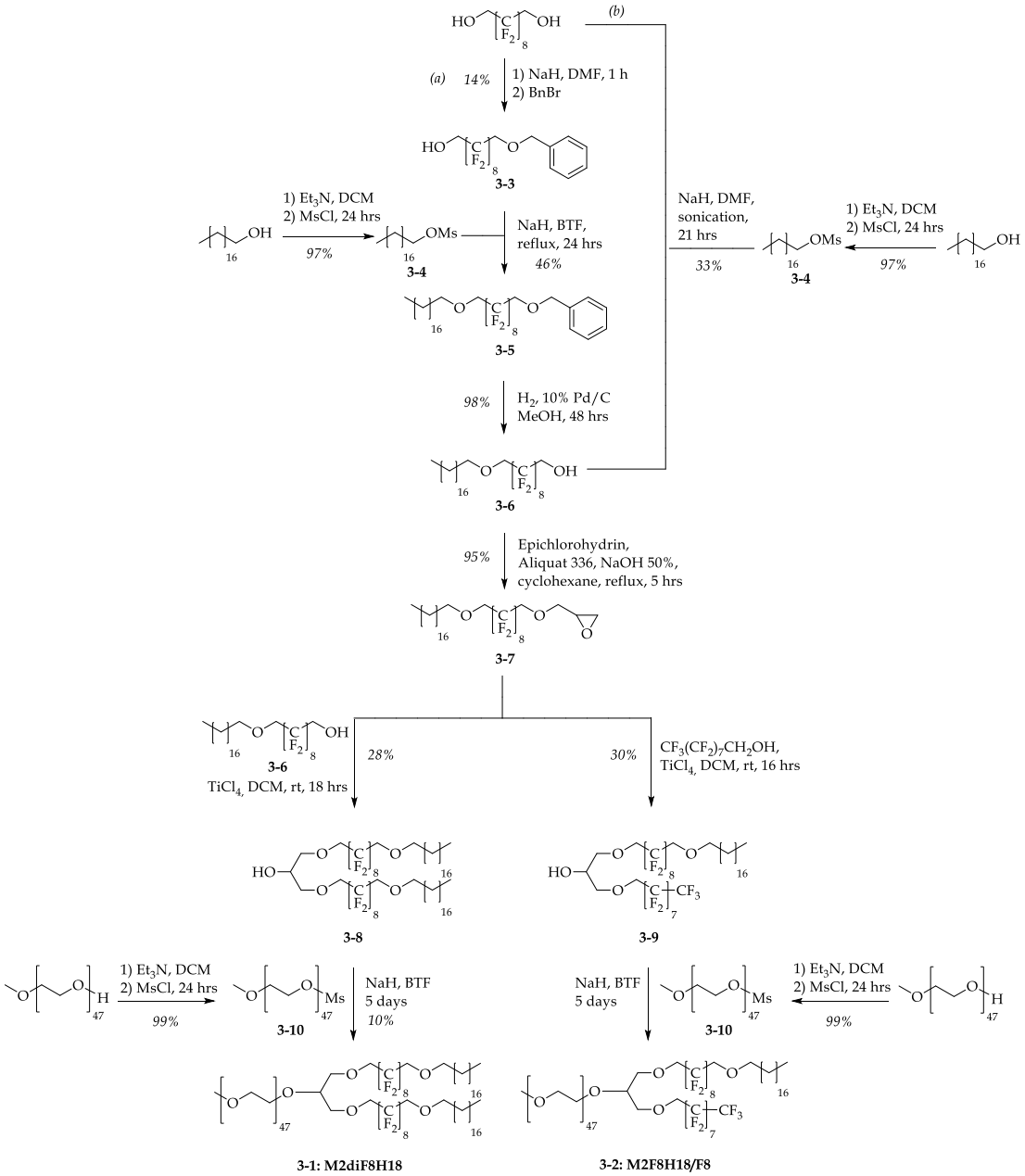

Scheme 3.1 Synthesis of **M2diF8H18** and **M2F8H18/F8**.

Intermediate **3-6** can be achieved following either route *(a)* or route *(b)*.

Route *(a)* involves the monoprotection of the commercially available 1H,1H,10H,10H-perfluoro-1,10-decanediol (HO-F8-OH) to afford intermediate **3-3**. Mono-benzylation reaction is chosen to protect the starting material HO-F8-OH and is carried out with NaH and benzyl bromide (BnBr) in DMF. Intermediate **3-3** is then alkylated by reaction with intermediate **3-4**, previously prepared by mesylation of the commercially available octadecan-1-ol. Intermediate **3-5** is achieved using benzotrifluoride (BTF) as solvent to promote the dissolution of intermediate **3-3**. Intermediate **3-5** is then deprotected by hydrogenolysis over palladium on carbon to afford intermediate **3-6** in quantitative yield.

The mono-benzylation of the HO-F8-OH shows a low yield (14%) and this is a great limitation for the whole synthesis since the monoprotection of the fluorous diol is the first step to get both **M2diF8H18** and **M2F8H18/F8** polymers. In order to overcome this issue, a different synthetic approach is tested, as illustrated by route *(b)*. In this procedure, HO-F8-OH is directly reacted with intermediate **3-4** to give intermediate **3-6**, skipping the mono-benzylation.[41] This shortens the whole synthesis by two steps, affording the desired intermediate **3-6** with a good yield (33%). This reaction requires NaH as a base to deprotonate the HO-F8-OH and the mixture is sonicated for 21 hours at rt. Intermediate **3-6** is then reacted with epichlorohydrin. This nucleophilic substitution (SN2) reaction is carried out using cyclohexane as solvent and an aqueous solution of NaOH as a base. Since two immiscible solvents (cyclohexane and water) are involved, a phase-transfer catalyst as tricaprylmethylammonium chloride (Aliquat 336®) is required. The mixture is heated to reflux for 5 hours to afford intermediate **3-7** in quantitative yield. Intermediate **3-7** is shared between the synthesis of **M2diF8H18** and **M2F8H18/F8.** Indeed, intermediate **3-7** is coupled with intermediate **3-6** to afford intermediate **3-8** and is also reacted with the commercially available 1H,1H-perfluoro-1-nonanol to give intermediate **3-9**. **M2diF8H18** is achieved

by reacting previously prepared intermediate **3-10** with intermediate **3-8** with a low yield (10%). The synthesis of intermediate **3-10** is a mesylation reaction of methyl-PEG 2000 and the product is obtained in quantitative yield. In contrast, the pegylation of intermediate **3-8** to afford **M2diF8H18** is quite difficult (10% yield) because of the poor reactivity of the fluorinated dibranched reactants as well as the steric hindrance due to the methyl-PEG 2000. Indeed, this reaction requires a strong base as NaH, BTF as a solvent to solubilize the fluorinated reactants and long reaction time. Another important issue is the purification of crude product containing pegylated compounds. In fact, PEG units strongly stick on silica gel, making chromatography a challenge. In order to promote the purification, pegylated polymers might be first precipitated with ether from various solvents to separate the unreacted intermediate **3-10** from **M2diF8H18**. Then, the final polymer must be purified by column chromatography. In conclusion, **M2diF8H18** was achieved while pegylation of intermediate **3-9** has not been attempted yet.

3.4 Optimization of Selected Reactions

The reactions with low yield have been optimized in order to obtain the desired product in a greater amount as well as reduce the consumption of the expensive fluorinated starting materials. In the following paragraphs, the optimization of the most problematic reactions is descussed.

3.4.1 Synthesis Optimization of Intermediate 3-3

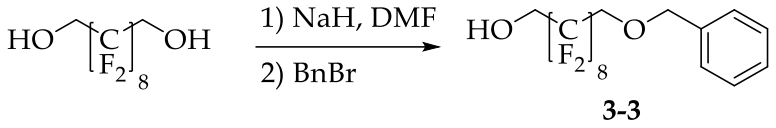

3-3

Scheme 3.2 Mono-benzylation of 1H,1H,10H,10H-perfluoro-1,10-decanediol

Benzyl group was chosen as protecting group for 1H,1H,10H,10H-perfluoro-1,10-decanediol since it can be removed easily by hydrogenolysis over Pd on carbon.

Various reaction conditions were investigated, as shown in **Table 3.1**.

Entry	Reaction time (h)	Temperature (°C)	Dilution of BnBr	Yield (%)
1	24	rt	-	2
2	42	rt	-	14
3	46	rt	4% in DMF	10

Table 3.1 Reaction conditions tested for the synthesis of intermediate **3-3**.

Previous work in Professor Mecozzi group demonstrated that the best reaction condition for mono-benzylation of fluorinated diols requires a 3-fold amount of HO-F8-OH compared to BnBr. This avoids large consumption of the expensive diol, giving only small amount of the di-benzylated product. The unreacted HO-F8-OH might be recycled and reacted again with BnBr. Moreover, after purification of the desired intermediate **3-3**, di-benzylated by-product might be deprotected and purified to obtain the starting HO-F8-OH.

The main issue related to this reaction is the formation of a sticky material after deprotonation of HO-F8-OH, making the following benzylation hard. In fact, as reported in **Table 3.1** (entry 1) only traces of intermediate **3-3** were found. To investigate the influence of the reaction time, the mixture was allowed to react for 42 hours (**Table 3.1**, entry 2). In this case, intermediate **3-3** was obtained in a low yield (14%). To better control the dripping rate of BnBr, this reactant was diluted in DMF and added to the mixture dropwise over 15 minutes (**Table 3.1**, entry 3). However, this did not improve the yield.

With the aim of increasing the yield, a different procedure was tested for the mono-benzylation of HO-F8-OH.[41] As shown in **Scheme 3.3**, the mixture was sonicated to promote both the deprotonation and the following benzylation.

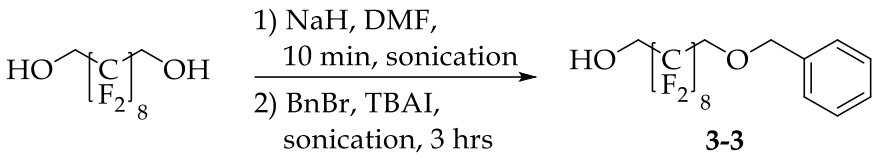

Scheme 3.3 Mono-benzylation of 1H,1H,10H,10H-perfluoro-1,10-decanediol.[41]

Different conditions were investigated, as resumed in **Table 3.2**.

Entry	TBAI	Sonication	Temperature (°C)	Yield (%)
1	+	+	rt	44
2	-	+	rt	41
3	+	-	rt	39
4	-	-	60	27

Table 3.2 Reaction conditions tested for the synthesis of intermediate **3-3** applying the procedure proposed by Hussein *et al*.[41]

All tested conditions afforded intermediate **3-3** with greater yields compared to those achieved with the procedure described previously. It seems that the presence of TBAI did not affect deeply the yield (**Table 3.2**, entry 1 *vs* entry 2). Moreover, the yield was just a little bit higher when the reaction mixture was sonicated instead of stirred at rt (**Table 3.2**, entry 1 *vs* entry 3). However, intermediate **3-3** was obtained in a lower yield when the mixture was stirred and heated to 60 °C (**Table 3.2**, entry 4). Since heating the mixture led to a lower yield (**Table 3.2**, entry 2 *vs* entry 4), we hypothesized that ultrasound might play an important role in increasing the reaction yield while the temperature has not a significant impact on the yield. In fact, we supposed that ultrasounds break NaH particles to form a fine suspension of smaller NaH particles in DMF, increasing their surfaces and thus, promoting the deprotonation of HO-F8-OH.

3.4.2 Synthesis Optimization of Intermediate 3-6

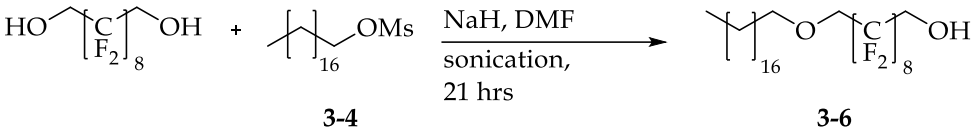

3-4 **3-6**

Scheme 3.4 Synthesis of intermediate **3-6**.

As shown in **Scheme 3.1**, intermediate **3-6** can be achieved starting from 1H,1H,10H,10H-perfluoro-1,10-decanediol by mono-benzylation followed by alkylation of the unprotected hydroxyl group and then debenzylation (route *a*). Due to the successful benzylation of 1H,1H,10H,10H-perfluoro-1,10-decanediol carried out with ultrasound, we hypothesized that the same reaction might be applied to the direct alkylation of the diol by intermediate **3-4** (**Scheme 3.1**, route *b*). This would allow skipping the monoprotection of HO-F8-OH and then shortening the synthesis by two steps.

Various reaction parameters were taken into account to optimize the direct alkylation of HO-F8-OH, as shown in **Table 3.3**.

Entry	Reaction solvent	TBAI	Sonication	Temperature (°C)	Reaction time (hrs)	Yield (%)
1	DMF/THF 7:3	+	+	rt	3	0
2	DMF	+	+	rt	3	28
3	DMF	+	-	60	3	20
4	DMF	-	-	60	21	18
5	DMF	+	+	rt	21	24
6	DMF	-	+	rt	21	33

Table 3.3 Optimization of alkylation reaction to obtain intermediate **3-6**.

First, a mixture of DMF and THF was used as solvent to promote the dissolution of all reagents (**Table 3.3**, entry 1). TBAI was considered as phase transfer catalyst and the mixture was sonicated for 3 hours. However, this did not lead to intermediate **3-6**. We hypothesized that THF was not a suitable solvent for this reaction. In fact, when the reaction was carried out using only DMF as solvent and keeping constant the other parameters (such as reaction time, temperature, the addition of TBAI as well as the sonication of the mixture), the formation of intermediate **3-6** was observed (28% yield; **Table 3.3**, entry 2). Then, the mixture was stirred at 60 °C both with (**Table 3.3**, entry 3) and without (**Table 3.3**, entry 4) TBAI. In these cases, intermediate **3-6** was achieved with the lowest yield, according to the results achieved previously for the mono-benzylation of HO-F8-OH (**Table 3.2**). Then, the mixture was sonicated for 21 hours both adding TBAI (**Table 3.3**, entry 5) and without TBAI (**Table 3.3**, entry 6). The highest yield (33%) was achieved when TBAI was not added to the reaction and the mixture was sonicated for 21 hours (**Table 3.3**, entry 6). According to the previously obtained results for the mono-benzylation of HO-F8-OH (**Table 3.2**), TBAI seems not to be needed. According to these results, the best reaction conditions require the sonication of the mixture for 21 hours at room temperature without adding TBAI (**Table 3.3**, entry 6).

The use of sound waves to generate chemical and physical effects has already been described in the literature. In particular, the term "sonochemistry" is referred to ultrasound, that is sound waves with a frequency above 20 kHz.[42] Sonochemical reactions in solutions have mainly been explained in terms of cavitation theory.[43] This theory assumes that the sonication leads to the formation, growth and implosion of microbubbles in a liquid. Ultrasound waves carry kinetic energy (particles of the liquid oscillate and move from their equilibrium position in the direction of propagation) as well as potential energy (fluid compression). When ultrasonic waves propagate in a liquid, the

local pressure in the liquid falls reaching a value lower than the vapor tension of that liquid. This causes the liquid to break down and microbubbles form. These vapor cavities are unstable and collapse rapidly. The implosion of the microbubbles releases a large amount of kinetic energy that drives a chemical reaction to completion.[42,43] Both mechanical and chemical effects are observed in a liquid medium. Mechanical effects result in enhanced mass and energy transfer, particle size reduction, liquid emulsification, surface activation, and intense local heating. Chemical effects occur inside the bubbles or at the bubble interface. They are represented by molecular sonolysis, which includes changes in solvation. In conclusion, microbubbles – created by the propagation of ultrasound waves through a liquid medium – act as microreactors with interior environmental conditions different from the bulk liquid.

The cavitation theory might explain the greater yield achieved using ultrasound instead of magnetic stirring for the synthesis of intermediate **3-6**.

The purification of intermediate **3-6** was quite simple and was achieved by silica gel column chromatography in gradient (hexanes and EtOAc as mobile phase). Despite intermediate **3-6** and unreacted intermediate **3-4** showed similar R_f (0.52 and 0.48 respectively), intermediate **3-6** was separated as a pure solid.

3.4.3 Synthesis Optimization of Intermediate 3-8

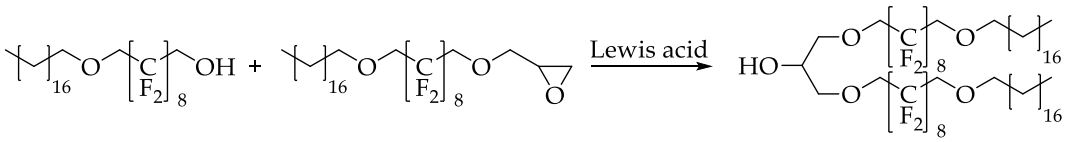

3-6 **3-7** **3-8**

Scheme 3.5 General synthetic scheme for the synthesis of intermediate **3-8**.

Scheme 3.5 shows the synthesis of intermediate **3-8** as described in the literature.[44] A Lewis acid is needed to promote the nucleophilic oxyrane opening. Boron trifluoride diethyl etherate, BF_3OEt_2, was selected as Lewis acid for the tests listed in **Table 3.4**.

Entry	Reaction solvent	Temperature (°C)	Reaction time (hrs)	Ratio intermediate 3-6/ intermediate 3-7/ BF_3OEt_2	Yield (%)
1	DCM	rt	1	1.1 : 1 : 0.2	16
2	DCM	rt	1	1.1 : 1 : 1	18
3	DCM	rt	1	1.1 : 1 : 2	10
4	DCM	rt	1	2 : 1 : 0.2	19
5	DCM	rt	1	5 : 1 : 0.2	13
6	DCM	rt	108	2 : 1 : 1.8	13
7	DCM	rt	1	1 : 2 : 0.4	15
8	cyclohexane	rt	1	2 : 1 : 0.2	19
9	cyclohexane	reflux	1	2 : 1 : 0.2	15
10	1,4-dioxane	reflux	1	2 : 1 : 0.2	20
11	1,4-dioxane	reflux	24	2 : 1 : 0.2	22
12	1,2-DCE + BTF (1:1)	reflux	41	2 : 1 : 0.2	14

Table 3.4 Reaction conditions tested for the synthesis of intermediate **3-8**.

First, DCM was considered as solvent for this reaction and the effect of a different ratio among the reactants was investigated (**Table 3.4**, entries 1-7). The yields achieved varying the ratio among intermediate **3-6**, intermediate

3-7, and the Lewis acid BF_3OEt_2 are very close, ranging from 10% (**Table 3.4**, entry 3) to 19% (**Table 3.4**, entry 4). As reported in **Table 3.4**, these tests were carried out at rt for 1 hour except for entry 6, in which the reaction time was significantly longer (108 hours). In this case, the aim was to verify if the low yield might have been due to a kinetic issue. These tests allowed us to select 2 : 1 : 0.2 as the best ratio among intermediate **3-6**, intermediate **3-7**, and BF_3OEt_2 (**Table 3.4**, entry 4). This is consistent with the mechanism of the reaction, in which the Lewis acid is used as catalyst and is recycled during the reaction. For that reason, just a catalytic amount of BF_3OEt_2 is required. Moreover, to promote the formation of intermediate **3-8**, an excess quantity of intermediate **3-6** was needed. However, the use of large quantities of intermediate **3-6** was not worth (**Table 3.4**, entry 5), since it did not improve the reaction yield. Then, the effect of the solvent, the temperature and the reaction time were investigated (**Table 3.4**, entries 8-12). Cyclohexane is the solvent used in the previous synthetic step, that is the synthesis of intermediate **3-7**. Due to the good solubility of intermediate **3-6** and intermediate **3-7** in cyclohexane, we took into account this solvent for the synthesis of intermediate **3-8** (**Table 3.4**, entry 8 and 9). The test was conducted both at rt (**Table 3.4**, entry 8) and to reflux (81 °C) (**Table 3.4**, entry 9). The yields were consistent with those achieved previously (19% and 15% respectively). Then, 1,4-dioxane was taken into account as solvent and the mixture was heated to reflux (101 °C) for 1 hour (**Table 3.4**, entry 10) and for 24 hours (**Table 3.4**, entry 11), without improving the yield significantly (20% and 22% respectively). Finally, to promote the dissolution of the starting materials, a mixture of two miscible solvents (1,2-DCE and BTF) was considered. 1,2-DCE has a chemical structure similar to DCM but the boiling point of 1,2-DCE is higher (83.5 °C *vs* 39.6 °C). This permits to reach a higher reaction temperature. BTF is commonly used as solvent to increase the solubility of fluorinated reactants by means of the fluorophilic effect. As

shown in **Table 3.4** (entry 12) the mixture of 1,2-DCE and BTF heated to reflux for 41 hours did not lead to better results.

Since the yields were low and very close to each other, we decided to investigate a different Lewis acid, such as $TiCl_4$. **Table 3.5** lists the reaction conditions tested. In all these tests, the ratio among intermediate **3-6**, intermediate **3-7**, and $TiCl_4$ was kept as 2 : 1 : 0.2.

Entry	Reaction solvent	Temperature (°C)	Reaction time (hrs)	Yield (%)
1	DCM	rt	1	22
2	DCM	rt	18	28
3	1,4-dioxane	reflux	24	20
4	1,2-DCE+BTF (1:1)	reflux	1	19
5	$N(CF_2CF_3)_3$	reflux	24	21
6	-	100 °C	1	18

Table 3.5 Reaction conditions tested for the synthesis of intermediate **3-8** using $TiCl_4$ as Lewis acid.

First, the reaction was carried out using DCM as solvent and stirring the mixture at rt for 1 hour (**Table 3.5**, entry 1). The yield was similar to that achieved when BF_3OEt_2 was used as Lewis acid (**Table 3.5**, entry 1 *vs* **Table 3.4**, entry 4). However, when the mixture was stirred for a longer period of time – 18 hours instead of 1 hour – intermediate **3-8** was isolated with a higher yield (**Table 3.5**, entry 2). Then, various solvents with higher boiling points than DCM were tested (**Table 3.5**, entries 3-5). This allowed us to heat the mixture to reflux and investigate the effect of the temperature on the yield. Noteworthy, we also tested perfluorotriethylamine $N(CF_2CF_3)_3$ as solvent (**Table 3.5**, entry 5), which should improve the solubility of

perfluorinated starting materials because of the fluorophilic effect. Moreover, the nitrogen atom of perfluorotriethylamine does not show basic properties due to the strong electron withdrawing effect of fluorines. For that reason, $N(CF_2CF_3)_3$ can be used as solvent in reactions involving Lewis acids without observing a reaction between the fluorinated base and the Lewis acid.[45] As shown in **Table 3.5** (entries 3-5), heating the mixture to reflux did not improve the yield, not even allowing the mixture to react for 24 hours. Interestingly, we tried to react the mixture without using a solvent (**Table 3.5**, entry 6). We reasoned that the yield might be improved increasing the concentration of the starting materials. To reach the highest concentration, no solvent was used and the solid mixture was melted. After 1 hour, intermediate **3-8** was isolated with low yield (18%).

The obtained results suggested that $TiCl_4$ worked better than BF_3OEt_2. Moreover, increasing the temperature or reacting the mixture for long time did not improve the yield. In conclusion, the best reaction conditions involved DCM as solvent and $TiCl_4$ as catalyst. The mixture should be reacted at rt for 18 hours (**Table 3.5**, entry 2). Nevertheless, the yield achieved following these conditions was still low (28%).

It is noteworthy that a mixture of intermediate **3-8** and its structural isomer was obtained in all tests. In fact, the nucleophilic ring-opening reaction led to a mixture of both secondary and primary alcohol, as shown in **Figure 3.10**. The separation of these two isomers was not possible by chromatography. The percentage of intermediate **3-8** in the mixture was estimated by ^{1}H-NMR to be 85%, according to the literature.[46] We reasoned that it is not required to obtain the pure intermediate **3-8** according to our purpose. Indeed, nanoemulsions prepared starting from a mixture of symmetric intermediate **3-8** and its structural isomer would show the same behavior – in term of ability to control the drug release – than nanoemulsions composed by the pure intermediate **3-8**.

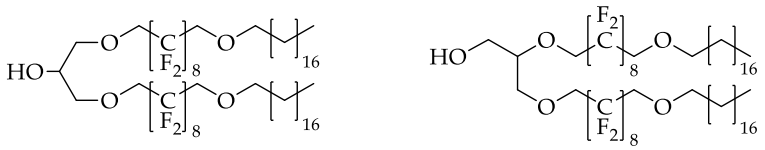

85% **15%**

Figure 3.10 Chemical structures of intermediate **3-8** (left-handed) and its structural isomer (right-handed) with their estimated molar percentages.

Since intermediate **3-8** is a symmetric molecule, we supposed that it might be synthesized in one step, starting from intermediate **3-6** and epichlorohydrin, as shown in **Scheme 3.6**.

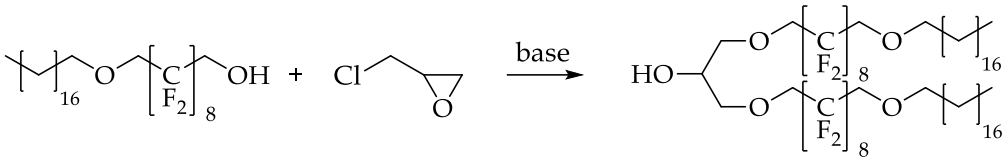

3-6 **3-8**

Scheme 3.6 General synthetic scheme to obtain intermediate **3-8** in one step.

This reaction requires a base like NaOH or NaH to deprotonate intermediate **3-6** and thus promote the nucleophilic attack to the epichlorohydrin ring. Intermediate **3-6** was kept in excess if compared with epichlorohydrin to promote the formation of intermediate **3-8** instead of intermediate **3-7**. **Table 3.6** summarizes the investigated reaction conditions.

Entry	Reaction solvent	Base	Temperature (°C)	Reaction time (hrs)	Ratio intermediate 3-6/ epichlorohydrin	Yield (%)
1	DMF	NaH	90	18	2.1 : 1	0
2	-	KOH	100	50	3 : 1	0
3	cyclohexane	NaOH 50%	90	5	1 : 0.5	small amount

Table 3.6 Reaction conditions tested for the synthesis of intermediate **3-8** in one step.

First, a strong base like NaH was used to deprotonate the hydroxyl group of intermediate **3-6**.[47] The mixture was heated to 90 °C for 18 hours without observing the formation of intermediate **3-8** (**Table 3.6**, entry 1). Then, a procedure previously used for a similar reaction by Professor Mecozzi group was tested (**Table 3.6**, entry 2). Crushed KOH and intermediate **3-6** were heated to 100 °C to melt the solid mass and then epichlorohydrin was added. The mixture was stirred for 50 hours. However, intermediate **3-8** was not isolated. We reasoned that intermediate **3-8** might be achieved following the procedure adopted for the synthesis of intermediate **3-7**.[44] Obviously, the ratio between intermediate **3-6** and epichlorohydrin must be adjusted to promote the isolation of intermediate **3-8** instead of intermediate **3-7** (**Table 3.6**, entry 3). These conditions allowed the formation of just small amount of intermediate **3-8**. Due to the poor achieved results, we tried a procedure based on ultrasounds (**Table 3.7**).[41] This approach started with the deprotonation of intermediate **3-6** by crushed NaOH or NaH in the presence of a phase-transfer catalyst. Epichlorohydrin was added and the mixture stirred at rt for 24 hours and then sonicated for further 7 hours. Intermediate **3-6** was four-fold than epichlorohydrin in terms of moles. **Table 3.7** summarizes the tested conditions.

Entry	Reaction solvent	Base	Catalyst	Yield (%)
1	DCM	crushed NaOH	TBABr	0
2	THF	NaH	TBABr	0
3	DCM	NaH	TBABr	7
4	DCM	NaH	TBAI	0

Table 3.7 Reaction conditions tested for the synthesis of intermediate **3-8** in one step.[41]

As shown in **Table 3.7**, this reaction was successful only one time (entry 3), where intermediate **3-8** was obtained with a very poor yield (7%).

In conclusion, basic conditions were not suitable for the one step synthesis of intermediate **3-8**. Increasing the temperature or lengthening the reaction time did not afford the desired product. Therefore, the symmetric intermediate **3-8** could not be achieved in one step.

3.4.4 Synthesis Optimization of Intermediate 3-9

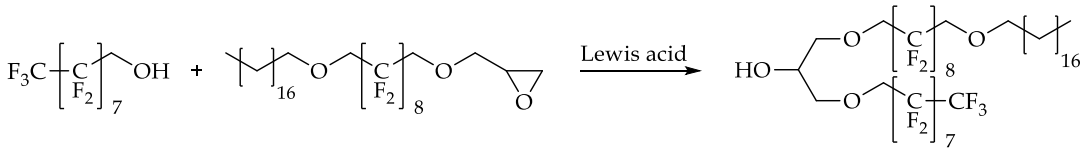

3-7 **3-9**

Scheme 3.7 General synthetic scheme for the synthesis of intermediate **3-9**.

Scheme 3.7 shows the synthesis of intermediate **3-9**. It is similar to the synthesis of intermediate **3-8**. **Table 3.8** describes the tested conditions.

Entry	Reaction solvent	Lewis acid	Temperature (°C)	Reaction time (hrs)	Ratio Perfluorononanol/ Intermediate 3-7/ Lewis acid	Yield (%)
1	DCM	BF_3OEt_2	rt	1	1.1 : 1 : 0.2	5
2	THF	BF_3OEt_2	rt	1	1.1 : 1 : 0.2	0
3	Et_2O	BF_3OEt_2	rt	1	1.1 : 1 : 0.2	0
4	DCM	BF_3OEt_2	rt	19	2 : 1 : 0.2	18
5	$N(CF_2CF_3)_3$	$TiCl_4$	reflux	24	2 : 1 : 0.2	25
6	DCM	$TiCl_4$	rt	16	3 : 1 : 0.2	30

Table 3.8 Conditions tested for the synthesis of intermediate **3-9**.

As reported in **Table 3.8**, BF_3OEt_2 and $TiCl_4$ were investigated as catalysts. Intermediate **3-9** was not obtained by using BF_3OEt_2, except when the reaction was carried out at rt with DCM as solvent (**Table 3.8**, entries 1 and 4). Remarkably, the desired product was obtained only when a double molar amount of 1H,1H-perfluoro-1-nonanol compared to intermediate **3-7** was used, according to the results previously accomplished for the synthesis of intermediate **3-8** (**Table 3.4**). Due to the poor yields achieved with BF_3OEt_2, $TiCl_4$ was considered as catalyst (**Table 3.8**, entry 5 and 6). First, $N(CF_2CF_3)_3$ was tested as solvent to promote the dissolution of fluorinated reactants. The mixture was heated to reflux and reacted for 24 hours, keeping the molar ratio among 1H,1H-perfluoro-1-nonanol, intermediate **3-7** and $TiCl_4$ as 2 : 1 : 0.2 (**Table 3.8**, entry 5). These conditions led to 25% yield. Then, DCM was tested as solvent (**Table 3.8**, entry 6). In this case, the reaction was carried out at rt and react for 16 hours. The molar amount of 1H,1H-perfluoro-1-nonanol was three-fold compared to intermediate **3-7**. The yield was close to the yield achieved using $N(CF_2CF_3)_3$ as solvent (30% *vs* 25% respectively). However, the conditions reported in **Table 3.8** entry 6 were selected as the best for

several reasons. First, DCM is a common solvent for chemical reactions and less expensive than $N(CF_2CF_3)_3$. Moreover, the synthetic procedure was simpler using DCM than $N(CF_2CF_3)_3$ since the mixture was neither heated nor reacted for long time. The excess of 1H,1H-perfluoro-1-nonanol could be easily recovered during chromatography purification of the crude product and used again.

3.5 Conclusions

The triphilic, dibranched and semifluorinated polymer **M2diF8H18** (compound **3-1**) has been successfully synthesized and characterized. However, the pegylation of intermediate **3-9** to afford **M2F8H18/F8** (compound **3-2**) has not been attempted yet. The synthesis of fluorinated polymers is a challenge because of the poor reactivity of fluorinated starting materials. Moreover, their purification is difficult due to the presence of large PEG unit that tend to have low R_f's and strongly stick on silica, making chromatography hard. Since the cost of fluorinated compounds are very high and the synthesis of polymers **3-1** and **3-2** requires several steps, we tried to increase the yield of the most problematic reactions. The most important improvement was the direct alkylation of the starting material 1H,1H,10H,10H-perfluoro-1,10-decanediol to afford intermediate **3-6** (**Scheme 3.1**). This allowed us to skip the mono-protection of 1H,1H,10H,10H-perfluoro-1,10-decanediol, shorten the synthesis by two steps as well as increase the yield. We also tried the synthesis of the symmetric intermediate **3-8** in one step without good results.

Semifluorinated polymers **3-1** and **3-2** will be used to prepare nanoemulsions. These colloidal systems will display an innovative design, different from that achieved with the linear polymer **M2F2H18** (**Figure 3.9**). The new design might affect the properties of the nanoemulsions – in term of

stability over time and drug release profile. The evaluation of these properties and their comparison with those achieved for the nanoemulsions prepared with the linear polymer **M2F2H18** will allow us to identify the best formulation for the controlled delivery of hydrophobic drugs.

3.6 Experimental Section

3.6.1 Materials and Methods

All fluorinated compounds were purchased from SynQuest Laboratories, Inc. (Alachua, FL, USA). All other reagents were obtained from Sigma-Aldrich (St. Louis, MO, USA) and used as received. All solvents were of ACS grade or higher and were purchased from Sigma-Aldrich (St. Louis, MO, USA) or Fisher Scientific (Hanover Park, IL, USA). Dry reactions were performed under argon using dry solvents and reagents. Reactions were monitored by thin-layer chromatography carried out on 0.25 mm Merck silica gel plates (60F-254) with UV light as the visualizing agent and potassium permanganate stain solution as developing agent. Chromatographic separation was performed using Silicycle 60 Å SiO_2. ^{1}H and ^{19}F NMR spectra were recorded on either Varian Unity-Inova 400 or Unity-Inova 500 spectrometers (University of Wisconsin-Madison, WI) using appropriate deuterated solvents and TMS as internal reference. The final polymer was purified by automated flash chromatography using a CombiFlash® Rf 4x system (Teledyne Isco, Lincoln, NE, USA) equipped with ELSD for compound visualization and a REDI-Sep Rf Gold C-18 silica high performance aqueous reverse phase cartridge. Polymer purity was analyzed by HPLC with a Gilson 321 Pump (Middleton, WI) equipped with Jordi Gel DVB 500Å (Bellingham, MA) column and a Gilson-Prep-ELS detector.

MALDI spectra were acquired on a Bruker ULTRAFLEX®III and high-resolution mass spectra were acquired on a Waters (Micromass) LCT®: electrospray ionization, time-of-flight, both in the University of Wisconsin-Madison Chemistry Department.

3.6.2 Specific Synthetic Procedures

Intermediate 3-3

10-(benzyloxy)-2,2,3,3,4,4,5,5,6,6,7,7,8,8,9,9-hexadecafluorodecan-1-ol

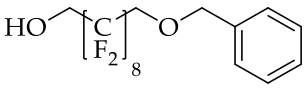

METHOD A

NaH (0.1582 g, 6.59 mmol) was added portionwise to a solution of 1H,1H,10H,10H-perfluoro-1,10-decanediol (2.0080 g, 4.34 mmol) in anhydrous DMF (50 ml). The reaction mixture was stirred under argon for 1 hour. BnBr (0.2 ml, 1.68 mmol) was diluted with DMF up to 5 ml and then added dropwise. The mixture was allowed to react at rt for 42 hours. The mixture was diluted with ether (40 ml) and extracted with aq. NH_4Cl (3 X 40 ml). The combined organic extracts were dried over $MgSO_4$, filtered and evaporated in vacuo to afford a yellow oil. The residue was purified by silica gel column chromatography (hexanes/EtOAc 100:0 to 93:7) to yield 0.1340 g (0.24 mmol, 14%) white powder.

R_f= 0.28 (hexanes/EtOAc 8:2)

^{1}H NMR (400 MHz, Chloroform-*d*) δ 7.45 – 7.30 (m, 5H), 4.68 (s, 2H), 4.10 (dt, *J* = 13.9, 7.5 Hz, 2H), 3.94 (t, *J* = 13.8 Hz, 2H), 1.93 (t, *J* = 7.6 Hz, 1H).

^{19}F NMR (376 MHz, Chloroform-*d*) δ -119.69 – -119.74 (m, 2F), -122.32 – -122.45 (m, 8F), -122.77 – -122.81 (m, 2F), -123.68 – 123.71 (m, 2F), -123.95 – -123.99 (m, 2F).

METHOD B

NaH (0.1050 g, 4.37 mmol) was added portionwise to a solution of 1H,1H,10H,10H-perfluoro-1,10-decanediol (2.0201 g, 4.37 mmol) in anhydrous DMF (20 ml). The reaction mixture was sonicated under argon for 10 minutes. BnBr (0.52 ml, 4.37 mmol) and TBAI (0.6465 g, 1.75 mmol) were added and the mixture was sonicated for 3 hours. The solvent was evaporated in vacuo and the residue was taken up in 5% HCl (20 ml). This solution was extracted with EtOAc (3 X 20 ml). The combined organic extracts were washed with 0.2M $Na_2S_2O_3$ (3 X 10 ml) and brine (10 ml), dried over $MgSO_4$, filtered and evaporated in vacuo to afford a yellow oil. The residue was purified by silica gel column chromatography (hexanes/EtOAc 100:0 to 93:7) to yield 1.0600 g (1.92 mmol, 44%) white powder, with spectra in agreement with those described above.

Intermediate 3-4

Octadecyl methanesulfonate

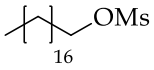

1-octadecanol (10.0351 g, 37.1 mmol) was dissolved in anhydrous DCM (125 ml) and flask flushed with argon. Anhydrous TEA (12.3 ml, 89 mmol) was added to the solution and flask cooled in ice bath. MsCl (3.7 ml, 48.1 mmol) was then added dropwise and reaction stirred overnight under argon, allowing the mixture to warm to rt. The reaction was then stopped, diluted with DCM (220 ml) and washed with saturated aqueous NH_4Cl (3 X 220 ml), dried over $MgSO_4$ and solvent removed under vacuum to yield 12.5450 g (36.0 mmol, 97%) white solid.

R_f= 0.48 (hexanes/EtOAc 8:2)

^{1}H NMR (400 MHz, Chloroform-*d*) δ 4.22 (t, *J* = 6.6 Hz, 2H), 3.00 (s, 3H), 1.75 (p, *J* = 6.8 Hz, 2H), 1.45 – 1.10 (m, 30H), 0.88 (t, *J* = 6.6 Hz, 3H).

Intermediate 3-5

(((2,2,3,3,4,4,5,5,6,6,7,7,8,8,9,9-hexadecafluoro-10-(octadecyloxy)decyl)oxy) methyl)benzene

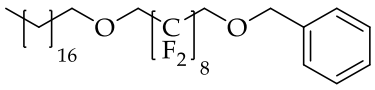

Intermediate **3-3** (1.7912 g, 3.24 mmol) was dissolved in anhydrous BTF (50 ml) and flask flushed with argon before NaH (0.1554 g, 6.48 mmol) was added. The mixture was stirred for 1 hour and then intermediate **3-4** (1.6961 g, 4.86 mmol) was added. The mixture was heated to reflux for 24 hours. The reaction was allowed to cool at rt, diluted with DCM (100 ml), and washed with saturated aqueous NH_4Cl (3 X 50 ml). The organic layer was dried over $MgSO_4$ and the solvent evaporated under reduced pressure to give a pale yellow solid. The residue was purified by silica gel column chromatography (hexanes/EtOAc 88:12) to yield 1.2523 g (1.54 mmol, 46%) white solid.

R_f= 0. 73 (hexanes/EtOAc 8:2)

^{1}H NMR (400 MHz, Chloroform-*d*): δ 7.46 – 7.29 (m, 5H), 4.68 (s, 2H), 3.97-3.88 (m, 4H), 3.59 (t, J = 6.6 Hz, 2H), 1.60 (p, J = 7.5 Hz, 2H), 1.25 (m, 30H), 0.88 (t, J = 6.6 Hz, 3H).

^{19}F NMR (376 MHz, Chloroform-*d*): δ -119.98 – -120.04 (m, 2F), -122.30 – -122.43 (m, 8F), -122.75 – 122.85 (m, 2F), -123.76 – -123.81 (m, 2F), -123.84 – -123.98 (m, 2F).

Intermediate 3-6

2,2,3,3,4,4,5,5,6,6,7,7,8,8,9,9-hexadecafluoro-10-(octadecyloxy)decan-1-ol

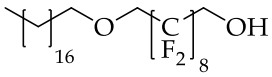

METHOD A

A solution of intermediate **3-5** (3.2000 g, 3.98 mmol) in methanol (250 ml) was flushed with argon before 10% Pd/C (400 mg) was added. Then, the mixture was placed under hydrogen for 2 days. The reaction was stopped and the mixture filtered over celite. The solvent was removed under reduced pressure to yield 2.7867 g (3.90 mmol, 98%) a white solid.

R_f= 0.52 (hexanes/EtOAc 8:2)

^{1}H NMR (400 MHz, Chloroform-*d*) δ 4.10 (dt, *J* = 13.9, 16 Hz, 2H), 3.92 (t, *J* = 14.0 Hz, 2H), 3.59 (t, *J* = 6.6 Hz, 2H), 1.93 (t, *J* = 7.5 Hz, 1H), 1.66 (p, *J* = 6.7 Hz, 2H), 1.36 – 1.20 (m, 30H), 0.88 (t, *J* = 6.7 Hz, 3H).

^{19}F NMR (376 MHz, Chloroform-*d*) δ -119.99 – -120.06 (m, 2F), -122.29 – -122.42 (m, 8F), -122.78 – 122.85 (m, 2F), -123.78 – -123.82 (m, 2F), -123.86 – -123.97 (m, 2F).

ESI-MS, *m/z* $[M+NH_4]^+$ calc'd: 732.3268; found: 732.3262.

METHOD B

NaH (1.2998 g, 54.2 mmol) was added portionwise to a solution of 1H,1H,10H,10H-perfluoro-1,10-decanediol (24.8443 g, 53.8 mmol) in anhydrous DMF (500 ml). The reaction mixture was sonicated under argon for 10 minutes. Intermediate **3-4** (18.7594 g, 53.8 mmol) was added and the

mixture was sonicated for 21 hours. The solvent was evaporated in vacuo and the residue was taken up in 5% HCl (500 ml). This solution was extracted with EtOAc (3 X 500 ml). The combined organic extracts were washed with brine (3 X 250 ml), dried over $MgSO_4$, filtered and evaporated under reduced pressure to afford a yellow oil. The residue was purified by silica gel column chromatography (hexanes/EtOAc 100:0 to 95:5) to yield 12.6875 g (17.8 mmol, 33%) white powder with spectra in agreement with those described above.

Intermediate 3-7

2-(((2,2,3,3,4,4,5,5,6,6,7,7,8,8,9,9-hexadecafluoro-10-(octadecyloxy)decyl)oxy) methyl)oxyrane

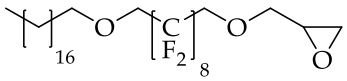

Epichlorohydrin (1.85 ml, 23.6 mmol) and Aliquat® 336 (0.14 ml, 0.31 mmol) were dissolved in cyclohexane (16 ml). Intermediate **3-6** (4.2222 g, 5.91 mmol) was added and the mixture was diluted with aqueous 50% NaOH (1.6 ml, 20 mmol). Under vigorous stirring, the two-phase system was heated to 90 °C for 5 hours. The mixture was then diluted with water (200 ml) and extracted with DCM (3 X 600 ml). The combined organic extracts were washed with saturated aqueous NH_4Cl (200 ml) and water (2 X 200 ml), dried over $MgSO_4$ and evaporated under reduced pressure to yield 4.3281 g (5.62 mmol, 95%) white powder.

R_f=0.60 (hexanes/EtOAc 8:2)

^{1}H NMR (500 MHz, Chloroform-*d*) δ 4.12 – 3.89 (m, 5H), 3.59 (t, *J* = 6.6 Hz, 2H), 3.54 (dd, *J* = 11.9 Hz, 5.9 Hz, 1H), 3.20 – 3.17 (m, 1H), 2.82 (t, *J* = 4.5 Hz, 1H), 2.64 (dd, *J* = 4.9, 2.6 Hz, 1H), 1.65 – 1.56 (m, 2H), 1.40 – 1.17 (m, 30H), 0.87 (t, *J* = 5 Hz, 3H).

^{19}F NMR (470 MHz, Chloroform-*d*) δ -119.52 – -119.58 (m, 2F), -119.75 – -119.80 (m, 2F), -121.78 – -121.82 (m, 4F), -121.92 – -121.96 (m, 4F), -123.35 – -123.38 (m, 4F).

Intermediate 3-8

21,21,22,22,23,23,24,24,25,25,26,26,27,27,28,28,36,36,37,37,38,38,39,39,40,40,41,41,42,42,43,43-dotriacontafluoro-19,30,34,45-tetraoxatrihexacontan-32-ol

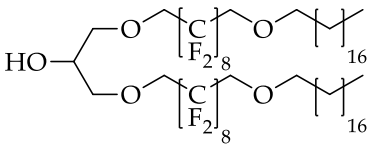

Intermediate **3-6** (8.1550 g, 11.4 mmol) and intermediate **3-7** (4.4097 g, 5.72 mmol) were dissolved in anhydrous DCM (130 ml) under argon. $TiCl_4$ (1.14 ml, 1.14 mmol) was added dropwise and the mixture was allowed to react for 18 hours at rt. The solvent was evaporated under reduced pressure and the residue was taken up in EtOAc (800 ml). The solution was washed with saturated aqueous $NaHCO_3$ (400 ml) and brine (400 ml), dried over $MgSO_4$, filtered and evaporated under reduced pressure. The residue was purified by silica gel column chromatography (hexanes/EtOAc 100:0 to 94:6) to yield 2.3772 g (1.60 mmol, 28%) white powder.

R_f=0.33 (hexanes/EtOAc 8:2)

^{1}H NMR (400 MHz, Chloroform-*d*) δ 4.07 – 4.00 (m, 5H), 3.91 (t, *J* = 14.0 Hz, 4H), 3.76 (d, *J* = 5.0 Hz, 2H), 3.62 (dd, *J* = 7.5 Hz, 5.5 Hz, 2H), 3.59 (t, *J* = 6.0 Hz, 4H), 2.37 (d, *J* = 6.0 Hz, 1H), 1.63 – 1.56 (m, 4H), 1.39 – 1.15 (m, 60 H), 0.88 (t, *J* = 6.7 Hz, 6H).

^{19}F NMR (470 MHz, Chloroform-*d*) δ -119.54 – -119.58 (m, 8F), -121.79 – -121.81 (m, 8F), -121.88 – -121.93 (m, 8F), -123.32 – -123.36 (m, 8F).

Intermediate 3-9

21,21,22,22,23,23,24,24,25,25,26,26,27,27,28,28,36,36,37,37,38,38,39,39,40,40,41,41,42,42,43,43-dotriacontafluoro-19,30,34,45-tetraoxatrihexacontan-32-ol

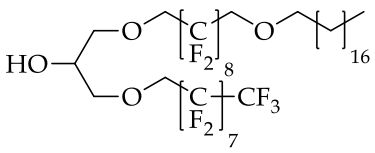

1H,1H-perfluoro-1-nonanol (8.8746 g, 19.7 mmol) and intermediate **3-7** (5.0500 g, 6.55 mmol) were dissolved in anhydrous DCM (400 ml) under argon. $TiCl_4$ (1.30 ml, 1.30 mmol) was added dropwise and the mixture was allowed to react for 16 hours at rt. The solvent was evaporated under reduced pressure and the residue was taken up in EtOAc (800 ml). The solution was washed with saturated aqueous $NaHCO_3$ (400 ml) and brine (400 ml), dried over $MgSO_4$, filtered and evaporated under reduced pressure. The residue was purified by silica gel column chromatography (hexanes/EtOAc 100:0 to 94:6) to yield 2.4061 g (1.97 mmol, 30%) white powder.

R_f=0.27 (hexanes/EtOAc 8:2)

^{1}H NMR (500 MHz, Chloroform-*d*) δ 4.11 – 3.97 (m, 5H), 3.92 (t, *J* = 13.9 Hz, 2H), 3.76 (d, *J* = 5.0 Hz, 2H), 3.64 (dd, *J* = 11.1, 5.5 Hz, 2H), 3.59 (t, *J* = 6.5 Hz, 2H), 2.43 (d, *J* = 6.0 Hz, 1H), 1.66 – 1.54 (m, 2H), 1.40 – 1.19 (m, 30H), 0.88 (t, *J* = 6.8 Hz, 3H).

^{19}F NMR (470 MHz, Chloroform-*d*) δ -80.76 – -80.80 (m, 3F), -119.57 – -119.62 (m, 6F), -121.80 – -121.85 (m, 8F), -121.88 – -121.93 (m, 8F), -123.35 – -123.37 (m, 8F).

Intermediate 3-10

mPEG2000-OMs

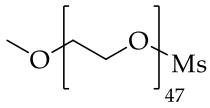

Anhydrous TEA (2 ml, 14.4 mmol) was syringed in a solution of mPEG2000-monomethyl ether (10.0642 g, 4.79 mmol) in anhydrous DCM (100 ml) under argon. MsCl (0.93 ml, 12.0 mmol) was then added and the reaction was stirred for 24 hours at rt under argon. The mixture was diluted with 100 ml DCM and washed with saturated aqueous NH_4Cl (3 X 100 ml). The organic layer was dried over $MgSO_4$, filtered and evaporated under reduced pressure to yield 10.3530 g (4.75 mmol, 99%) white solid.

^1H NMR (400 MHz, Chloroform-*d*) δ 4.42 – 4.35 (t, *J* = 4 Hz 2H), 3.72 – 3.54 (m, PEG), 3.38 (s, 3H), 3.09 (s, 3H).

Compound 3-1

M2diF8H18

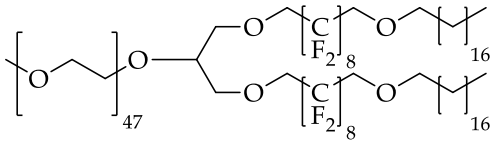

Intermediate **3-8** (303.9 mg, 0.20 mmol) was dissolved in BTF (5 ml) and flask flushed with argon. The solution was cooled at 0 °C before NaH (48.5 mg, 2.02 mmol) was added. Then, intermediate **3-10** (425.5 mg, 0.20 mmol) was added and the mixture heated to reflux for 5 days. The reaction was cooled, diluted with 150 ml DCM, washed with saturated aqueous NH_4Cl (150 ml), brine (90 ml), and dried over $MgSO_4$. The organics were concentrated to a minimum volume under reduced pressure and the product precipitated upon addition of cold ether. The solid was filtered and purified by silica gel column chromatography (DCM/methanol 100:0 to 90:10) and then by reverse phase column chromatography (water/methanol 100:0 to 0:100) to yield 68 mg (0.02 mmol, 10%) white powder.

^{1}H NMR (400 MHz, Chloroform-*d*) δ 4.04 – 3.97 (m, 5H), 3.95 – 3.88 (t, *J* = 14 Hz, 4H), 3.83 – 3.81 (m, 2H), 3.74 – 3.55 (m, PEG), 3.48 – 3.45 (m, 2H), 3.38 (s, 3H), 3.17 – 3.10 (t, *J* = 4 Hz, 4H), 1.61 – 1.56 (m, 4H), 1.35 – 1.25 (m, 60H), 0.90 – 0.86 (t, *J* = 8 Hz, 6H).

^{19}F NMR (376 MHz, Chloroform-*d*) δ -119.66 – -119.81 (m, 8F), -121.94 – -122.06 (m, 16F), -123.44 – -123.52 (m, 8F).

Mass (MALDI): dispersion around 3458.266

3.7 References

1. Riess, J. G. Highly Fluorinated Amphiphilic Molecules and Self-Assemblies with Biomedical Potential. *Curr. Opin. Colloid Interface Sci.* **14,** 294–304 (2009).
2. Kataoka, K., Harada, A. & Nagasaki, Y. Block Copolymer Micelles for Drug Delivery: Design, Characterization and Biological Significance. *Adv. Drug Deliv. Rev.* **64,** 37–48 (2012).
3. Know, G. S. & Kataoka, K. Block Copolymer Micelles as Long-Circulating Drug Vehicles. *Adv. Drug Deliv. Rev.* **64,** 237–245 (2012).
4. Torchilin, V. P. Multifunctional Nanocarriers. *Adv. Drug Deliv. Rev.* **64,** 302–315 (2012).
5. Ferlay, J., Shin, H. R., Bray, F., Forman, D. & Mathers, C. Estimates of Worldwide Burden of Cancer in 2008: GLOBOCAN 2008. *Int J Cancer* **127,** 2893–2917 (2010).
6. Jhaveri, A. M. & Torchilin, V. P. Multifunctional Polymeric Micelles for Delivery of Drugs and siRNA. *Front. Pharmacol.* **5,** 1–26 (2014).
7. Kim, T. Y. *et al.* Phase I and Pharmacokinetic Study of Genexol-PM, a Cremophor-Free, Polymeric Micelle-Formulated Paclitaxel, in Patients with Advanced Malignancies. *Clin. Cancer Res.* **10,** 3708–3716 (2004).
8. Gothwal, A., Khan, I. & Gupta, U. Polymeric Micelles: Recent Advancements in the Delivery of Anticancer Drugs. *Pharm Res* **33,** 18–39 (2016).
9. Gelderblom, H., Verweij, J., Nooter, K. & Sparreboom, A. Cremophor EL: the Drawbacks and Advantages of Vehicle Selection for Drug Formulation. *Eur. J. Cancer* **37,** 1590–1598 (2001).
10. Singh, S. & Dash, A. K. Paclitaxel in Cancer Treatment: Perspectives and Prospects of Its Delivery Challenges. *Crit. Rev. Ther. Drug Carrier Syst.* **26,** 333–372 (2009).

11. Yoon, H. J. & Jang, W. D. Polymeric Supramolecular Systems for Drug Delivery. *J. Mater. Chem.* **20,** 211–222 (2010).
12. Known, G. S. & Katoaka, K. Block Copolymer Micelles as Long-Circulating Drug Vehicles. *Adv. Drug Deliv. Rev.* **64,** 237–245 (2012).
13. Rosler, A., Vandermeulen, G. W. M. & Klok, H. A. Advanced Drug Delivery Devices via Self-Assembly of Amphiphilic Block Copolymers. *Adv. Drug Deliv. Rev.* **64,** 270–279 (2012).
14. Wilhelm, S. *et al.* Analysis of Nanoparticle Delivery to Tumors. *Nat. Rev.* **1,** (2016).
15. Otsuka, H., Nagasaki, Y. & Katoaka, K. PEGylated Nanoparticles for Biological and Pharmaceutical Applications. *Adv. Drug Deliv. Rev.* **64,** 246–255 (2012).
16. Matsumura, Y. & Maeda, H. A New Concept for Macromolecular Therapeutics in Cancer-Chemotherapy - Mechanism of Tumoritropic Accumulation of Proteins and the Antitumor Agent Smancs. *Cancer Res.* **46,** 6387–6392 (1986).
17. Zarzar, L. D. *et al.* Dynamically Reconfigurable Complex Emulsions via Tunable Interfacial Tensions. *Nature* **518,** 520–524 (2015).
18. Zhang, L. *et al.* Nanoparticles in Medicine: Therapeutic Applications and Developments. *Clin. Pharmacol. Ther.* **83,** 761–769 (2008).
19. Blair, H. A. & Deeks, E. D. Albumin-Bound Paclitaxel: a Review in Non-Small Cell Lung Cancer. *Drugs* **75,** 2017–2014 (2015).
20. Mishra, A. K. *Nanomedicine for Drug Delivery and Therapeutics.* (Wiley, 2013).
21. Ma, P. & Mumper, R. J. Paclitaxel Nano-Delivery Systems: a Comprehensive Review. *J Nanomed Nanotechnol* **4,** (2013).
22. Kumar, G. P. & Divya, A. Nanoemulsion Based Targeting in Cancer Therapeutics. *Med Chem* **5,** 272–284 (2015).
23. Matsumura, Y. *et al.* Phase I Clinical Trial and Pharmacokinetic

Evaluation of NK911, a Micelle-Encapsulated Doxorubicin. *Br. J. Cancer* **91,** 1775–1781 (2004).

24. Alani, A. W. G., Bae, Y., Rao, D. A. & Kwon, G. S. Polymeric Micelles for the pH-Dependent Controlled, Continuous Low Dose Release of Paclitaxel. *Biomaterials* **31,** 1765–1772 (2010).
25. Li, X. R. *et al.* Self-Assembly and Characterization of Pluronic P105 Micelles for Liver-Targeted Delivery of Silybin. *J. Drug Target.* **17,** 739–750 (2009).
26. Maeda, H., Wu, J., Sawa, T., Matsumura, Y. & Hori, K. Tumor Vascular Permeability and the EPR Effect in Macromolecular Therapeutics: a Review. *J. Control. Release* **65,** 271–284 (2000).
27. Ven, A. *et al.* Rapid Tumoritropic Accumulation of Systemically Injected Plateloid Particles and their Biodistribution. *J. Control. Release* **158,** 148–155 (2012).
28. Paciotti, G. F. *et al.* Synthesis and Evaluation of Paclitaxel-Loaded Gold Nanoparticles for Tumor-Targeted Drug Delivery. *Bioconjug. Chem.* **27,** 2646–2657 (2016).
29. Fang, J., Nakamura, H. & Maeda, H. The EPR Effect: Unique Features of Tumor Blood Vessels for Drug Delivery, Factors Involved, and Limitations and Augmentation of the Effect. *Adv. Drug Deliv. Rev.* **63,** 136–151 (2011).
30. Allen, T. M. & Cullis, P. R. Drug Delivery Systems: Entering the Mainstream. *Science (80-.).* **303,** 1818–1822 (2004).
31. Yuan, F. *et al.* Vascular Permeability in a Human Tumor Xenograft - Molecular Size Dependence and Cutoff Size. *Cancer Res.* **55,** 3752–3756 (1995).
32. Frank, D. *et al.* Overview of the Role of Nanotechnological Innovations in the Detection and Treatment of Solid Tumors. *Int. J. Nanomedicine* **9,** 589–613 (2014).

33. Duncan, R. & Gaspar, R. Nanomedicine(s) under the Microscope. *Mol. Pharm.* **8,** 2101–2141 (2011).
34. Bae, K. H., Lee, Y. & Park, T. G. Oil-Encapsulating PEO-PPO-PEO/PEG Shell Cross-Linked Nanocapsules for Target-Specific Delivery of Paclitaxel. *Biomacromolecules* **8,** 650–656 (2007).
35. Jee, J., Mccoy, A. & Mecozzi, S. Encapsulation and Release of Amphotericin B from an ABC Triblock Fluorous Copolymer. *Pharm Res* **29,** 69–82 (2012).
36. Harris, J. M. & Chess, R. B. Effect of Pegylation on Pharmaceuticals. *Nature* **2,** 214–221 (2003).
37. Riess, J. G. Perfluorocarbon-Based Oxygen Delivery. *Artif. Cells Blood Substitutes Biotechnol.* **34,** 567–580 (2006).
38. Taylor, P. Ostwald Ripening in Emulsions: Estimation of Solution Thermodynamics of the Disperse Phase. *Adv. Colloid Interface Sci.* **106,** 261–285 (2003).
39. Kabalnov, A. S. & Shchukin, E. D. Ostwald Ripening Theory: Applications to Fluorocarbon Emulsion Stability. *Adv. Colloid Interface Sci.* **38,** 69–97 (1992).
40. Parlato, M. C., Jee, J. P., Teshite, M. & Mecozzi, S. Synthesis, Characterization, and Applications of Hemifluorinated Dibranched Amphiphiles. *J. Org. Chem.* **76,** 6584–6591 (2011).
41. Hussein, W. M. *et al.* Synthesis of Nickel-Chelating Fluorinated Lipids for Protein Monolayer Crystallizations. *J. Org. Chem.* 1473–1479 (2009).
42. Cintas, P., Cravotto, G., Barge, A. & Martina, K. Interplay between Mechanochemistry and Sonochemistry. *Top Curr Chem* **369,** 239–284 (2015).
43. Tuulmets, A., Piiskop, S., Järv, J. & Salmar, S. Sonication Effects on Non-Radical Reactions. A Sonochemistry beyond the Cavitation? *Ultrason. Sonochem.* **21,** 997–1001 (2014).

44. Bauer, J. & Rademann, J. Hydrophobically Assisted Switching Phase Synthesis: the Flexible Combination of Solid-Phase Reactions Employed for Oligosaccharide Preparation. *J. Am. Chem. Soc.* **127,** 7296–7297 (2005).
45. Chambers, R. *Fluorine in Organic Chemistry*. (Blackwell Publishing Ltd., 2004).
46. Wang, Y. *et al.* Investigation on RAFT Polymerization of a Y-Shaped Amphiphilic Fluorinated Monomer and Anti-Fog and Oil-Repellent Properties of the Polymers. *Macromol. Rapid Commun.* **31,** 1816–1821 (2010).
47. Laurent, N., Lafont, D. & Boullanger, P. Syntheses of α-D-Galactosamine Neoglycolipids. *Carbohydr. Res.* **341,** 823–835 (2006).

Scientific Publications

Published Article	Gambini, L., Rizzi, L., Pedretti, A., Taglialatela-Scafati, O., Carucci, M., Pancotti, A., Galli, C., Read, M., Giurisato, E., Romeo, S., Russo, I. Picomolar inhibition of Plamepsin V, an essential malaria protease, achieved exploiting the prime region. *PloS One* **2015**, 10 (11).
Published Article	Pancotti, A., Parapini, S., Dell'Agli, M., Gambini, L., Galli, C., Sangiovanni, E., Basilico, N., Bosisio, E., Taramelli, D., Romeo, S. Discovery of oxybisbenzoylamides as a new class of antimalarial agents. *Med. Chem. Commun.* **2015**, 6, 1173.
Published Article	Gabriele E., Porta, F., Facchetti, G., Galli, C., Gelain, A., Meneghetti, F., Rimoldi, I., Romeo, S., Villa, S., Ricci, C., Ferri, N., Asai, A., Barlocco, D., Sparatore, A. Synthesis of new dithiolethione and methanethiosulfonate systems endowed with pharmaceutical interest. *Arkivoc*, **2017**, (ii), 235-250.
Abstract in Conference Proceedings	Galli, C., Barres, A., Mecozzi, S. Synthesis of dibranched semifluorinated polymers for fluorous nanoemulsion-based drug delivery. ACS Congress. Philadelphia (August 21-25, **2016**).
Abstract in Conference Proceedings	Galli, C., Pellino, M., Ceppi, L., Ambrosini, D., Romeo, S. Noncovalent fluorous-fluorous interactions: a new approach for drug discovery. 53rd International Conference on Medicinal Chemistry. Toulouse (July 5-7, **2017**).